UNIVERSIDADE FEDERAL DO PARANÁ

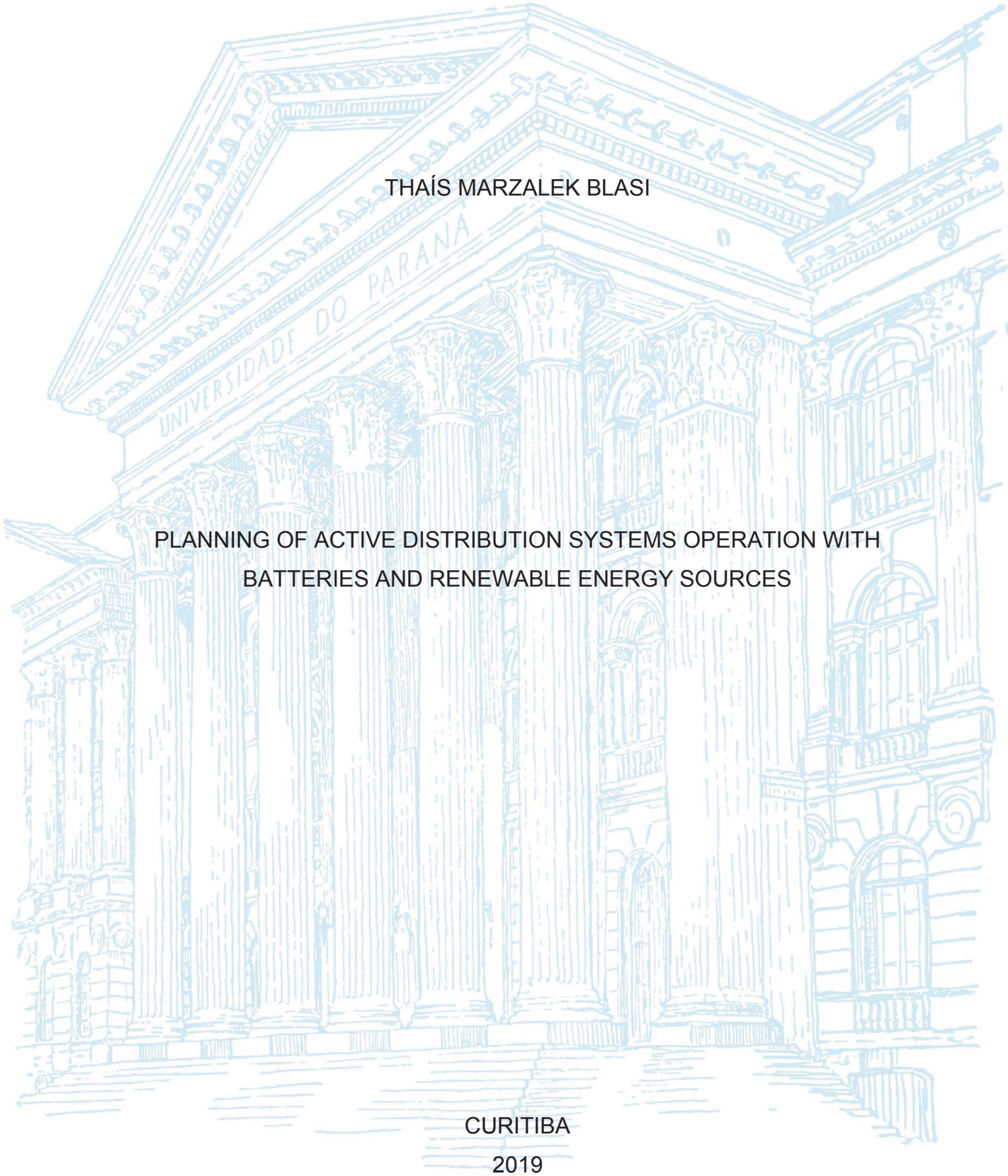

THAÍS MARZALEK BLASI

PLANNING OF ACTIVE DISTRIBUTION SYSTEMS OPERATION WITH BATTERIES AND RENEWABLE ENERGY SOURCES

CURITIBA
2019

THAÍS MARZALEK BLASI

PLANNING OF ACTIVE DISTRIBUTION SYSTEMS OPERATION WITH BATTERIES AND RENEWABLE ENERGY SOURCES

Dissertação de Mestrado apresentada ao curso de Pós-Graduação em Engenharia Elétrica, Setor de Tecnologia, Universidade Federal do Paraná, como requisito parcial à obtenção do título de Mestre em Engenharia Elétrica.

Orientadora:

Prof. Dra. Thelma S. P. Fernandes (UFPR)

Coorientadores:

Prof. Dr. Alexandre Rasi Aoki (UFPR)

Prof. Dr. Daniel Navarro Gevers (THI)

CURITIBA

2019

Catalogação na Fonte: Sistema de Bibliotecas, UFPR
Biblioteca de Ciência e Tecnologia

B644p BlasiThaís Marzalek
Planning of active distribution systems operation with batteries and renewable energy sources [recurso eletrônico] / Thaís Marzalek Blasi– Curitiba, 2019.

Dissertação - Universidade Federal do Paraná, Setor de Tecnologia, Programa de Pós-graduação em Engenharia Elétrica.

Orientadora: Profa. Dra. Thelma Solange Piazza. P. Fernandes
Coorientador: Prof. Dr. Alexandre Rasi Aoki
Coorientador: Prof. Dr. Daniel Navarro Gevers

1. Baterias. 2. Rede Elétrica – Fluxo de Potência. 3. Sistemas Fotovoltaicos. I. Universidade Federal do Paraná. II. Fernandes. Thelma Solange Piazza. III. Aoki, Alexandre Rasi. IV. Gevers, Daniel Navarro. V. Título.

CDD: 621.312424

Bibliotecária: Roseny Rivelini Morciani CRB-9/1585

MINISTÉRIO DA EDUCAÇÃO
SETOR DE TECNOLOGIA
UNIVERSIDADE FEDERAL DO PARANÁ
PRÓ-REITORIA DE PESQUISA E PÓS-GRADUAÇÃO
PROGRAMA DE PÓS-GRADUAÇÃO ENGENHARIA
ELÉTRICA - 40001016043P4

TERMO DE APROVAÇÃO

Os membros da Banca Examinadora designada pelo Colegiado do Programa de Pós-Graduação em ENGENHARIA ELÉTRICA da Universidade Federal do Paraná foram convocados para realizar a arguição da dissertação de Mestrado de **THAÍS MARZALEK BLASI** intitulada: **Planning of Active Distribution Systems Operation with Batteries and Renewable Energy Sources**, sob orientação da Profa. Dra. THELMA SOLANGE PIAZZA FERNANDES, que após terem inquirido a aluna e realizada a avaliação do trabalho, são de parecer pela sua APROVAÇÃO no rito de defesa.

A outorga do título de mestre está sujeita à homologação pelo colegiado, ao atendimento de todas as indicações e correções solicitadas pela banca e ao pleno atendimento das demandas regimentais do Programa de Pós-Graduação.

CURITIBA, 03 de Fevereiro de 2020.

THELMA SOLANGE PIAZZA FERNANDES
Presidente da Banca Examinadora (UNIVERSIDADE FEDERAL DO PARANÁ)

CRESENCIO SILVIO SEGURA SALAS
Avaliador Externo (INSTITUTO DE TECNOLOGIA PARA O DESENVOLVIMENTO)

JOÃO AMERICO VILELA JUNIOR
Avaliador Interno (UNIVERSIDADE FEDERAL DO PARANÁ)

ROMAN KUIAVA
Avaliador Interno (UNIVERSIDADE FEDERAL DO PARANÁ)

I dedicate this dissertation to my mother, Marília and to my brother Raphael that are my best friends and are who always supported and encouraged me.

ACKNOWLEDGMENT

First, I thank God for the gift of life and always show me the paths that I should follow.

I would like to thank my family, my mother Marília Marzalek Blasi, my brother Raphael Marzalek Blasi and my father Paulo Küster Blasi for all the love, affection, dedication, support and incentive during all my life and for encouraging me to follow my dreams.

I would like to thank my professor supervisor Dra. Thelma Solange Piazza Fernandes for the friendship and for all her dedication, patience, support and help to develop this work.

I would like to thank my professor auxiliary supervisor, Dr. Alexandre Rasi Aoki, for the friendship and for all his support, dedication, patience and for always encouraging me to develop this work and also for always give me opportunities to learn more and more.

I would like to thank my professor auxiliary supervisor, Dr. Daniel Navarro Gevers from Technische Hochschule Ingolstadt, for the friendship and for all his dedication and support, especially during my exchange time in Germany.

I would like to thank all my colleagues from UFPR and Lactec for all the knowledge shared and support during the development of this work.

I would like to thank my supervisor at Lactec, Dr. Eduardo Kazumi Yamakawa for the friendship, support and incentive to develop this work.

I would like to thank the Lactec for financial support and for the opportunities provided, including the R&D project PD-2866-0444/2016 entitled “Algoritmo Multicritério Espacial para Aplicação de Baterias para Qualidade do Fornecimento" coordinated by Dr. Patricio Rodolfo Impinnisi and supported by Companhia Paranaense de Energia (Copel Distribuição).

“Be humble to avoid pride, but fly high to attain wisdom”.

Saint Augustine

RESUMO

A operação das redes de distribuição mudou nos últimos anos devido à inserção de recursos energéticos distribuídos. Esses sistemas ativos consistem em sistemas de geração, como sistemas fotovoltaicos, ou mesmo sistemas de armazenamento, como baterias. Uma vez que as redes de distribuição não foram projetadas considerando a presença de sistemas de geração e armazenamento, é necessário verificar o impacto desses elementos quando conectados ao sistema elétrico em diferentes níveis de penetração. Para avaliar os impactos desses novos elementos, foram realizados estudos de fluxo de potência, permitindo compreender o comportamento da rede elétrica distribuída considerando um estado operacional definido. Para essa análise, foi utilizada a ferramenta de software OpenDSS, sendo considerados diferentes níveis de penetração, calculados de acordo com dois critérios diferentes: um baseado na relação da potência instalada da carga e da geração e outros baseado na capacidade de suporte do alimentador. Para realizar o planejamento da rede de distribuição, considerando o horizonte de um dia à frente, foi proposto o aprimoramento do fluxo ótimo de energia por períodos múltiplos, também chamado de fluxo ótimo de energia dinâmico. A formulação clássica ideal de fluxo de energia multiperíodo é normalmente usada para resolver o despacho de energia e o gerenciamento do lado da demanda. Portanto, foi necessário propor modelagem estendida, na qual foi possível inserir o modelo correspondente ao funcionamento da bateria. Esse novo fluxo de energia ideal de vários períodos tem o objetivo de minimizar as perdas de energia elétrica e os custos operacionais do sistema e da bateria. As simulações realizadas compreenderam duas etapas: na primeira, o impacto dos elementos ativos nas redes de distribuição foi avaliado por simulações de fluxo de potência com diferentes níveis de penetração nos sistemas de geração, e a segunda consistiu na simulação do fluxo de potência ideal. prorrogado por vários períodos para avaliar o planejamento da operação da rede e do sistema de baterias de acordo com as previsões de geração e demanda para o dia seguinte. Nos dois casos, a rede de distribuição foi modelada considerando a presença de bancos de capacitores e também a operação de reguladores de tensão, uma vez que esses dispositivos já existem na rede de distribuição, mesmo antes da inserção dos elementos ativos. Dessa forma, os resultados encontrados evidenciaram os impactos da inserção de recursos energéticos distribuídos nas redes de distribuição, principalmente quando os níveis de penetração são maiores, reduzindo, neste caso, as perdas de energia do sistema. Em relação ao planejamento da operação do sistema, verificou-se que as descargas das baterias ocorrem durante o pico da carga, a propósito, que os períodos de carregamento variam de acordo com a disponibilidade de geração fotovoltaica. As abordagens propostas destacam a possibilidade de avaliar e planejar a operação ideal dos sistemas de distribuição existentes, considerando a inserção de novos elementos.

Palavras-chave: Fluxo de Potência Ótimo Multi-Período. Fluxo de Potência. Sistemas Ativos de Distribuição. Baterias. Sistemas Fotovoltaicos. Níveis de Penetração.

ABSTRACT

The operation of the distribution networks has changed over the last years due to the insertion of distributed energy resources. These active systems consist of generation systems, such as photovoltaic systems, or even storage systems, such as batteries. Since distribution networks were not designed considering the presence of generation and storage systems, it is necessary to verify the impact of these elements when connected to the electrical system at different penetration levels. In order to evaluate the impacts of these new elements, power flow studies were performed, allowing to undestand the behavior of the electric distributed network considering a defined operating state. For this analysis, the OpenDSS software tool was used, being considered different penetration levels calculated according to two different criteria: one based on the relation of the installed power of the load and the generation, and others based on the feeder supportability. In order to carry out the planning of the distribution network, considering the horizon of a day ahead, it was proposed the enhancement of multi-period optimum power flow, also called dynamic optimum power flow. The classical multi-period optimal power flow formulation is normally used to solve energy dispatch and demand-side management. Therefore, it was necessary to propose an extended modeling, in which it was possible to insert the model corresponding to the operation of the battery. This new multi-period optimal power flow has the objective to minimize the electrical power losses and system and battery operating costs. The simulations carried out comprised two stages: in the first one, the impact of the active elements in distribution networks was evaluated by power flow simulations with different levels of penetration of generation systems, and the second one consisted on the simulation of the optimal power flow multi-period extended to evaluate the planning of the network operation and the battery system according to the forecasts of generation and demand for the day ahead. In both cases, the distribution system was modeled considering the presence of capacitor banks and also the operation of voltage regulators, since these devices already exist in the distribution system, even before the insertion of the active elements. In this way, the results found evidenced the impacts of the insertion of distributed energy resources in the distribution networks mainly when the penetration levels are higher, reducing, in this case, the power losses of the system. Regarding the planning of system operation, it was verified that the battery discharges happen during the peak of the load, by the way, that the charging periods vary according to the availability of photovoltaic generation. The proposed approaches highlight the possibility to evaluate and plan the optimal operation of existing distribution systems considering the insertion of new elements.

Keywords: Multi-period Optimum Power Flow. Batteries. Photovoltaic Systems. Penetration Levels.

LIST OF ILLUSTRATIONS

LIST OF TABLES

LIST OF ABBREVIATIONS

AC	Alternating Current
ADN	Active Distribution Network
Ah	Ampère hour
ANEEL	Brazilian Electricity Regulatory Agency
BESS	Battery Energy Storage System
BMS	Battery Management System
C	Battery Capacity
CAES	Compressed Air Energy Storage
CAIDI	Customer Average Interruption Duration Index
CAIFI	Customer Average Interruption Frequency Index
CAPES	Brazilian Foundation from the Ministry of Education to coordinate efforts related to education improvement
DC	Direct Current
DER	Distributed Energy Resources
DG	Distributed Generation
DIgSILENT	Digital Simulation and Electrical Network
DMS	Distribution Management System
DoD	Depth-of-Discharge
DSM	Demand Side Management
DSO	Distribution System Operator
EIA	U.S. Energy Information Administration
EPE	Energy Research Office
EPRI	Electric Power Research Institute
ESS	Energy Storage System
IEA	International Energy Agency
IEC	International Electrotechnical Commission
IEEE	Institute of Electrical and Electronics Engineering
INMET	Brazilian National Institute of Meteorology
LCO	Lithium Cobalt Oxide battery
LFP	Lithium Phosphate battery
LMO	Lithium Manganese Oxide battery

LTO	Lithium Titanate battery
LV	Low Voltage
LVR	Line Voltage Regulator
MPOPF	Multi-period Optimum Power Flow
MV	Medium Voltage
NaNiCl	Sodium-nickel-chloride battery
NaS	Sodium-Sulfur battery
NCA	Nickel-Cobalt-Aluminum Oxide battery
NiCd	Nickel-Cadmium battery
NiMH	Nickel-Metal Hydride battery
NMC	Nickel-Manganese-Cobalt battery
NR	Normative Resolution
OLTC	On-load TAP Changes
ONS	National System Operator
OPENDSS	Open Distribution System Simulator
OPF	Optimum Power Flow
PBE	Brazilian Energy Efficiency Program
PES	Power and Energy Society
PF	Power Factor
PRODIST	Procedures for Distribution of Electric Energy in the National Electric Power System
Prosumer	Consumers that produce energy
p.u.	*per unit*
PV	Photovoltaic
SAIDI	System Average Interruption Duration Index
SAIFI	System Average Interruption Frequency Index
SCADA	Supervisory Control and Data Acquisition
SOC	State of Charge
TAP	Transformer Adjustment Position
VR	Voltage Regulator
VRFB	Vanadium Redox Flow Battery
VRLA	Valve Regulated Lead-Acid Battery
ZBFB	Zinc-bromine flow battery

LIST OF SYMBOLS

a_j^t	Tap position of voltage regulator at branch j and period t
$amax_j^t, amin_j^t$	Maximum and minimum limit of taps of voltage regulator at branch j and period t
c_i^t	Capacitive susceptance of the bank of capacitors at bus i and period t [S]
$cost^t$	Hourly cost of energy [Brazilian Reais]
$cost\_bat$	Cost of battery operation [Brazilian Reais]
$cost_{BB}$	Cost of battery energy storage bank [Brazilian Reais]
$cost_{degradation}$	Cost of battery degradation [Brazilian Reais]
$cost\_total$	Cost of energy generated at substation [Brazilian Reais]
$cmax_i^t$	Maximum capacitive susceptance of the bank of capacitors at bus i and period t [S]
$cycles$	Number of cycles to failure
$DGpenetration$	Distributed generation penetration level [%]
$Ebat$	Total Energy of battery system [kWh]
$Ebat_i^t$	Total Energy of battery system at bus i and period t [kWh]
$Ebat\_acum_i^t$	Effective value of energy storage at bus i and period t [kWh]
eta	Efficiency of battery energy storage system [%]
fl_j^t	Power flow at branch j and period t [kVA]
$flmax_j^t$	Maximum power flow at branch j and period t [kVA]
nb	Number of buses
nl	Number of branches
np	Number of periods
$Pbat_i^t$	Active power of battery system at bus i and period t [kW]
pf	Power factor
P_i^t	Injection active power at bus i and period t [kW]
Pd_i^t	Active power load at bus i and period t [kW]
$P_{generation}$	Active power generated [kW]
P_{gh}	Active power provided by the substation [kW]

Pg_i^t	Active power generation at bus i and period t [kW]
$Pgsol_i^t$	Active solar power generation at bus i and period t [kW]
P_k	Active power injection at bus k [kW]
P_{load}	Load active power [kW]
P_m	Active power injection at bus m [kW]
$Qbat_i^t$	Reactive power of battery system at bus i and period t [kvar]
Q_i^t	Injection reactive power at bus i and period t [kvar]
Qg_i^t	Reactive power generation at bus i and period t [kvar]
$Qgsol_i^t$	Reactive solar power generation at bus i and period t [kvar]
Qd_i^t	Reactive power load at bus i and period t [kvar]
Q_k	Reactive power at bus k [kvar]
Q_m	Reactive power at bus m [kvar]
r_{km}	Resistance of the line between buses k and m [ohm]
R_{SC}	Short circuit ratio
S_{SC}	Short circuit power
SI_m	Stability index of bus m
Δt	Time interval between two consecutive periods
$\dot{V}_i^t$	Phasor of voltage at bus i and period t
$Vmax_i^k, Vmin_i^k$	Maximum and minimum limit of voltage magnitude at bus i and period t [V]
V_k	Voltage magnitude at bus k [V]
V_m	Voltage magnitude at bus m [V]
x_{km}	Reactance of line between buses k and m [ohm]

SUMMARY

1 INTRODUCTION

The use of electricity is an intrinsic necessity for human life nowadays. The demand for electricity has been growing year after year during the last century, and the forecasts show that it will continue increasing, according to the International Energy Agency (IEA) research. However, this growth will be more noticeable in growing economy countries, led by China and India as shown in FIGURE 1 (IEA, 2018).

FIGURE 1 - GLOBAL ELECTRICITY DEMAND BEHAVIOR.

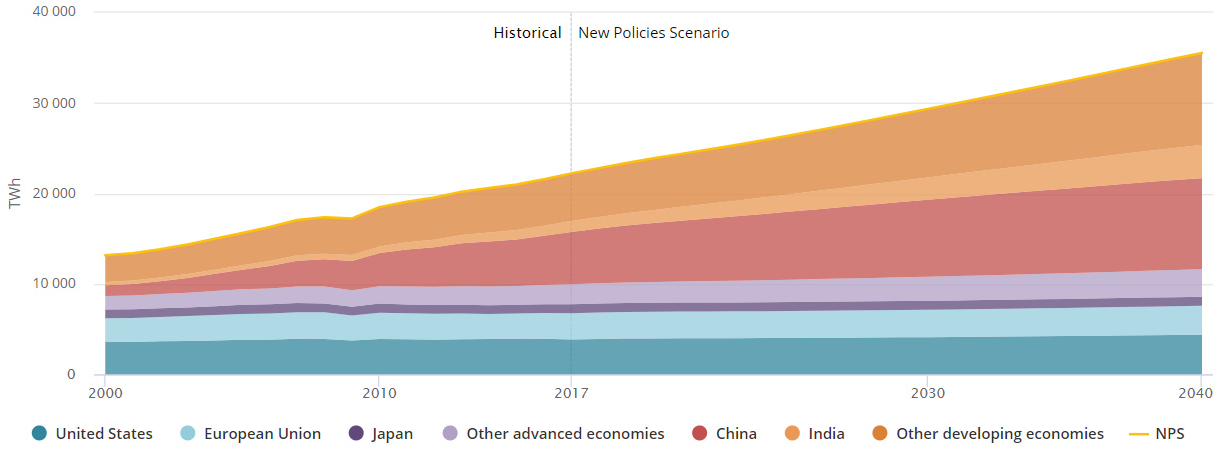

SOURCE: IEA (2018).

During the last ten years, China presents the biggest growth of electricity due to different aspects combined as shifts in the economy that presents a growth of 4.5% per year, strong energy efficiency policies and demographic changes (IEA, 2017). Only in 2018, the energy demand grows 8.5% in the year, largely driven by the growth of the secondary industry (YANG, 2019). Other countries as the United States and European Countries do not present the same electricity demand growth due to more energy efficiency' technologies and towards services industries that tends to grow more than the energy-intensive industries. In the USA, for example, according to the U.S. Energy Information Administration (EIA) forecast, the electricity demand will grow by 0.8% per year until 2050 (EULE, 2019).

Nonetheless, in Brazil, according to the Energy Research Office (EPE), the demand growth forecast from 2017 to 2026 is 3.6% each year, reaching 653.93 GWh in 2026. However, this growth is not as high as other emerging countries, such as China and India, and is even lower than the forecasts made by EPE for the country in 2010 to 2019, which had a growth forecast of 5%. It is important to highlight that in

Brazil, around 40% of the load corresponds to industrial consumers, followed by 30% of residential consumers, 20% of commercial and 10% of another kind of consumers as public services and street lighting (EPE, 2017).

Due to the growth of the demand, it is necessary to increase the electricity capacity of all the electrical power system. In Brazil, for example, from 2019 to 2023 the total installed capacity of generation from central power stations will present a growth from 161,552 MW to 177,971 MW of installed power, according to the forecast of National System Operator (ONS). At the same time, the growth of the system will happen in transmission level, with the insertion of more 44 thousand kilometers of transmission lines (ONS, 2019a). Furthermore, the changes in the power system will happen also at the distribution level (medium and low voltage) mainly due to the insertion of distributed generation (DG), close to the consumers. This corresponds to a new paradigm, since new elements are being installed into the grid, by the way, at generation and transmission levels, there will only be the expansion of existing elements.

1.1 CONTEXT

The increase of DG associated with the growth of load demand significantly changed the planning and operation of the distribution network. Until some years ago, the energy flowed only in the one-directional way (FIGURE 2-a), from generation centers, most of the time located far from the consumer's centers, to transmission and distribution systems. Yet, with the insertion of generation units at the distribution level, as active elements into the grid, the flow of energy starts to happen in a multidirectional way (FIGURE 2-b) (CAMPILLO, 2016).

Since the distribution system was not planned to operate considering generation systems inserted on it, these elements may present impacts on distribution system operation in terms of voltage and power quality, load and voltage profile management, security and safety issues and, in case of high penetration, it can tease reverse power flow at the substation, being this level of penetration known as extreme penetration. These changes in the distribution network brought the necessity to improve the monitoring and communication systems, allowing the distribution system operator (DSO) to develop new coordinate control strategies (CIGRE, 2011).

According to ANEEL (Brazilian Electricity Regulatory Agency), the DG can be defined as generation systems directly connected to the distribution power system or connected by the consumer's installations (ANEEL, 2018a). In the present approach distributed generation consisted on micro and minigeneration systems, following the definition presented at ANEEL Normative Resolution 482/2012, in which is outlined microgeneration generation systems connected to the main grid by consumers units and that present installed power lower than 75kW, whereas minigeneration systems presents installed power higher than 75kW and lower than 5MW (ANEEL, 2012).

Most of the time the distributed generation systems consisted of renewable energy resources, mainly photovoltaic systems, on account of its ease implementation with consumers and the decrease of market and technology costs. According to a Fraunhofer ISE research, the costs of photovoltaic systems will decrease from approximately 550 euros/kW in 2015 to 140-360 euros/kW by 2050 for modules prices. The same effect will be noticed in inverters prices that will reduce from 110 euros/kW in 2015 to 23 – 39 euros/kW in 2050 (FRAUNHOFER ISE, 2015).

FIGURE 2 – PASSIVE (A) AND ACTIVE (B) DISTRIBUTION NETWORK.

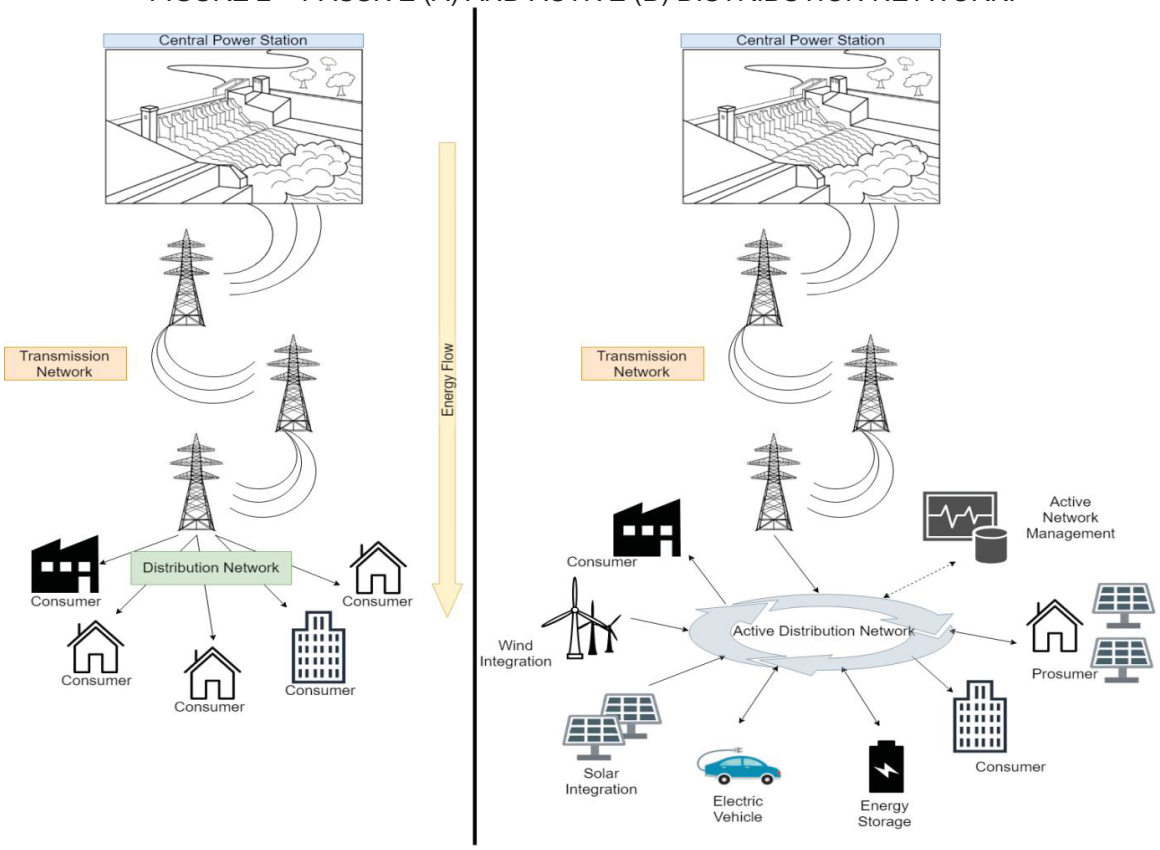

(a) (b)

SOURCE: The Author (2019).

The connection of DG systems at the distribution network needs to be studied and approved by DSOs and, moreover, needs to follow specific regulations.

In Brazil, the first regulation about the connection of distributed generation was the Article 14 of the Law Decree number 5,163 from July, 30th 2004, in which was defined the possibility of the connection of distributed generation systems limited to the installed power of 30 MW for hydropower systems and the efficiency of 75% to thermal systems of generation (PEREIRA, 2019).

In 2012, the Normative Resolution (NR) nº 482/2012 from ANEEL allowed the consumer to produce their own electricity and to provide the surplus of electricity to the power grid (ANEEL, 2012). Moreover, the NR n° 482 characterizes the differences between micro and mini-generation systems and also introduces the concepts about the compensatory system of electricity between the power utility and the prosumers[1], which was detailed later in the NR nº 687/2015 (ANEEL, 2015). Therefore, with the definition of these resolutions, the number of DG systems starts to grow, moving from tested systems installed in universities and industries to systems that are marketed and installed close to electricity consumers.

Nowadays in Brazil, there are more than 102,653 distributed generation systems that totalize an installed power of 1,240,138.62 kW (ANEEL, 2019a). The considered technologies of distributed generation systems are solar photovoltaic generation, wind power systems, thermal generation, which included biogas and biomass generation and small hydropower generation central. The most expressive technology used is photovoltaic systems, presenting 102,333 systems installed, corresponding to 1,094,802.08 kW of installed power (ANEEL, 2019a). FIGURE 3 represents the location of all distributed photovoltaic systems, allowing to verify the regions with the greatest concentration of these systems, in the southwest of the country, with 48,685 DGs. It is important to highlight that in the north region there is just a few numbers of systems due to the Amazon Forest.

[1] Prosumers are consumers that also produce energy

FIGURE 3 - DISTRIBUTION OF THE PHOTOVOLTAIC SYSTEMS IN BRAZIL.

SOURCE: ANEEL (2019a).

The state with the highest amount of DG systems is Minas Gerais, with 22,612 photovoltaic units installed, totalizing an installed power of 225,739.77 kW. In the context of the R&D Copel DIS project, it is important to foucus at the Paraná state, which currently has 5,146 distributed photovoltaic systems, corresponding to 56,070.59 kW of installed power, most of them concentrated in the west of the State and close to the Curitiba city, that is the State's Capital City, as it is possible to visualize at FIGURE 4 (ANEEL, 2019a).

FIGURE 4 - DISTRIBUTION OF THE PHOTOVOLTAIC SYSTEMS AT PARANÁ STATE.

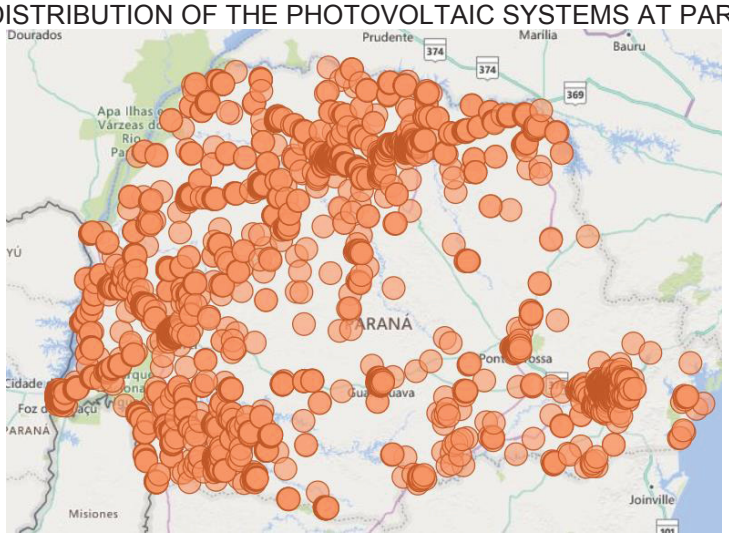

SOURCE: ANEEL (2019a).

As aforementioned, the distributed energy generation represents a disruptive idea on distribution system operation and about the potential of electricity generation. The increase of these systems into the power grid is dependent of different factors, being one of the most relevant the economic one, that will be the key to instigate the consumer to install the system, becoming a prosumer. Meanwhile, looking for the energy planning perspective, the increase of the DG implies a greater uncertainty on energy demand and how the load could be supplied at each instant. At the same time, the DG systems can be useful for grid operation, contributing, for example, to the reduction of the electric losses, since the generation is placed close to the consumers, and thus, reducing the flow of energy through the lines (ENERGY RESEARCH OFFICE - EPE, 2018).

In order to improve the distribution system operation, the DSOs are evaluating the insertion of storage elements, to contribute with the definition of the best operational strategy, reducing losses, costs and improving the reliability of the distribution system. However, there are a lot of options for energy storage systems technologies and their use had been growing, mainly of battery systems, as show FIGURE 5.

FIGURE 5 – TECHNOLOGY MIX OF STORAGE SYSTEMS, EXCLUDING PUMPING HYDRO.

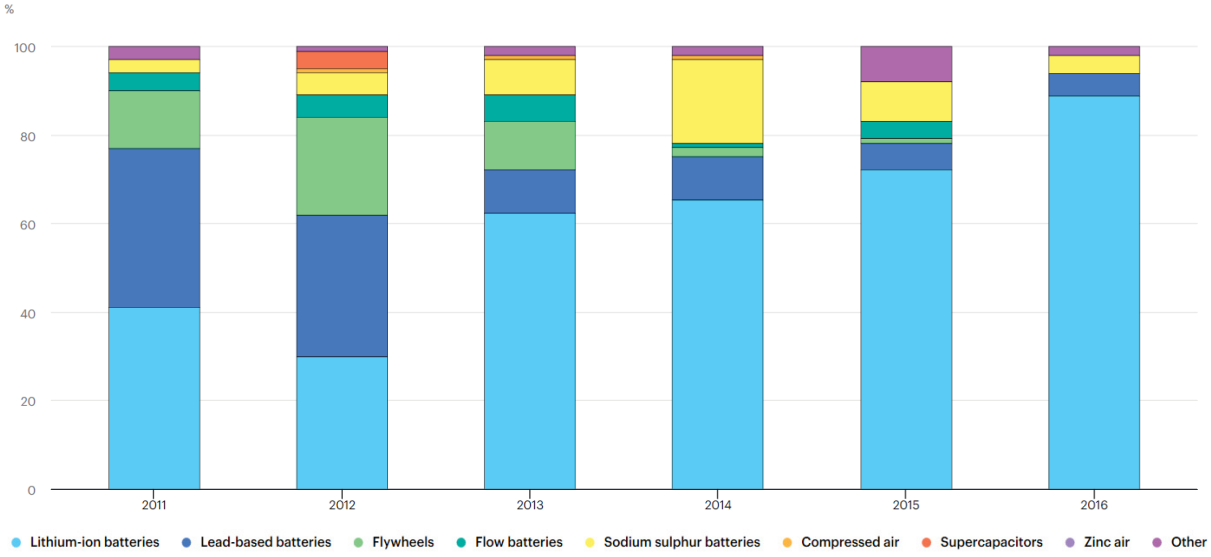

SOURCE: IEA (2019).

The growth of battery systems use is related to the cost reduction and technologies improvement, with new chemistries and more application possibilities (PALIZBAN; KAUHANIEMI, 2016).

The main advantage of battery systems is the multiple options of operation, being able to provide power quality improvement by mitigating voltage deviation, suppling frequency regulation, improving the grid operation quality and, in addition these systems can change the charge and discharge period in order to realize load shifting, load leveling and peak shaving, contributing with the load management of the feeder (DAS et al., 2018).

In this way, the present work aims to analyze how mainly electrical aspects of distribution systems are affected by the insertion of distributed generation and battery energy storage systems. The electrical aspects considered are voltage profile, losses, number of taps changes by the voltage regulator located at substation, voltage stability index and power flow directions.

Moreover, the planning of distribution system operation will be evaluated using a multi-period optimum power flow (MPOFP) formulation to define network control actions and battery charging and discharging behavior considering different compositions of the grid and the elements inserted on it.

1.2 OBJECTIVES

The main objectives of the present work are to analyze how the main electrical aspects are affected by the insertion of distributed generation and battery energy storage systems at distribution feeders as well analize the optimum planning of distribution grid operation, looking for a day ahead scenario, also considering the operation of photovoltaic and battery systems.

With the aim to reach the main objective of the work, some specific objectives were defined:

- Define how to evaluate the performance of a distribution system considering conventional infrastructure with and without insertion of distributed generation and battery system;
- Compare the grid operation behavior ex-ante and ex-post the insertion of distributed generation and battery connection, evaluating how each one of the new grid elements can impact the operation planning based on different scenarios;
- Insert a battery model in a multi-period optimum power flow to operate the distribution system along with a day-ahead dispatch;

- Develop a complete grid modeling at the multi-period optimum power flow;
- Consider the placement of the battery system in different points along the distribution feeder, sighting how the location of the storage system can impact the operation based on different scenarios.

1.3 JUSTIFICATIVE

According to the forecasts for grid evolution in the future, as shown before, it is possible to verify the necessity to study and evaluate the grid planning and operation, considering the insertion of new elements for different grid behaviors. Moreover, it is important to monitor the operation of equipment that is already installed on the grid, and how they are affected by the distributed generation and the battery system.

Most of the time the distributed generation is composed of the renewable energy systems, placed at consumer's houses. As this system generation changes according to weather behavior, it is possible to make a prediction of the energy generation in a day-ahead horizon, considering the weather forecast. Nowadays, the technics used to estimate the weather forecast are very trustworthy, presenting reliability of 98% (INPE, 2019). In this way, it is possible to use this information to estimate the generation for photovoltaic and also wind systems. The energy generated, in these cases, are firstly used to supply the consumer's demand, being the surplus provided to the distribution system, once the systems considered do not present storage.

On the other hand, the operation of the battery energy storage system is done by the power utility, once it is installed by them to improve the grid operation. In real cases, the DSOs integrates the BESS management systems to the Distribution Management Systems (DMS), usually integrated into the Supervisory Control and Data Acquisition (SCADA) system. It is relevant, therefore, to have the planning of load demand and generation considering the day-ahead predictions.

In this way, a multi-period optimum power flow simulation was developed, using the classical formulation of interior points method, as proposed by Borges, Fernandes, and Almeida (2011), considering the insertion of photovoltaic generation and battery energy storage systems at the distribution network, looking for a day-ahead

forecast. In the same system voltage regulator, capacitor banks, transformer, and other grid equipment were modeled, and their operation was also considered.

The use of the optimum power flow at the distribution system operation planning will provide a solution looking at a day-ahead time horizon and these results can contribute to the real-time simulations, providing a better starting point for the problem solution and reducing the making decision time.

1.4 STRUCTURE OF THE DISSERTATION

The present work presents in chapter 2 the theoretical foundation of the work, detailing the information about active distribution networks, voltage regulators, capacitor banks, photovoltaic systems, and energy storage systems, explaining their concepts and operation with the power grid. In chapter 3 the literature review is presented, showing the papers used to base the proposed work. In chapter 4 the tools for distribution system planning are explained, in this case, the power flow and the optimum power flow, being detailed the extended formulation proposed to insert the battery behavior at multi-period optimum power flow. In chapter 5, the scenarios to be simulated are defined as well the results from different power flow grid configurations and the impacts of new elements into the power grid are evaluated. In chapter 6, the extended multi-period optimum power flow system configuration is detailed as well as the results obtained for different simulations are presented and discussed. In the end, chapter 7 presents the main conclusions obtained from work development and the suggestions for future works.

2 THEORETICAL BASIS

In this chapter the main concepts of active distribution networks and the elements considered for the modeling of this grid will be detailed, explaining their main functionalities and characteristics.

2.1 ACTIVE DISTRIBUTION NETWORK

The growth of electricity demand and the connection of renewable energy resources are changing the distribution systems. Moreover, new elements as electric vehicles and also storage systems are making changes in grid operation and planning. Also, the evolution of control strategies associated with new monitoring and communication systems are providing the possibility to manage all these resources together. For the DSOs the challenges are increasing significantly, once they need to control, operate and integrate all these systems together, inside of the network under their responsibility. In this way, the concept of Active Distribution Network (ADN) can be defined as distribution systems that have systems in place to coordinate and control distributed energy resources (DER), for example, distributed generation, energy storage, electric vehicles and controllable loads, as an example shown at FIGURE 6 (CIGRE, 2014).

FIGURE 6 - ACTIVE DISTRIBUTION NETWORK ARCHITECTURE.

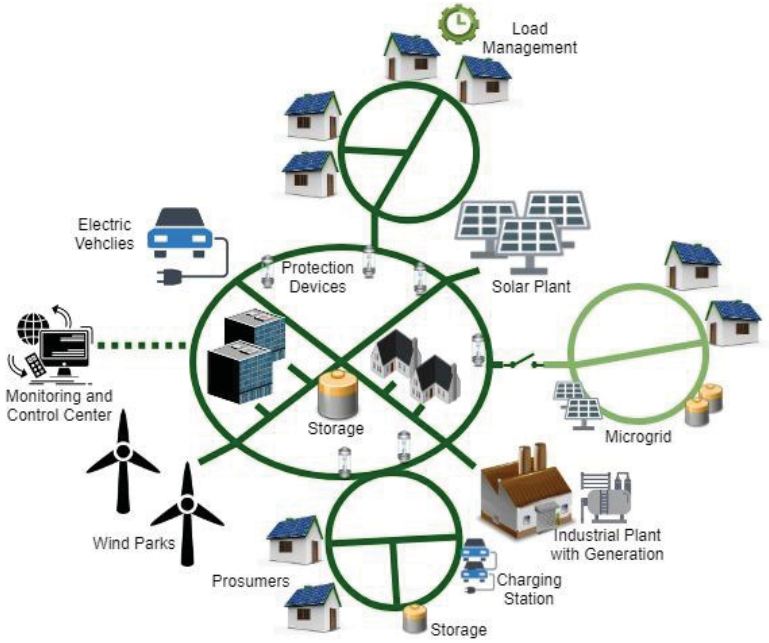

SOURCE: Adapted from Silva (2016).

The work developed by D'Adamo et al. (2009) highlights the main features of active distribution networks, as shown in TABLE 1. As presented by the author, the ADN have an important management system, able to coordinate the operation of the elements contributing to improve the power grid, providing power flow management and DG and load control, for example. Moreover, to perform this control some specifications are required, as protection systems and communication infrastructure, as well the in order to guarantee the maintenance of the grid reliability.

TABLE 1 - ACTIVE DISTRIBUTION NETWORKS MAIN FEATURES.

Functionalities	Specifications	Driver / Benefit
• DG and Load Control • Fast grid reconfiguration • Voltage Management • Power flow congestion management • Data collection and management	• Integration with existing systems • Communication • Protection • Flexible network topology	• Improve access for DG • Improve reliability • Network stability • Alternative to network reinforcement • Increase asset utilization

SOURCE: Adapted from D'Adamo et al. (2009).

Intelligent control strategies have been applied in ADN in order to allow the DSOs to keep the operation objectives, what means voltage and frequency levels, even in this new context. The typical controls are voltage and frequency control, congestion management and loss minimization, which operate together within a coordinated way. Nowadays the voltage control in ADN consists of adjusts of tap position of on-load tap changer (OLTC). For the future, the voltage control can have the participation of smart metering data acquisition and also partial household load controls, via consumer's equipment (CIGRE, 2011).

About the communication aspect, there are a lot of new studies about how to provide a safety communication, with high-speed and full integration to the power grid. To have access to data information is needed to improve the sensor technologies that will provide power grid information, in terms to evaluate the equipment health, the integrity of the grid and protection devices operation (IEEE, 2013).

The ADN infrastructure is more complex than the one that exists nowadays at distribution systems, even so, the reliability and power quality needed to be kept. The limits of SAIDI (System Average Interruption Duration Index), SAIFI (System Average

Interruption Frequency Index), CAIDI (Customer Average Interruption Duration Index) and CAIFI (Customer Average Interruption Frequency Index) defined for the DSO do not change with the insertion of new elements into the power grid (CIGRE, 2011). In this way, the DSO needs to invest in new solutions to keep the satisfactory grid operation. Thus DG, load management and storage system can operate in order to support the grid providing ancillary services and contributing to the flexibility of the system. Besides that, the DSO can use protection equipment communication and control to isolate some area, or even develop new possibilities of self-healing strategies including the support of new elements (HALLBERG, 2013).

Some of the equipment and techniques that enable the ADN operation are described in TABLE 2, which explains the application of the technology and also the main benefits that its use can provide to the power grid.

So, the ADN incorporates the operation of traditional grid elements as voltage regulators and capacitor banks with also the insertion of the active elements, as DG, storage systems and load management. These elements will be detailed in the next chapters of this work.

TABLE 2 - ACTIVE DISTRIBUTION NETWORKS ENABLING TECHNOLOGIES.

Enabling Technologies	Application	Benefits
Power Electronics at Distribution Network	Power Control (Active and Reactive Power)	• Increased power transfer • Grid stability
Intelligent Devices and Communication Systems	Information and Communication Technologies (ICT)	• Distribution system management • Network information collection • Coordination and control of new and existing elements
Advanced Metering Infrastructure (AMI)	Demand-side management (considering the variable pricing)	• Reduce consumer costs • Peak Shaving • Peak shifting
Advanced Protection Devices	ADN management with high DG penetration	• Increase of DG penetration • Grid reliability and power quality • Sensitivity and selectivity with communication-based protection
Energy Storage System (ESS)	Islanding, load peak shaving, integration of intermittent generation	• Increase DG integration • Peak Shaving • Islanding capability
Distributed Power Interconnection and Control Interface	Power quality control	• Islanding capability
Automatic Voltage Control	Voltage regulation	• Facilitates the increase of DG • Avoid voltage rise on networks

Demand Side Management (DSM)	Load reduction, load shifting, price responsive, load control	• Frequency control • Reduce consumers cost • Avoid grid reinforcement • Peak Shaving

SOURCE: Adapted from CIGRE (2011).

2.2 VOLTAGE REGULATOR

Voltage regulator (VR) is a passive equipment developed to keep the voltage value inside of the limits defined for the distribution network. Most of the time the VR is placed close to the end of the feeder and or places with high load levels, since in these points the voltage levels tends to be lower. In Brazil, the voltage levels for distribution networks are defined by ANEEL at PRODIST Module 8 and present the bands shown in TABLE 3.

TABLE 3 - CLASSIFICATION OF VOLTAGE LEVELS.

$\mathbf{0.93 \leq V \leq 1.05\ pu}$	Adequate
$\mathbf{0.90 \leq V < 0.93\ pu}$	Precarious
$\mathbf{V < 0.9\ or\ V > 1.05\ pu}$	Critical

SOURCE: ANEEL (2018b).

The voltage levels need to be maintained even with the connection of DG systems, in order that, if the DG operates out of the predefined range of voltage, it must be disconnected from the main grid (ANEEL, 2018b). This process is called the mandatory disconnection of the DG units and the operating voltage range and time of disconnection changes according to the DSO. It is important to highlight that the disconnection of the DG must happen if the voltage of the grid or of the DG system violates the established limits in the point of the common coupling (COLOMBARI et al., 2019). Some examples of under-voltage operation limits and times for disconnections are presented at TABLE 4 based on DSOs regulation. It is possible to visualize that the most restrictive in voltage levels are more flexible in time, and the opposite is also valid. Considering the overvoltage values, most of the DSO adopted the supportability of 1.1 pu during at maximum 0.2 s.

TABLE 4 - MANDATORY DISCONNECTION LEVELS FOR DISTRIBUTED GENERATION IN DIFFERENT DSOs.

Voltage at the Point of Common Coupling	Maximum Time for DG Disconnection	Distribution System Operator (DSO)
V < 0.8 pu	0.2 s	ELEKTRO
	0.4 s	CEMIG, Light, Cocel, Energisa, Eletropaulo
V < 0.85 pu	1.0 s	Celesc
V < 0.95 pu	2.0 s	Copel

SOURCE: Adapted from Celesc (2018) CEMIG (2012), Cocel (2017), Copel (2016), ELEKTRO (2017), Eletropaulo (2018), Energisa MT (2016) and Light (2018).

In order to keep the voltage levels of the grid and avoid the disconnection of the DG systems, and moreover prevent the voltage collapse on the power grid, voltage regulators can be connected at the distribution systems.

The VR consists of an autotransformer that usually presents 32 different tap positions, allowing to increase or decrease the voltage level around +/- 10%. Each tap position corresponds to a different winding ratio. For equipment placed in the middle of the feeder, the tap position is defined in the configuration fit-and-forget, which is a fixed tap position, defined according to previous studies and measurements in the point of connection. In this case, the VR actuated to increase or reduce the voltage in a defined point at the feeder, changing the voltage level downstream to fit into the limits. FIGURE 7 shows the line voltage regulator (LVR) behavior. The equipment is placed in the middle of the line and in the case (a), the voltage intends to be higher, once there are DER generating, so, the LVR will reduce the voltage level, keeping inside of the acceptable limits. Hence, in (b) is possible to verify the operation when the voltage tends to reduce since there are only loads in the circuit. So, for this case, the LVR will increase the voltage level (HOLT; GROSSE_HOLZ; REHTANZ, 2018).

FIGURE 7 - VOLTAGE REGULATOR ACTUATION FOR REDUCE THE VOLTAGE (a) AND TO INCREASE THE VOLTAGE LEVEL (b).

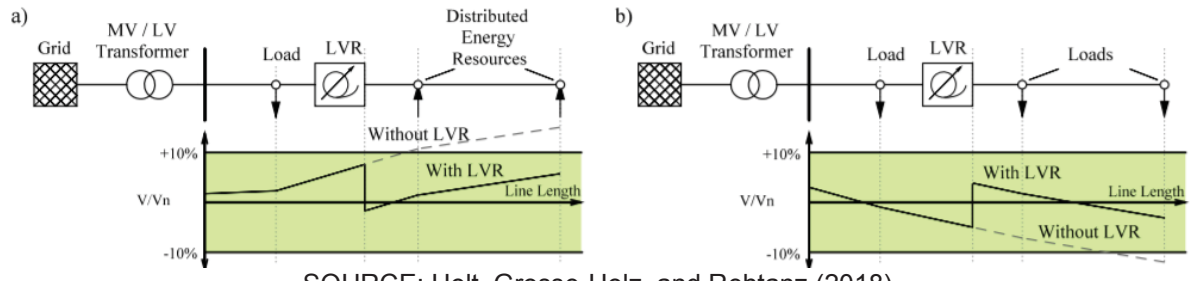

SOURCE: Holt, Grosse-Holz, and Rehtanz (2018).

At the substation, it is interesting to install an OLTC (FIGURE 8), which consists of equipment able to change the tap position during the system operation and in an automatic way, based on online grid measurements. The tap change happens with the connection of a reactor to avoid power interruptions into the power grid during the tap change process, and also contributing to extend the lifetime of the contactors, once it limited the current (BURATTI, 2016). The behavior of OLTC operation into the grid is the same that the one of a voltage regulator, with the difference that, in this case, the equipment can change the tap while it is connected at the power circuit.

FIGURE 8 - EXAMPLE OF OLTC INTERNAL CIRCUIT.

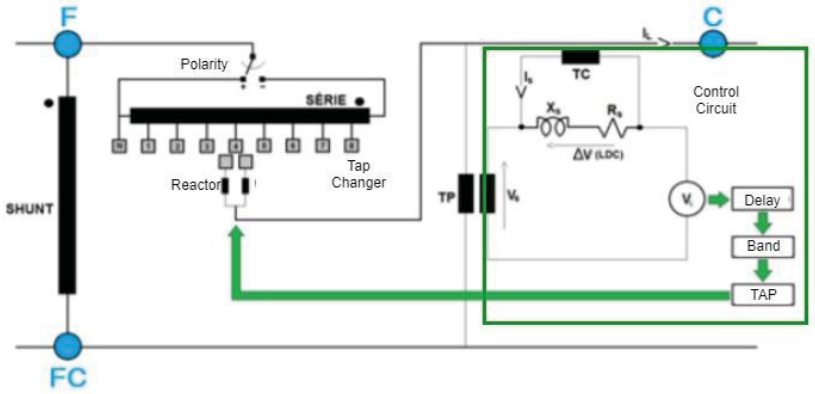

SOURCE: Adapted from Buratti (2016).

In a circuit with a high penetration of distributed generation sources, the voltage regulator can operate in different control modes in order to ensure safe and reliable operation. There are different operation modes, being bi-directional, reactive bi-directional and co-generation modes the most common. These modes defined which voltage will be controlled, according to the power flow direction, as illustrated in FIGURE 9 (SHIREK, 2014).

FIGURE 9 - POSSIBLE VOLTAGE REGULATOR OPERATION MODES.

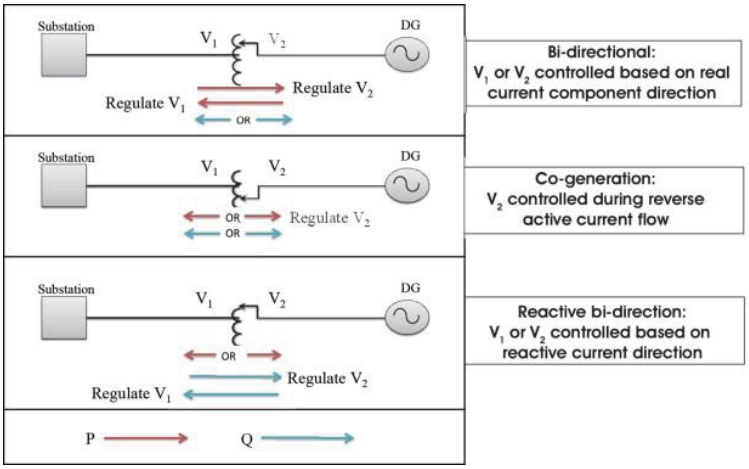

SOURCE: SHIREK (2014).

2.3 CAPACITOR BANK

The capacitor bank is an element able to inject reactive power into the power grid, bestowing to reactive power compensation, improving voltage regulation and power factor correction, allowing the increase of transmission line flow of energy and also contributing to the reduction of the power losses (MASOUM; FUCHS, 2015).

Capacitor banks could be fixed, being connected to the grid during all time, or automatics, being connected and disconnected to the power grid according to the operation necessity. Define the best capacitor bank allocation into the distribution system is a big challenge. For this, a lot of studies have been developed using different optimization techniques as nonlinear programming and artificial intelligence.

2.4 PHOTOVOLTAIC SYSTEMS

Distributed energy generation is mostly composed of photovoltaic (PV) systems. As known, the PV systems are capable to transform the sun irradiation into electricity, due to the semiconductor thin layers that compose the photovoltaic cells. The cells present around 13 cm in square sizes and the material that composes the cell will define the technology of the equipment, being the most common the mono or polycrystal usually made with silicon (97% of the cells production), or a more recent technology that is thin-films made from amorphous silicon or nonsilicon materials. To increase the power output of the cells, they are connected in order to build a PV module, typically between 50 W and 400 W. Those modules can also be connected in

series or in parallel to improve the output voltage and current, being this arrange named PV system (IEA-PVPS, 2018).

The output of a PV module is given in direct current (DC), so it is required to install an inverter, providing alternating current (AC) to the grid or to the load in which the PV system is connected. The inverters present different output power capacities, since few kW values to hundreds of kW. In terms of connection configuration, the inverters can be connected to one or more strings of PV modules or can consist of a central inverter, presenting, in this case, a higher power output. In addition to performing the power conversion, the inverters have different functions for the PV generation systems as (PORTAL SOLAR, 2020):

- low-loss conversion, that consists of the present a high efficiency during the conversion process (efficiency over 90%);
- inverter present a self-consumption around of 2% of the nominal power;
- power optimization, finding the optimum operating point for the PV system, being this point called Maximum Power Point (MPP);
- monitoring and security, in case of a problem in the power grid the system must be disconnected from the main grid or must support the grid during the contingency, being this decision taken by the grid operator;
- communication interface, allowing control and monitoring the PV generation, being the data sent using different possible interfaces as a network connection, RS485 Fieldbus or even wireless communication;
- temperature management, allowing to keep the conversion efficiency even in low temperatures (PORTAL SOLAR, 2020; SHARENERGY, 2020; SMA, 2019).

Before installing a PV system it is necessary to check if the equipment is certified following the international standards IEC 61215:2005, IEC 61730-2:2004, IEC 61701:2011 for PV modules and IEC 61683:1999, IEC 62109-1, IEC 62116 and IEC 62446 for PV system inverters (SALAS et al., 2011). In Brazil, the equipment must follow international standards and in addition the Inmetro (Brazilian National Institute of Metrology Standardization and Industrial Quality) Standards 004/2011 and 357/2014, allowing the equipment to be certificated by the Brazilian Energy Efficiency

Program (PBE). Nowadays, the PBE homologate 857 PV modules and 95 inverters for PV applications, from different manufacturers.

The output power of each PV module changes according to the environmental irradiation and temperature. Looking for the world atlas presented in FIGURE 10, it is possible to visualize the regions with the highest daily and annual irradiation.

Even with more radiation levels than European countries, Brazil does not present so many PV systems like Germany, Spain, France and also China. This happens because those countries presented government subsidies mainly related to incentives to change the electricity matrix, replacing fossil generators for clean energy. In the Brazilian case, around 74% of the electricity matrix is composed of renewable sources, is 64% of hydropower generation, 9% of wind power and 1% of photovoltaic systems (ANEEL, 2019b).

FIGURE 10 - WORLD RADIATION MAP.

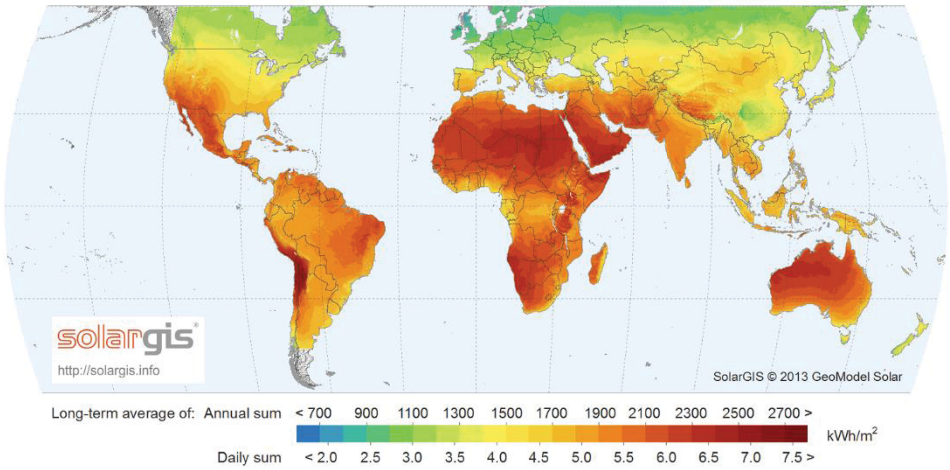

SOURCE: Solargis (2013).

A photovoltaic system can be installed in two different ways: grid-connected or off-grid. The grid-connected installation could be in a centralized way, working as a generation center and usually presenting ground-mounted PV panels, or in a decentralized way, being in this case associated with a consumer installation. For off-grid PV systems, a storage system is required to allow the power supply during no-light periods, being most of the time used lead-acid batteries. Moreover, a charge controller is needed to control the storage charge and discharge operation (IEA-PVPS, 2018).

The photovoltaic systems are increasing significantly worldwide. This growth is related to economies of scaled manufacturing, technologies improvements,

innovations and supporting in financial investments. The biggest amount of PV module manufactures is placed in Asia Countries, concentrating around of 84.8% of the production, being 3.1% in Europe and 3.7% in the USA and Canada. Looking for the learning rate shown in FIGURE 11 it is possible to verify the module price behavior during the last years, which presents a reduction of 24% in 38 years. The module price is shown considering all the PV technologies available and also the cumulative production worldwide (BURGER et al., 2018). In Brazil, there are also some initiatives to improve photovoltaic cell production in the country, as actions led by ANEEL, BNDES (National Development Bank) and FINEP (Research and Innovation Funder), that contributes to reduce the costs or even providing more financing options to the next installations.

FIGURE 11 - LEARNING RATE OF PV MODULE OF COST EVOLUTION.

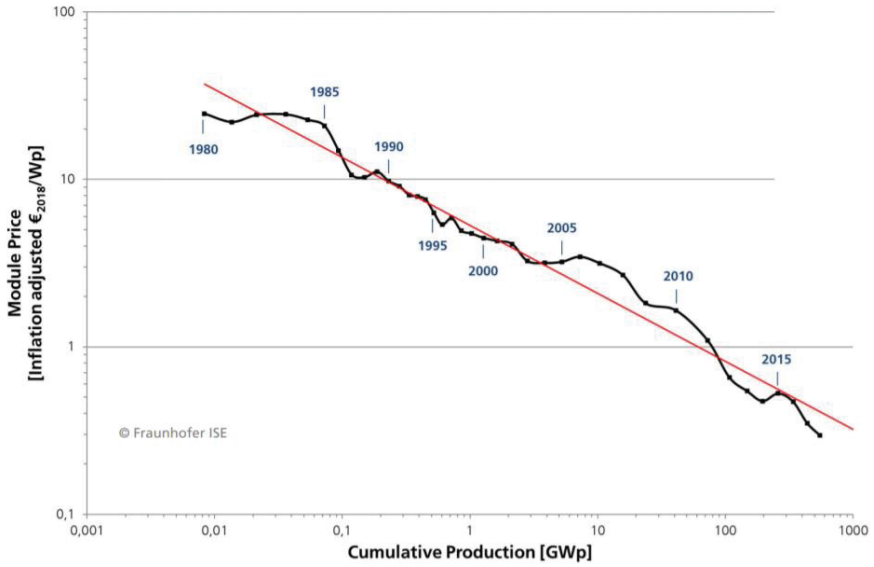

SOURCE: Burger et al. (2018).

A great amount of these systems is being connected to the distribution systems, as in Germany that will present 80% of the solar photovoltaic generation interconnected to the distribution network in 2020. In this way, the high penetration of PV generation requires that utilities study the grid balancing and control, the interaction between PV and grid equipment and moreover, the forecasting of PV generation, based on meteorology behavior, for load balancing (HUDSON; HEILSCHER, 2012).

2.5 ENERGY STORAGE SYSTEMS

There are different types of energy storage systems (ESS) applied to power systems, as supercapacitors, flywheels, compressed air energy storage systems (CAES), pumped hydro, batteries and others that could be characterized according to how the energy is stored (FIGURE 12). The definition of the most appropriate ESS depends on different factors like the lifetime, power, and energy relation, self-discharge rate, cycling efficiency, environmental impact, technology maturity, cost of investment and others as market availability (BEAUDIN et al., 2010).

The ESS could present large (GW), medium (MW) or small (kW) scale application according to the function and location, being in all cases composed by a grid interface, control, and communication system that will be responsible to define the charge and discharge behavior, and the storage element, that consists in a system able to convert electricity into another form of energy to be stored.

FIGURE 12 - ENERGY STORAGE TECHNOLOGIES.

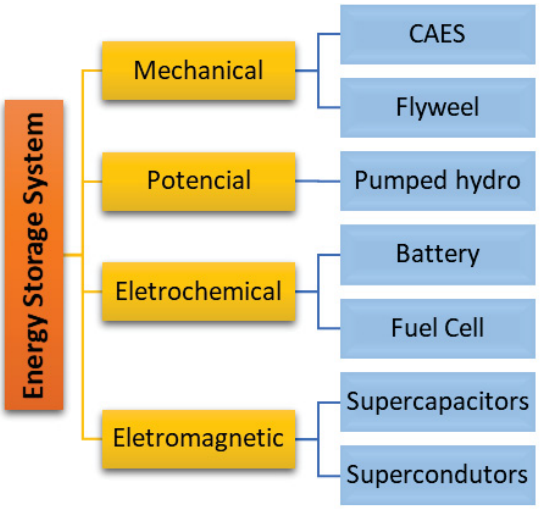

SOURCE: Adapted from McDowall (2018).

Compressed Air Energy Storage System (CAES) consists of a large underground site, as a salt cave or a rock cavern, in which air is storage with high pressure. During the moments with low demand on the power system, the compressors and turbines will store air into the cave. When the demand is higher, the stored pressured air will pour through the turbines, generating power electricity to be provided to the power grid.

Nowadays there are only two CAES plants in operation in the world, one in McIntosh in the United States with 110 MW / 2.86 GWh, being able to provide power to the grid during 26 hours, and another in Huntorf, Germany with 290 MW / 580 MWh, being this one under operation since 1978 and in last years was integrated with wind power generation (MEYER, 2007). There are few plants implemented once these are large systems that demand high investments and also require a very specific location due to the cave necessity.

Pumped hydro consists of a storage system that uses potential energy, once it is based in two water reservoirs at different heights. When it is needed to store energy, the water is pumped from the lower reservoir to the upper one, by the way, that when it is required to provide power to the grid, the water flows from the upper to the down reservoir, working similar to a hydropower plant. The greatest amount of PHSs can be found in countries as Japan, China, and the United States according to the International Hydropower Association (2017).

It is important to highlight that the CAES and PHSs are systems that present a high capacity of energy storage, that is even with a low number of installed systems, they represent a large amount of installed capacity of storage energy around the world, as presented at FIGURE 5.

Flywheel consists of a motor with a high inertia moment, capable to store and provide energy very fast to the grid, once the energy is storage changing the rotational speed. This technology presents high efficiency and also a high live-cycle (around 15 to 20 years), but at the same time requires high investment costs and the technology still is being developed.

Superconductors and supercapacitors are technologies under development, based on the electro and magnetic effects respectively, to store energy. These systems do not yet present applications at power grid system operation.

Batteries and fuel cells are the technology based on a chemical process. Battery energy storage systems (BESS) are electrochemical elements capable to store energy from an oxi-reduction reaction and are the most common ESS, since it presents some benefits as large number of technologies available in the market, different sizes applications, high energy density, market gain over last years and high efficiency. Another good feature in batteries is that energy and power are decoupled, by the way, that it is possible to define the specific power and energy according to the application use.

As the present work focuses on the application of battery systems, the main characteristics of these systems will be explained in detail in subchapter 2.5.1.

BESS can be used for small scale application into the power grid, e.g. connected to prosumers installations, sized for the consumer demand supply (tens of kW and kWh), or even can be installed for large applications, close to power plants generations. Examples of large applications of battery systems can be seen at Australia, that presents five energy storage systems up to MW, being the largest one installed at Riverland with 100MW/400MWh lithium-ion BESS integrated to a solar power plant of 253MW in which the Transmission System Operator (TSO) planned to have a dispatchable solar power plant using the ESS (LYON GROUP, 2019a, 2019b).

The ESS can be used for different grid applications according to the location of the system in the power grid (FIGURE 13) and according to energy storage capacity. Battery energy storage systems are capable to cover a wide range of applications from short-term power quality to long-term energy management. The BESS can improve the grid reliability and moreover can contribute with bulk energy, ancillary services, customer energy management applications, and renewable energy integration.

Bulk energy application is related with energy arbitrage and peak shaving. Energy arbitrage consists of storage the electricity when the price is low and sell it when the price is high at peak times. Peak shaving presents a very similar behavior then energy arbitrage, with the difference that in this case there is not an economic target. Peak shaving is installed close to the consumer and it is done to improve the system, contributing to supporting the peak demand of the consumer without stress the entire feeder capacity (ADB, 2018).

The ancillary services consist of operation models that can contribute to grid operation as frequency regulation and voltage support, improving system reliability with black start and spinning reserve and also load-leveling service.

According to PRODIST Module 8, the frequency limits for the power grid in Brazil are defined between 59.9 and 60.1Hz, being acceptable variations just for small periods of time. The charge and discharge of the BESS can contribute to frequency regulation absorbing energy when the frequency is higher than the upper limit and providing energy when the frequency is lower than the lower limit. The BESS time of operation, in this case, can vary from 5 seconds to 30 minutes, according to the control strategy and the causes of frequency fluctuation (ADB, 2018).

FIGURE 13 - ENERGY STORAGE SYSTEM APPLICATIONS IN POWER SYSTEM.

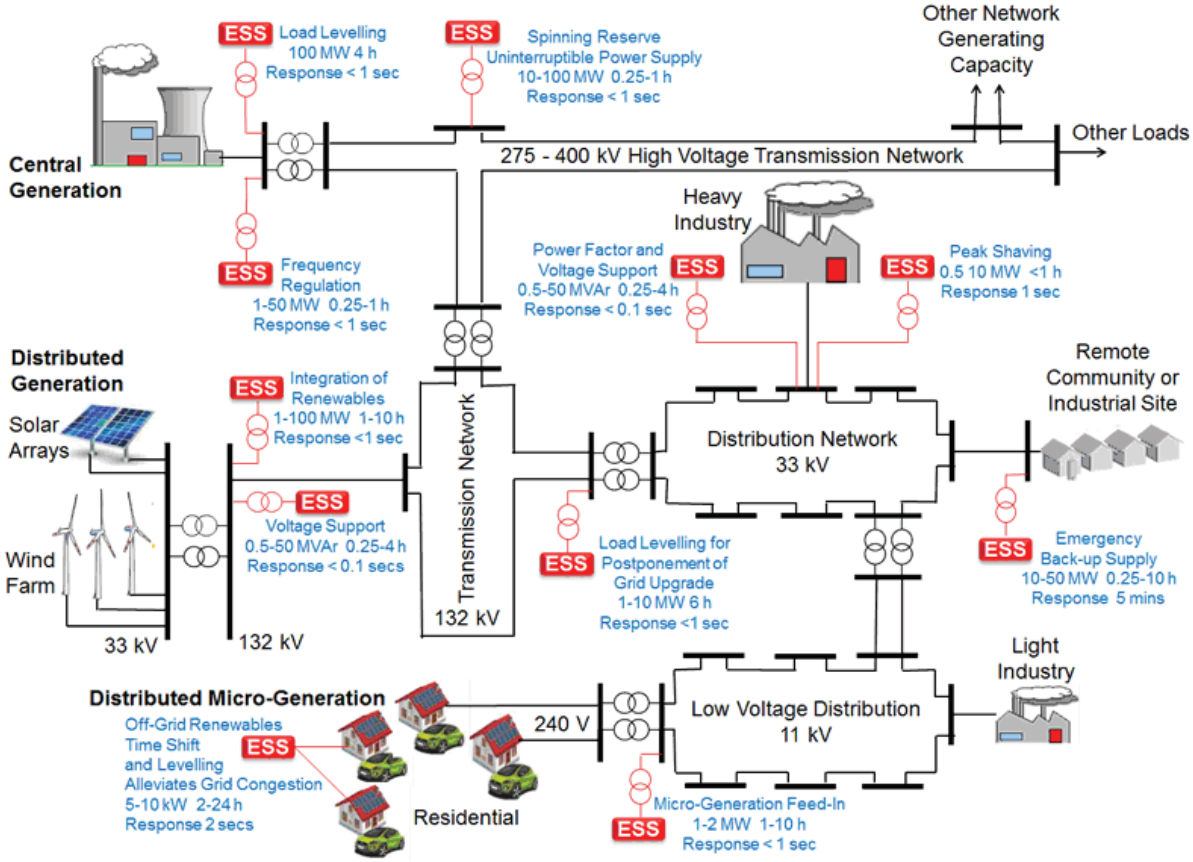

SOURCE: Woodbank Communications (2020).

For voltage support, the BESS need to actuate by controlling the power factor of the inverter, in order to provide more reactive power to the grid. In this case, the BESS will provide locally the voltage support, suppling more reactive power when the voltage levels are lower.

The restoring process after a blackout is called black start process and is not simple to be done, once it is necessary to get some power levels to start auxiliary's equipment and plants without pulling electricity from the grid. Moreover, for each part of the system is needed to know which should be the procedure to restart the grid operation. During this process is needed to take care of the synchronization aspects and the BESS can contribute to providing a controlled voltage and frequency as a black start source.

During the normal operation of the power system, there is a spinning reserve, mainly from rotating machines of generators connected to the system, consisting of a reserve of power that can be used to supply load changes or transmission lines failures. In this way, the BESS can operate as a reserve, being prepared to provide energy contributing to improving grid reliability (ADB, 2018).

Load leveling consists of stored energy in the moments when the load demand is lower, and provide energy when the demand is higher. This is similar to peak shaving but does not consider the discharge of the BESS only in peak time, but always when the load is higher than a pre-defined value. Load leveling application allows the postponement investments on grid updates or in generation expansions.

Looking for the power quality and reliability of the power system, BESS can be used for customer energy management applications.

The BESS can contribute to keeping voltage and frequency levels, as explained before, but moreover, it can contribute to improve power quality, mitigating harmonics and voltage distortion, and can protect downstream load against short-duration events. In the same way, the BESS can contribute to improving power reliability, providing power for downstream loads in case of a system blackout. It is important to highlight that in this case, it is necessary to have a coordinated protection and control system, capable to isolate part of the system and reconnect after the fault.

The intermittency of renewable energy generation reflected in fluctuations in the output power of solar and wind generation. The BESS can smooth the output variation and contribute to control the ramp, mitigating power and voltage and frequency swings. This application is known as capacity, voltage and frequency firming respectively. This supportability on power grid quality levels can be provided by active and reactive control, requiring a time of responde in seconds or even less time, in order to compensate the renewables intermittence effects. In the case of off-grid systems with renewable energy sources, the BESS is required to provide consumers electricity during no-generation periods, which is essential in these cases (PALIZBAN; KAUHANIEMI, 2016).

All these possibilities of battery applications cannot be defined for the same equipment, once different application requires different sizing of power and energy for the battery systems, is defined according to the time response required for each application, as illustrated in FIGURE 14.

FIGURE 14 - APPLICATIONS TIME RESPONSE.

Seconds or Less	Minuts	Hours
Flicker Effect Compensation	Black Start Blackouts Reserve for frequency control	Load Leveling Load Shaving Intermitent Energy Resources Island Operation

SOURCE: Adapted from Hayes (2012).

Projects for BESS insertion into the power grid nowadays present more viability than some years ago. First, because the results of some applications are getting more relevance and also the batteries' prices are getting lower. Second, because the technology is becoming more consolidated, reducing the price of the technology, being this the main reason why lead-acid batteries presents, now and in the close future, the lowest cost of energy, as it is shown at FIGURE 15. In this graphic, it is possible to compare the installation costs of different batteries technologies, showing the $/kWh in 2016 and a forecast in 2030. In the graphic, it is also shown, in the bottom part, the prediction of cost reduction percentages.

FIGURE 15 - INSTALLATION PRICE OF ENERGY FOR DIFFERENT BATTERY ENERGY STORAGE SYSTEMS.

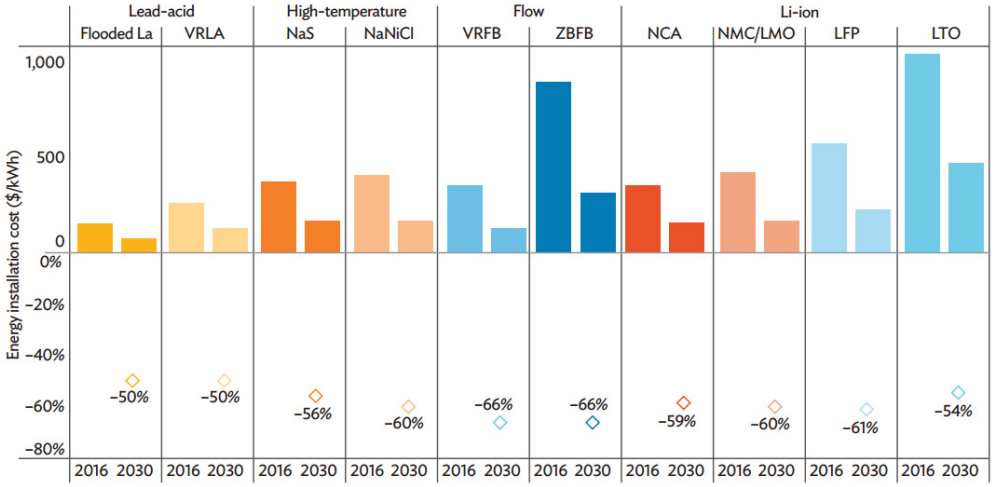

SOURCE: ADB (2018).

2.5.1 Battery Energy Storage Systems Characteristics

In 1800, Alexandre Volta created the first electric battery and since then the evolution of this system grows exponentially. The battery systems present a lot of terminologies and definitions that will be explained in the present chapter, allowing a better understanding of these systems' behavior.

Batteries can be defined as a group of voltage cells, that consist of the smallest electrochemical unit, responsible to deliver a voltage according to the chemical composition defined to build it. When cells are connected in series, the voltage values of each cell are summed and when are connected in parallel the voltage is kept the same and the currents are summed, improving the current capacity of the entire system. Each battery technology presents a specific energy density, that corresponds to the amount of energy that can be stored per weight (Wh/kg) or volume (Wh/l or Wh/m³) unit.

There are different battery technologies, which use different chemical combinations for the building of the cells, being the most common:

- lead-acid: that was the first one to be used in grid applications, consists of a positive and negative electrode with sulfur-acid as the electrolyte. The structure could be flooded, or valve regulated (VRLA), and one of the disadvantages is that presents a memory effect and self-discharge (BATTERY UNIVERSITY, 2019a);
- nickel-cadmium: this battery presents one of the first technologies that does not require electrolyte maintenance. It presents high energy density, but have memory effect and low-efficiency, around 65% (BATTERY UNIVERSITY, 2019b);
- lithium-ion: it is the most recent technology, with a solid electrolyte, high energy density, and storage efficiency higher than 90%, low self-discharge rates and it is not affected by memory effect. This is one of the technologies with high growth of application possibilities, considering the market gain and the reduction of the costs (DIVYA; OSTERGAARD, 2009). Lithium-ion batteries are increasing their recognition due to the diversity of applications and for changing the use of electricity in different areas, resulting in the awarding of the Nobel Prize in Chemistry 2019 to its inventors: Akira Yoshino, Michael Stanley

Whittingham, John Bannister Goodenough (THE NOBEL PRIZE, 2019);

- flow batteries: it is a cross of a battery and a fuel cell. It presents two liquid electrolytes storage in barrels, and these fluids flow through a permissive membrane. The most common technology, in this case, is the redox-flow battery. One of the advantages of these batteries is the capacity to develop deep discharges without impact the life cycle. The disadvantages consist of high costs and the large size of the equipment (SUSCHEM, 2018).

At FIGURE 16 the energy densities for different batteries technologies are presented, being visible that the lithium technologies batteries (LTO, LFP, LMO) present much more capacity than other technologies, as lead-acid and nickel-cadmium, but also less than nickel manganese cobalt (NMC) and nickel cobalt aluminum (NCA) batteries.

The BESS is composed of the electrochemical components, corresponding to the battery cells responsible to store the energy, that has their operation manage and controlled system named Battery Management System (BMS) (HATZIARGYRIOU, 2018).

FIGURE 16 - ENERGY DENSITY FOR DIFFERENT BATTERIES TECHNOLOGIES.

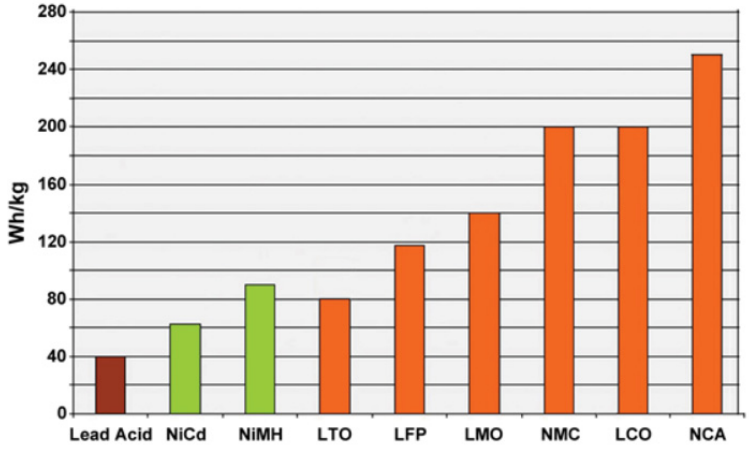

SOURCE: Battery University (2019b).

FIGURE 17, illustrates the integration of the BESS with the power system, considering the control and hardware layers. At the control level, the utility system supervisory control (SCADA) communicate with system control algorithms that will be

responsible to make the decision about the BESS operation, providing information to the inverter control system and the BMS, the latter being responsible for managing the operation of the battery cells, considering the operating and safety limits. As the BMS is responsible to define the operation of the storage part of the system, there is also the local control to the system inverter, which is responsible to manage the power factor relation, as well the voltage and frequency levels. All the control system algorithms are feed with signal measures in the point of connection with the main grid, allowing to take new decisions. All this structure is enclosure inside of a container or a specific structure, that is designed to protect the equipment of environmental conditions and contributes to providing the best grid system operation (MCDOWALL, 2018).

FIGURE 17 - EXAMPLE OF BATTERY ENERGY STORAGE SYSTEM INTEGRATION TO POWER SYSTEM.

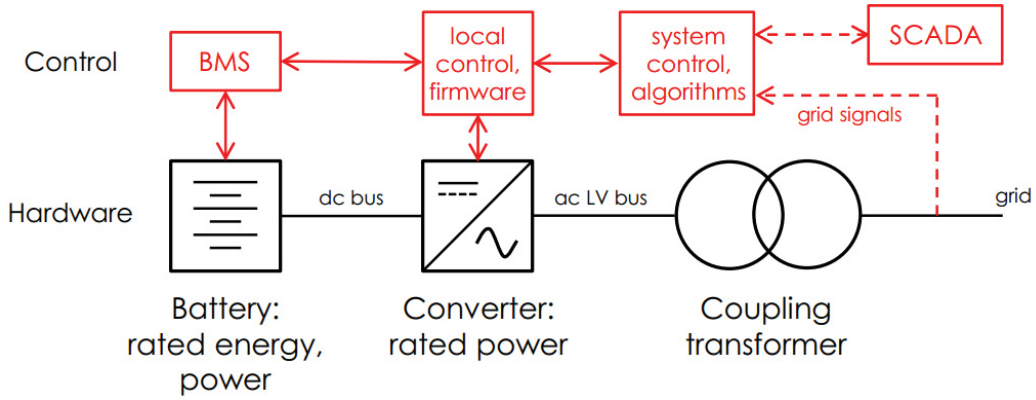

Source: McDowall (2018).

The battery system inverter most of the time are able to operate in the four-quadrant configuration, being able to provide the most different levels of active or reactive power to the system during the charge and discharge process (FIGURE 18) (RHOLDEN; CEBALLOS, 2018).

FIGURE 18 - FOUR-QUADRANT INVERTER MODELS OF OPERATION.

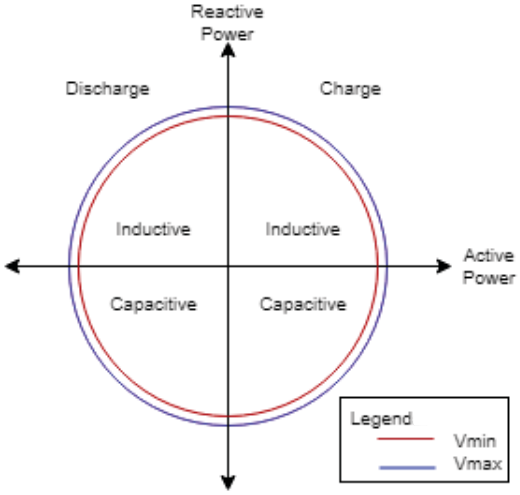

SOURCE: Adapted from Rholden and Ceballos (2018).

Part of the BMS responsibilities is related to monitor the State of Charge (SOC) of the battery cells, which corresponds to the amount of power that yet remains from the full battery capacity. The SOC level must respect the Depth-of-Discharge (DoD) level defined to the battery operation, which corresponds to the maximum that the battery can be discharged (e.g. when the battery presents a DoD of 70% it corresponds to reach a SOC of 30%). The DoD is defined according to with the battery application and also with the expected life-cycling for the systems, once as much higher the DoD, lower are the lifetime of the system, as shown at TABLE 5 for nickel manganese cobalt and lithium-ion phosphate batteries (BATTERY UNIVERSITY, 2019c).

Another important parameter related to the battery systems is the Capacity rates (C-rates), that correspond to the BESS performance, once represents the maximum amount of current that can be charged or discharged from the battery, related to the battery defined Capacity (C) in Ah. If a battery with a nominal capacity of 2 Ah operates with 1C-rate, it means that the system will operate with a current of 2 A for one hour to completely discharge the battery. By the way that, if the maximum rate of the system is a 5C-rate, it means that the maximum discharge current to operate in safety conditions is 10 A and the system will take 12 minutes to be completely discharged (RODGERS, 2019). The information about the battery capacity and the possible C-rates are presented by the batteries manufactures in the datasheets.

TABLE 5 - LIFE CYCLING ACCORDING WITH DEPTH-OF-DISCHARGE AT 1C-RATE.

Depth-of-Discharge	Discharge cycles	
	NMC	$LiPO_4$
100% DoD	~ 300	~ 600
80% DoD	~ 400	~ 900
60% DoD	~ 600	~ 1500
40% DoD	~ 1000	~ 3000
20% DoD	~ 2000	~ 9000
10% DoD	~ 6000	~ 15000

Source: Battery University (2019c).

The IEEE Standard 2030.3-2016 titled IEEE Standard Test Procedures for Electric Energy Storage Equipment and Systems for Electric Power System Applications presents the test items and procedures related to ESS applications, providing information about the test type, production test, installation evaluation, commissioning test at the site and periodic tests instructions. Another document that provides information about tests of ESS operation at power grids is from EPRI on the technical update 3002011739 – Energy Storage Integration Council (ESIC) Energy Storage Test Manual, defined to support the definition of performance and functional tests of the ESS.

Battery degradation is important information about the system since it is possible to define the lifecycle of the system. However, battery degradation depends mainly on system application and therefore on SOC, DoD, temperature and C-rates of operating conditions (SUFYAN et al., 2019).

Battery operation cost is dependent on the battery degradation cost, since each time that the system operates to charge or discharge, part of their capacity is lost, due to the chemical reaction.

According to Tazvinga, Zhu, and Xia (2015) proposed a degradation cost model ($cost_{degradation}$) defined by the relation of the cost of the battery bank, with the DoD in percentage, the number of cycles that the BESS can be developed with the DoD and the total energy storage capacity of the system ($Ebat$) given in kAh:

$$cost_{degradation} = \frac{cost_{BB}}{DoD.cycles.Ebat} \quad \left[\frac{R\$}{MWh}\right] \tag{2.1}$$

where:

$cost_{BB}$: cost of battery energy storage bank in brazillian reais;

$cycles$: number of cycles to failure.

In order to get the maximum payback of the investment to buy the system, the cost of degradation should be minimized, respecting the applications for which the system was developed.

It is important to highlight that the maintenance cost of the battery changes based on system chemistry, since batteries with liquid electrolyte as lead-acid, requires constant supervision and electrolyte level maintenance should be done frequently. On the other hand, technologies with a solid electrolyte, as lithium-ion batteries needs not often maintenance, being necessary only visual inspection of the construction aspects of the equipment, for example, is there are cracks or corrosion points (COPETTI; MACAGNAN, 2007; KEYSIGHT TECHNOLOGIES, 2017).

2.6 CHAPTER FINAL CONSIDERATIONS

The insertion of DERs into the power grid associated with load management is changing the distribution systems operation. This is not anymore, a challenge for the future, but is a reality in power systems around the world.

The placement of new elements, mainly renewable sources, insert uncertainty to the operation of the distribution systems, caused by the intermittency of the generation. At the same time, energy storage systems can contribute to reducing this intermittency being capable to provide capacity firming to the system.

To operate the system in a coordinated way it is required control, monitoring and communication systems capable to provide information in real-time to DSOs, allowing immediately responses of manageable systems. Moreover, the grid operator has the challenge to coordinate the operation of equipment that already exists into the power grid as voltage regulators and capacitor banks in conjunction with these new elements.

Voltage regulators and capacitor banks operate in order to contribute with power grid operation, improving voltage levels. Due to the insertion of DG and load management, the voltage profiles change more frequently into the grid. In this way, change the tap position of voltage regulators allocated along the distribution feeder can be required, by the way, that capacitor banks could be reallocated to improve the system operation.

The insertion of energy storage elements can also contribute to distribution system operation since these systems can provide different grid services. The sizing of these systems requires the specification of power and energy according to the application that the system will be used for.

Batteries are the most common ESS for power grid applications, being inserted into the grid by power utilities or even by consumers, in conjunction with the distributed generation systems or even with electrical vehicles. The operation of BESS can also increase power quality and grid reliability.

Considering the integration of all these equipment, the active distribution networks are requiring more and more studies and analysis about the grid operation, in order to guarantee the maintenance of reliability and safety levels, besides the minimum operational costs as well the reduction of greenhouse gases emissions.

3 LITERATURE REVIEW

The literature review bibliographic portfolio selection process is based on the methodology proposed by Ensslin et al. (2010).

The first step of the process consists in the definition of the keywords, based on articles that inspired the proposition of the present work. The keywords are divided according to the axis of research, that in this case consists of approach and application. Four different keywords were defined for each area, as presented in TABLE 6.

TABLE 6 - KEYWORDS DEFINITION.

Approach	Optimum Power Flow
	Optimization
	Storage Management
	Day-ahead Scheduling
Application	Renewable Energy
	Renewable Integration
	Battery Energy Storage
	Distribution System

SOURCE: The Author (2019).

The next step consists of a search for papers and works already developed related to the topic of this work. However, develop a search in the bibliographic portfolio is a challenge nowadays, mainly due to the facility to information access that provides a large number of results being not all of then relevant and trustworthy. In this way, the Publish or Perish software tool was chosen to assist in the searching process of the most relevant bibliographic portfolio.

Publish or Perish consists of a retriever and analysis citation software, that uses different databases like Google Scholar, based on combinations of keywords, and provide as a result of one list of citations, presenting at maximum one thousand works, being those the most relevant ones. The software also presents some metrics of the found articles, calculating the number of citations per year, citations per author, h-index[2] , and g-index[3] (FIGURE 19).

[2] h-index: it is an index to quantify an individual's scientific research.
[3] g-index: it is an index from an improvement of the h-index calculation, giving more weight to papers with more citations.

FIGURE 19 - PUBLISH OR PERISH INTERFACE WITH THE RESULTS FOR A SEARCH USING GOOGLE SCHOLAR DATABASE.

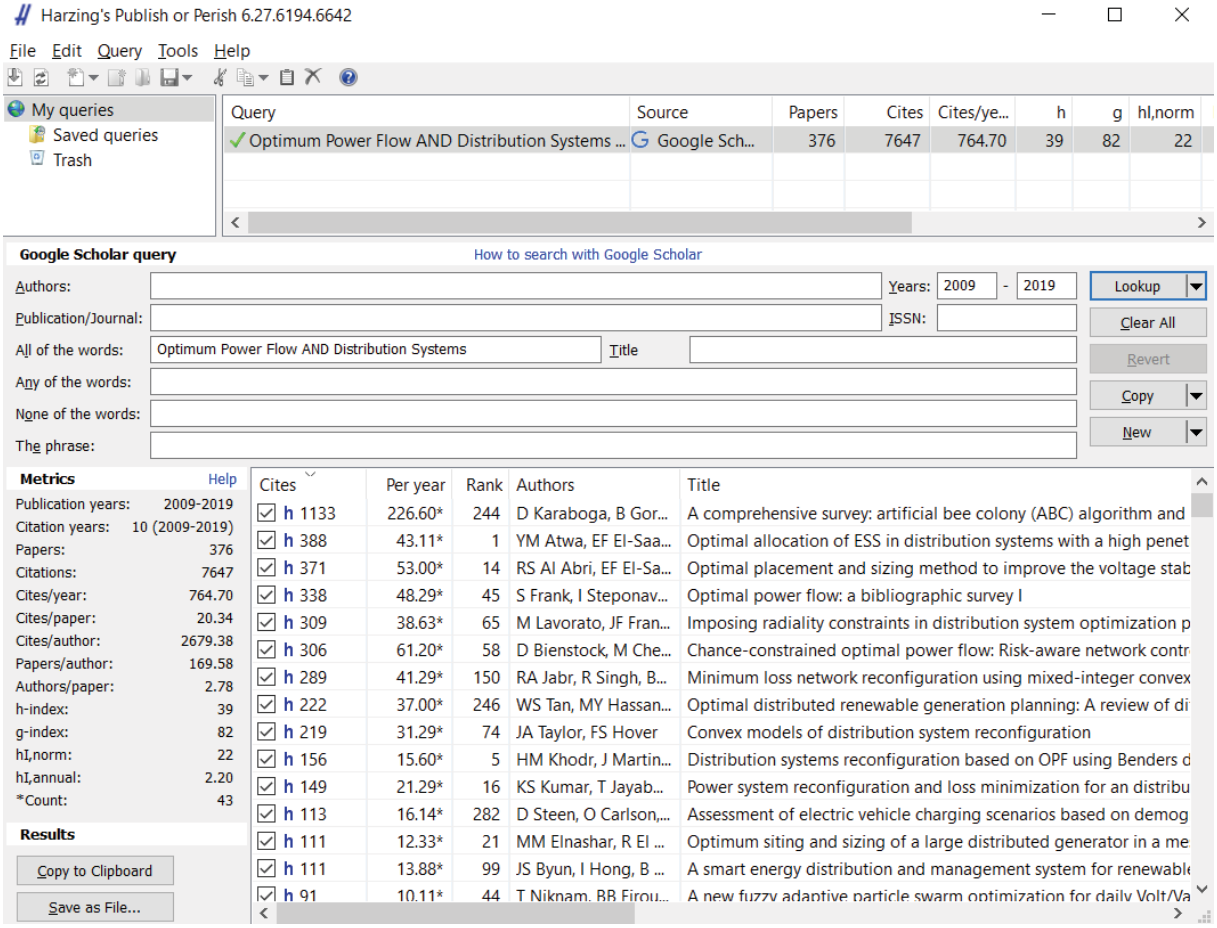

SOURCE: The Author (2019).

Searches on Publish or Perish were developed for all possible combinations of keywords, always considering one of them from the approach and other from the application group, resulting in 16 different combinations. The total number of articles founded was 10,727 articles, when the searching application is used.

The same searches were realized using the CAPES journal's portal, in which the number of results is not limited and they are not organized according to works relevance. The results of both processes are compared in TABLE 7, in which is possible to verify that articles resulting from CAPES search are much higher than the number of articles that comes from the Publish or Perish search, since in this case the number of articles in a search is limited to one thousand, being presented the articles with higher number of citations. In this way, it is clearly known the relevance of using an analysis citation software.

TABLE 7 - NUMBER OF PAPERS FROM SEARCHES USING CAPES JOURNAL'S PORTAL AND PUBLISH OR PERISH SOFTWARE.

Keywords Combination	CAPES	Publish or Paresh			
	Results	Total	Citations	G-index	H-index
Optimum Power Flow + Renewable Energy	16754	342	4646	62	33
Optimum Power Flow + Renewable Integration	5984	20	413	20	5
Optimum Power Flow + Battery Energy Storage	4376	46	938	30	11
Optimum Power Flow + Distribution System	56995	401	7261	80	38
Optimization + Renewable energy	55800	920	143075	305	199
Optimization + Renewable Integration	18787	1000	19328	106	68
Optimization + Battery Energy Storage	15265	1000	68237	224	112
Optimization + Distribution System	408568	1000	113030	254	166
Storage Management + Renewable Energy	31641	1000	38252	156	100
Storage Management + Renewable Integration	13432	270	2819	46	24
Storage Management + Battery Energy Storage	19813	986	13168	92	55
Storage Management + Distribution System	144148	1000	60822	194	129
Day-ahead scheduling + Renewable Energy	1882	920	27323	119	78
Day-ahead scheduling + Renewable Integration	1269	225	3346	53	28
Day-ahead scheduling + Battery Energy Storage	879	617	6212	62	42
Day-ahead scheduling + Distribution System	2095	980	13980	89	62
Total Number of Articles	**797688**	**10727**			

SOURCE: The Author (2019).

In order to verify whether the results were reliable, some articles emerging from the search were drawn and it was verified whether the key words presented included those used in the search process.

Furthermore, it is important to highlight that the search using Publish or Perish can exclude recent papers, since the classification process is based on the number of citations, and a relevant but new article may not have had enough time to achieve a significant number of citations. Therefore, it is important to develop a complementary search looking for recent papers.

From the survey of the articles, it is necessary to perform the process of filtering them. The first step consists of defining the relevant sources, and thus, the articles' publisher on them, excluding citations of books and patents. Moreover, the results of all searches are overlapped, in order to exclude the articles duplicated. Both strategies together reduce the number of articles to 6,650.

In this way, the next step consists of reading the titles, separating those related to the theme of this work. At this stage, it is tried to reduce as much as possible the number of articles, keeping only those that present great adherence to the theme of the work, mainly focusing on the ones that present the keywords defined on title

composition and excluding the ones that present different approaches, for example, all titles that presented electrical vehicles or microgrids were excluded from the results. From the title's reading process, the number of articles was reduced to 93, being split overall the ten years considered to the research process, according to TABLE 8.

TABLE 8 - NUMBER OF ARTICLES PUBLISHED IN EACH YEAR, FROM TEXT READING FILTERING PROCESS.

Year of Publication	Number of articles
2010	4
2011	4
2012	3
2013	11
2014	11
2015	8
2016	16
2017	7
2018	26
2019	3

Source: The Author (2019).

The next step on Ensslin et al. (2010) proposed process consists of reading the abstract of the filtered articles, in order to verify if the work developed on them is really related to the present work. Reading the 93 abstracts was possible to identify that lots of works were related to the microgrids scenarios or considered photovoltaic systems with battery systems coupled on it, being both cases not related to the analysis developed in the present work. Therefore, the abstract reading process was possible to reduce the number of articles to 35.

In the sequence, all articles should be read, considering the scientific reading process, i.e., the reading begins with the introduction, followed by the conclusion, for a subsequent reading of the complete article.

At this time, some more articles were also excluded. This happens because it was possible to find articles not related to the aim of the present work, for example, studies related to the grid reconfiguration or with microgrid management.

From the reading process was founded 19 articles, listed in TABLE 9.

TABLE 9 - SELECTED ARTICLES FROM THE LITERATURE REVIEW BIBLIOGRAPHIC PORTFOLIO SELECTION PROCESS.

Number	Title	Year
1	Short-term scheduling and control of active distribution systems with high penetration of renewable resources	2010
2	Active-reactive optimal power flow in distribution networks with embedded generation and battery storage	2012
3	Optimal power flow with large-scale storage integration	2013
4	Optimal power flow solution using fuzzy evolutionary and swarm optimization	2013
5	A multi-period optimal power flow model including battery energy storage	2013
6	Loss minimization in medium voltage distribution grids by optimal management of energy storage devices	2013
7	Dynamic optimal power flow for active distribution networks	2014
8	A flexible mixed-integer linear programming approach to the AC optimal power flow in distribution systems	2014
9	Optimal power flow with energy storage systems: Single-period model vs. multi-period model	2015
10	A robust approach to chance constrained optimal power flow with renewable generation	2016
11	Energy management at the distribution grid using a Battery Energy Storage System (BESS)	2016
12	Day-ahead smart grid cooperative distributed energy scheduling with renewable and storage integration	2016
13	Incorporating price-responsive customers in day-ahead scheduling of smart distribution networks	2016
14	A multi-temporal optimal power flow for managing storage and demand flexibility in LV networks	2017
15	Active distribution grid management based on robust AC optimal power flow	2018
16	Multi-objective chance-constrained optimal day-ahead scheduling considering BESS degradation	2018
17	Optimal Distributed Energy Storage Management Using Relaxed Dantzig-Wolfe Decomposition	2018
18	A Linear Multi-Objective Operation Model for Smart Distribution Systems Coordinating Tap-Changers, Photovoltaics and Battery Energy Storage	2018
19	Multiperiod Coordination of Local Voltage Controllers and Energy Storage for Voltage Regulation in Distribution Feeder-Connected Renewable Energy Sources	2018

SOURCE: The Author (2019).

From the selected articles the optimization techniques used to solve optimization problems related to distribution power system grids and battery systems behavior were also compared and are presented at TABLE 10. It is possible to verify that the same approach, e.g. OPF was solved in different articles using different methods or even solvers, as GAMS (optimization solver programming using algebraic notation) or Interior Points Method, as proposed by the author of the present work.

Reading the articles, it was possible to verify that most of them present just new formulation approaches and changes in the equation to adapt them to the problem related to each case of study. However, most of the articles consider small grid representation, being composed only by a few loads and few generators. Moreover, the articles frequently present the operation of the battery system integrated into the power grid considering the renewable sources as wind power. In case when photovoltaic systems are considered, usually the battery system is coupled to them.

TABLE 10 - OPTIMIZATION TECHNIQUES AND SOLVED USED IN THE SELECTED ARTICLES.

NUMBER	CALCULATION APPROACH	SOLVING METHOD / SOLVER
1	AC 3-Phase Power Flow	Mixed Integer Linear Programming
2	OPF	GAMS[4]
3	OPF	SeDuMi[5]
4	OPF	Fuzzy-PSO[6]
5	OPF	GAMS
6	Genetic Algorithms	Genetic Algorithms
7	Dynamic OPF	Matpower Interior Point Algorithm Solver
8	AC OPF	Mixed Integer Linear Programming
9	AC OPF	Not Informed
10	Robust Chance Constrained OPF	CPLEX[7]
11	Linear Regression Method	Dynamic Programming Techniques
12	Cooperative Distributed Energy Scheduling	Matlab fmincom function
13	Information Gap Decision Theory	KKT[8]+Mixed Integer Linear Programming
14	OPF	Interior Points Method
15	Multi-period AC OPF	GAMS
16	Chance-Constrained Goal Programming	CPLEX
17	AC OPF	Dantzing-Wolfe Decomposition
18	OPF	PARETO set
19	AC OPF	Genetic Algorithms
PROPOSED ARTICLE	OPF	Interior Point Primal-Dual Version

SOURCE: The Author (2019).

Related to the objective function of the optimization problems, most of them are related only to the cost's minimization, considering as constraints the limits of grid operation, related to the generation, lines flow capacity and voltage limits.

Besides the articles selected from the literature review bibliographic portfolio selection process developed, some other articles were added to the literature review survey. Those articles are from a previous search developed in order to get some previous information, contributing to the definition of the research topic of the proposed work.

The sequence will be presented a summary of the main articles for the present work. First will be present the articles related to the penetration levels and the impacts of the renewable energy sources in distribution networks, and in the sequence the

[4] GAMS: Optimization solver programming language using algebraic notation.
[5] SeDuMi: Matlab toolbox for optiization over symnetric cones.
[6] Fuzzy – PSO: both are artificial intelligent techniques. PSO is Particle Swarm Optimization.
[7] CPLEX: optimization software that uses SIMPLEX methods to solve optimization problems.
[8] KKT: Karush-Kuhn-Tucker conditions. Consist on optimization base conditions.

articles related to the optimization approach of the work, following the same sequence of ideas presented in this work.

Penetration levels of distributed energy resources correspond to a relation between the installed power of DERs and distribution system parameters, being calculated in different ways, considering different approaches.

Looking for the penetration levels of distributed generation, Bernards et al. (2017) developed a probability model to estimate the penetration levels of photovoltaic generation in a test area of the Netherland, considering the probability of household adoption. Using the developed model, the authors estimate three different scenarios, with 6, 8 and 11% of PV penetration levels, considering the medium load of the feeder. In the sequence, the authors evaluated the impact of this amount of generation on feeder load.

In the work of Chathurangi et al. (2018) the approach focus was on power quality in a distribution feeder on Sri Lanka, considering high penetration levels of PV generation. In this analysis the authors presented the main impacts of PV generation, related with voltage rise and reverse power flow, considering 50, 60 and 70% of PV penetration levels, calculated based on the transformation ratio of the substation transformer.

The work developed by Aziz and Ketjoy (2017) presented a study of different penetration levels of PV generation in a distribution feeder, looking mainly for voltage behavior and the limit of PV penetration that does not reach the voltage limits of the feeder. According to the work, the main causes of the voltage rises with DG are the reverse power flow and the reactive power disturbance. The voltage control should be applied to avoid voltages to reach the limits. This control should be stronger when the penetration levels are higher than 20%.

Considering different distributed generation penetration levels, the impacts on distribution systems change. One of the parameters that allow verifying these impacts is the voltage stability index. The work developed by Lebid (2017) presents the calculation of stability index for distribution systems considering different formulation proposes, as index SI and L. However, the work developed do not consider the insertion of distributed sources, by the way, that the operation of voltage regulators and capacitor banks are taking in the account. Ali, Eid and Abdel-Aker (2012) used the index L to evaluate the voltage levels for a distribution system with photovoltaic generation from the power flow simulation using backward/forward sweep analysis,

allowing to find the weakest bus in the system, considering the probability to present a voltage collapse.

Looking for the optimization of grid operation considering the insertion of distributed energy resources and storage systems, the articles presented in the sequence present different approaches to develop this analysis.

The work developed by Chandy et al. (2010) considered the insertion of a large-scale battery energy storage at the transmission system without renewable systems. The optimum power flow approach was used to optimize the cost of generation across time. The proposed formulation is based on an optimum power flow classical formulation, inserting the storage system power and energy limits as well as the battery costs that depend on the state of charge. In this way, minimizing the battery cost it is looked to maintain the battery levels, avoiding cycling. To solve the optimum power flow, the authors used a convex program obtained as the Lagrangian dual to the rank relaxation.

Considering the connection of photovoltaic systems with storage, the work developed by Riffonneau et al. (2011) presented an optimum power flow solved with multi-period programming. The main objective was to reduce the energy costs for the consumer, managing the power flow of its system to the power grid, and also reduce the aging cost of the batteries. In this work, a grid equivalent was used to simulate the utility power grid and a detailed formulation was developed to the consumer system (photovoltaic, battery and load). The power flow management proposed to consider three different time horizon: (1) the forecasting stage, in which the predictions and forecast of input variables are learning from the past, considering month to hours period, (2) predictive optimization stage, that takes the horizon of hours to a few minutes and (3) local control stage, that consists of the local command of batteries controller system. The battery modeling developed by the authors includes the state-of-charge, the voltage and the aging process of the battery. From the optimum power flow solution, the resulted battery behavior presented the charge of the system during the solar generation and discharging during the peak load time.

The work developed by Gabach and Li (2012) proposes an OPF approach for a distribution system with wind generation and battery energy storage systems, in which the optimal problem is divided into two sub-problems: one optimization for active and another for reactive power. Using this approach, the authors proposed an optimal grid operation strategy minimizing power losses and improving voltage profiles. In the

modeling, the authors considered the tariff cost of the energy provided by the distribution network and defined also that the battery can perform just one cycle per day. From the optimization of power's dispatch was possible to reduce the system power losses by 12% and the importation of energy from the transmission network in 90%.

Following the OPF approach, the study developed by Gayme and Topcu (2013) consider an extension model of the classical formulation, in order to characterize the battery system operation. To allow the dynamic model of multiple BESS distributed in the system, authors used an extended semi-definite program relaxations, being this an equivalent process to the Lagrangian Dual. From the optimization, authors evaluate the different possible contributions of energy storage dispatch, considering grid cost operation minimization when modeled as a linear or quadratic function, however, the BESS cost operation is not considered.

The authors Wang et al. (2013), proposed a multi-period OPF including a battery energy storage system, in order to predict the behavior of the system looking for a forecasted 24 hours in advance. The main objective of the optimization problem is to reduce the cost of the generation and the prices of battery charge and discharge, applying the constraints of active and reactive power flow balance, voltage limits, generators limits of operation, and the battery system constraints of state-of-charge, storage capacity limits, and charge and discharge systems. In this case, the optimization process is performed with GAMS software and the results show the best operation for the generators and the battery system considering different price scenarios.

Levron, Guerrero, and Beck (2013) developed an optimum power flow tor a microgrid application, considering photovoltaic and wind generation as well as battery energy storage system connections. The main objective in the formulation developed consisted of minimizing the price of energy imported from the main grid, represented as an equivalent, and optimize the voltage profile. For this the authors proposed an optimum power flow that integrated storage devices, presenting the global optimization for network domain and time domain. The storage limitations, as voltage, currents, and power were considered in addition to internal losses. The problem is solved using multi-period programming and recursive search is used to determine the operation grid parameters. In this case, the battery operation consisted of store energy when there is

over-generation and it is discharged in the moments when the solar and wind generation reduces momentarily.

Also considering a microgrid application, the work developed by Maffei et al. (2014) developed an alternate current optimal power flow (ACOPF), in which the battery energy storage system is defined to mitigate the fluctuation of renewable energy generation, being placed close to a wind park and, contributing to guarantee the network power balance. The battery formulation presented the power and energy limits as well as a fixed degradation of the system for all time samples. The cost function of the battery depends only on the state of charge of the system, by the way, that the generation cost is defined by a linear function. The main goal of the ACOPF in this work consisted in determine how much generators and storage systems need to provide power to cover the entire microgrid load, respecting the constraints, minimizing the cost of generation, the storage level change and the power exchanged with the utility grid. In this case, the ACOPF consisted of a non-convex optimization problem solved using an interior-point optimization solver in the GAMS environment.

In order to compare the performance between a single-period and a multi-period OPF, Nguyen et al. (2015) modeled a distribution power system with battery systems and wind park considering both approaches to determine the optimal schedule of BESS and wind generation operation. In this case, the authors defined an objective function to minimize the generation costs, as well as the costs of battery operation. Implementing both methods in Matlab, the single-period runs the calculation for each period independently, by the way, that with multi-period all the periods are calculated for each iteration. Both methods were used in a 14-bus system and in a 57-bus system. From the results was possible to visualize that when the multi-period method is used, the generation costs are lower than in the case of a single-period. Besides, with the multi-period approach, the battery behavior presents better performance than in single-period, charging and discharging according to wind generation variation.

The work developed by Jayasekara, Masoum, and Wolfs (2016) evaluated the integration of battery energy storage systems in distribution systems that also present renewable energy systems connected, being in this case, photovoltaic and wind systems. The total load of the system corresponds to 3.556 MW, by the way that the installed renewable generation totalized 5.2 MW. The battery system sizing was calculated by the authors considering grid requirements of storage energy based on

previous studies of grid operation. To evaluate the integration of the systems, a multi-objective problem was defined, in which the battery modeling is defined by the state-of-charge and state-of-health, which considers the cycle aging and the temperature effects. In this way, the battery dispatch was defined considering the daily energy balance constraint and charging and discharging constraint, being represented along the simulation period using a Fourier coefficient vector. In this case, the objective function of the optimization problem consisted in minimize the distribution system costs, including the cost of power losses, the peak demand, and the voltage regulation. Battery and distribution system constraints were considered, resulting in a nonlinear optimization problem solved using the interior-point method. This work presented the conclusion that the best operation for battery in an LV or MV distribution system is the peak shaving.

The study developed by Reihani et al. (2016) propose the optimization of BESS (1MW/1MWh) operation, considering that the system will operate to develop peak shaving, voltage regulation and power smoothing to the distribution system. The objective function of the proposed work consisted in minimize power losses, using dynamic programming techniques. Yet, the power grid model is simplified, presenting just an equivalent model. From the results was possible to evaluate different BESS behaviors, according to different scenarios of grid operation and considering the main goal of battery operation, becoming visible mainly the results of peak shaving developed. In case to reduce the smoothing of renewable energy sources, the BESS presented a highly variable output with low depth-of-discharge, and the proposed optimization technique was not so successful in comparison with the peak shaving results due to system time of response required to smoothing operation.

Considering more than one BESS connected to the distribution system, the work developed by Zhang et al. (2016) propose a Cooperative Distributed Energy Scheduling, in which each bus is modeled as an agent with scheduled capacity. Being simulated as an optimization problem with the minimization of the multiple generators cost, all the equations related to battery systems behavior on time domain are presented, characterizing also systems operational limits. Power system losses, generators limits and power flow through the lines are also represented, being solved the problem using an expanded Lagrangean approach with KKT conditions applied. The study case considered a 30 bus system with six generators, five battery systems,

three photovoltaic systems and twenty loads. From the results, it is possible to verify the different behavior for each battery, due to their different locations.

In order to evaluate the insertion of energy storage element operation into the distribution feeder, the work developed by Viola, da Silva, and Rider (2017) presented the mathematic modeling using non-linear programming for the optimal distribution system operation, considering the insertion of battery systems and energy storage systems with hydrogen (H_2). In this work the analysis of grid operation was done considering only battery operation, only hydrogen storage and with both storage technologies operation. The authors presented the power flow formulation using backward formulation, considering the power losses of the system and operational constraints, as power limits at the substation, voltage limits in all buses and the current through all lines. The formulation of capacitor banks, storage systems, and renewable energy sources was also developed. Solving the system power flow, it was possible to verify the storage systems operation, considering different possibilities, like peak shaving, respecting the best electricity price for grid operation.

Specifically, on classical OPF formulation, there are several efficient methods for solving it, as the Primal-Dual version Interior Points Method techniques used by Granville, Mello and Mello (1996), Carvalho (2006), Paiva (2006) and others, optimizing the active and reactive power dispatch.

One of the most used formulations to evaluate the energy storage systems connected at power grids is the optimum power flow, however, it is also possible to consider different approaches as the implementation of artificial intelligence techniques. The work developed by Li et al. (2018) proposes a fuzzy multi-objective bi-level optimization for active distribution networks with battery energy storage systems and renewable energy distributed resources. In this case, the battery optimization system is formulated in a similar way that it is done for the OPF approach, but considering a retrofit system based on two different objective functions, one for planning and another for operational considerations. For the planning objective function, the goal is to reduce the costs of the system, by the way, that for operation objective function it consists in a composition of objective functions defined to control the battery operation to realize the peak load shaving, restraining volatility and improve the reserve capability of the battery. The authors conclude that the formulation and solution technique propose was satisfactory to plan and operate a battery system behavior in active distribution networks.

There are a lot of works that use optimum power flow formulation to planning the optimized battery behavior. Different grid scenarios were already considered, as operation in a microgrid, or in off-grid systems, or looking for consumer's benefits of storage operation and even the power utility grid operation, considering the insertion of storage systems. However, studies that considered the large-scale battery operation in distribution systems that also presented photovoltaic systems are uncommon being more frequently studies in which renewable energy corresponds to wind systems.

This work is based on the formulation of the OPF proposed by Fernandes (2004), in which is modeled the voltage phasor using rectangular coordinates to overcome the numerical problems in excessively long and radial networks, being applied by Borges, Fernandes, and Almeida (2011) in a multi-period OPF to dispatch hydrothermal system. Following these previous studies, an extended formulation was developed in the present work considering the battery modeling for a multi-period OPF, in addition to a detailed grid modeling, that also takes into account the operation of voltage regulators and capacitor banks installed at the power grid. This is a similar approach to the work developed by Oliveira (2019) that modeled the electric vehicle batteries using a multi-period optimum power flow. Unlike vehicle batteries, in this work, the battery is always connected to the power grid and in the same placement of the network.

3.1 CHAPTER FINAL CONSIDERATIONS

Renewable energy systems integration with the power distribution network and more recently, storage systems are becoming frequently topics for different studies all over the world.

Different approaches are founded nowadays in the literature, and as with internet access, it is possible to found information from different sources. Developing a structured process for the survey of bibliographic material is essential in order to ensure the analysis of the most relevant material.

With the literature review process performed in this work, it is possible to get access to articles with the greatest amounts of citations, presenting higher relevance. However, this process to not consider brand new articles, since, they had no time to

get citations. In this way, it is necessary to develop extra searching, looking for articles that were not cached in the previous selection.

Moreover, when the theme of the present work was being under the definition, a first search was developed, and those articles are also very important references to the present study.

From reading the articles it is possible to state that the OPF approach is well used to plan the optimized grid operation, considering different elements modeled in the distribution network, as well as different objective functions. Furthermore, the optimization problem solution can be calculated using different techniques or solvers, as it is possible to conclude from the literature review process.

In order to compare the selected works from the literature review process, TABLE 11 was defined based on the definition of some criteria, being each article evaluated if the developed study present (Y - Yes) or not (N - No) the element or approach that are being looked for. From the comparation it is possible to visualize that none of the articles developed a study like the one that is presented in this work.

TABLE 11 - COMPARISON TABLE OF ELEMENTS AND APPROACHES CONSIDERED ON SELECTED ARTICLES.

	Article Number																		
Criteria	**1**	**2**	**3**	**4**	**5**	**6**	**7**	**8**	**9**	**10**	**11**	**12**	**13**	**14**	**15**	**16**	**17**	**18**	**19**	**Proposed Method**
Day-ahead approach	Y	Y	N	N	N	N	N	N	N	N	Y	Y	Y	Y	N	Y	N	N	N	Y
Multiperiod	Y	Y	Y	Y	Y	Y	Y	N	Y	Y	Y	N	Y	Y	Y	Y	Y	Y	Y	Y
PV System	Y	N	N	N	N	N	N	N	N	N	Y	Y	N	N	Y	N	N	Y	Y	Y
PV Different Penetration Levels	N	N	N	N	N	N	N	N	N	N	N	N	N	N	N	N	N	N	N	Y
BESS	Y	Y	Y	N	Y	Y	Y	N	Y	N	Y	Y	Y	Y	Y	Y	Y	Y	Y	Y
Model of Ebat and Pbat	Y	Y	Y	N	Y	Y	Y	N	Y	N	Y	Y	Y	Y	Y	Y	Y	Y	Y	Y
Response to Cost Variation	Y	Y	Y	Y	Y	N	Y	Y	N	Y	N	Y	Y	N	Y	Y	Y	N	N	Y
Cost of BESS Operation	N	N	N	N	Y	N	N	N	N	N	Y	N	Y	N	N	Y	N	N	N	Y
System Losses Minimization	N	Y	N	N	N	Y	Y	N	N	N	N	N	N	Y	N	N	N	Y	Y	Y
Consider some OLTC	Y	N	N	N	N	N	Y	N	N	N	Y	N	N	N	Y	N	N	Y	Y	Y
Efficiency of Storage Operation	N	N	N	N	Y	N	Y	N	Y	N	N	Y	Y	Y	N	Y	Y	N	Y	Y
Optimization Problem	Y	Y	Y	Y	Y	Y	Y	Y	Y	Y	Y	Y	Y	Y	Y	Y	Y	Y	Y	Y
Optimization of Grid Operation	Y	Y	Y	Y	Y	Y	Y	Y	Y	Y	N	N	Y	Y	Y	Y	N	Y	Y	Y
Optimization of BESS Operation	N	N	Y	N	Y	N	Y	N	Y	N	Y	Y	Y	Y	N	Y	Y	N	N	Y

SOURCE: The Author (2019).

4 TOOLS TO DEVELOP THE PLANNING OF ELECTRICAL DISTRIBUTION SYSTEM OPERATION

There are different possibilities to evaluate the grid operation, looking into different approaches and considering the different fields of studies being, some of them, related to the power flow behavior inside of the grid. For the power flow (PF) calculation, it is considered a predefined grid configuration, specifying the number and behavior of loads and generators units during the defined time-horizon of study. In this case, it is necessary to provide a slack bus, able to coordinate the equilibrium between demand and generation.

Thus, it is possible to model the system in different software tools and solve the PF using different iterative methods as Newton-Raphson, Decoupled Method, Fast-Decoupled Method, Backward-Forward and Current Injections techniques.

In this way, to evaluate the impacts of different active elements into the distribution power grid, power flow simulations were performed. The theoretical approach of PF will be explained in section 4.1, presenting the results of the simulations in chapter 5.

However, with the necessity to improve the control and operation strategies of power grids, mainly for active distribution networks, the planning of operation can be optimized, using optimization techniques as Optimum Power Flow (OPF). This concept can be implemented for a single period or in a dynamic way, considering multiple periods. In this case, the variables of the system as the generator's behavior can be defined in order to minimize or maximize an objective function.

The classical formulation of a Multi-period OPF is detailed in section 4.2, being also explained the extended formulation used to model also the batteries. Furthermore, the scenarios simulations and results of the proposed OPF are presented in chapter 6.

4.1 POWER FLOW

Power flow analyses can be developed in order to analyze the grid operation under different steady-state scenarios.

Power flow calculation consists of determining the magnitudes and angles of the voltages, allowing to calculate from these results the other grid parameters as

currents, active and reactive power of a system under defined load conditions. However, these analyses can be done considering a specific operation set or a specific period of time. For these simulations, the characteristics of the system, as load and generators profiles are predefined and a slack bus should be considered in order to provide active and reactive power balancing.

There is different software that can simulate distribution power systems, considering different analysis, as fault studies, power quality studies and also solve power flow simulation. Some software tools able to solve PF analysis are DIgSILENT PowerFactory, GridLAB-D, OpenDSS, PowerWorld, and Matlab, in which the calculation can be implemented using script programming or can use predefined tools as Matpower or SimPowerSystems at Simulink toolbox. These computational tools already present photovoltaic system representation and battery models that can be configurated to actuate according to the programmer's necessity.

DIgSILENT PowerFactor is a commercial software capable to simulate generation, transmission and distribution system, industrial systems, renewable energy, and distributed sources, using graphical interface or programming language, in this case, DPL (DIgSILENT Programming Language). The photovoltaic system can be modeled using a typical profile behavior for a sunshine day or the user can provide the data using for example measurement information. Yet, for battery simulations, there are different options of configurations being possible to define a profile behavior, set a controller, use a manufactory’s model and also allow the user to develop their own BESS model (DIGSILENT, 2017).

Developed by the U.S. Department of Energy (DOE) at Pacific Northwest National Laboratory (PNNL), GridLAB-D is an open-source power distribution system simulation tool. Power flow simulations are solved using Newton-Raphson, and the PV system can be simulated as an object which specification can be the system characteristics as PV module technology, temperature ambient, area of the system, or directly the output power provided by the system. For BESS there is not a default battery model, being in this case, modeled as a generic energy storage device, which behavior is provided by the user (DOE, 2018).

The Open Distribution System Simulator (OpenDSS or simply DSS) is an open-source system simulation tool for electric utility distribution systems, developed by Electrical Power Research Institute (EPRI) (EPRI, 2019). To develop simulations using this computational tool it is required to program a script providing the information

of the system configuration as well the characteristics of the PV System and Storage element. For PV System is required the temperature, efficiency, and irradiation profiles, as well as the power of the installed system and the power factor established to the system inverter. Furthermore, for the storage element, a profile should be defined corresponding to the charge and discharge behavior, being not a control variable for the simulation (EPRI, 2011a).

PowerWorld Simulator is a power system simulator highly interactive and able to develop different studies, including economic analysis. The newest versions of the software provide predefined models for different ESS such as batteries, concentrated solar power, flywheel, and others (Power World Corporation, 2019).

A widely used and well-known tool is Matlab. In this software, it is possible to perform analysis of different knowledge areas, including electric power systems. To develop a simulation in Matlab it is possible to develop a programming scrip with the related equations to model the grid and the equipment, as well the mathematical model to solve analysis implementing, for example, the Newton-Raphson model to solve power flow calculations. However, it is also possible to use the Simulink toolbox, which consists of a block diagram in which equipment is already modeled and formulated. The modeling developed at the block diagram environment can be also integrated into script formulation.

All the simulation tools described before are able to solve power flow simulations considering PV and BESS operation. As the PV model is very similar to be modeled in all computational tools analyzed, it is important to compare the battery modeling strategies.

Thus, the work developed by Blasi, Fumagalli, and Pereira (2018) present the survey and comparison between the battery models in each software. For the comparison between the software tools, it was defined as an impact effort matrix, present in FIGURE 20. The matrix was created based on criteria evaluation for efforts and impacts. For the effort criteria evaluation were considered: cost of the software, if it presents predefined models and how much the interface is user-friendly. On the other hand, for the impact criteria evaluation were considered: the possible simulations to be developed in the software, how much flexibility software presents to the modeling implementation and how many technologies of ESS can be modeled on it. With the evaluation of each criteria it is possible to define the best power flow simulation software aiming for a tool with low effort and a high impact. However, from the matrix

it is also needed to split the softwares more appropriated for steady state or dynamics simulations, being PSCAD, ATP and EMTP tools more used for dynamic analysis.

FIGURE 20 - IMPACT EFFORT MATRIX OF SOFTWARE FOR POWER FLOW SIMULATIONS.

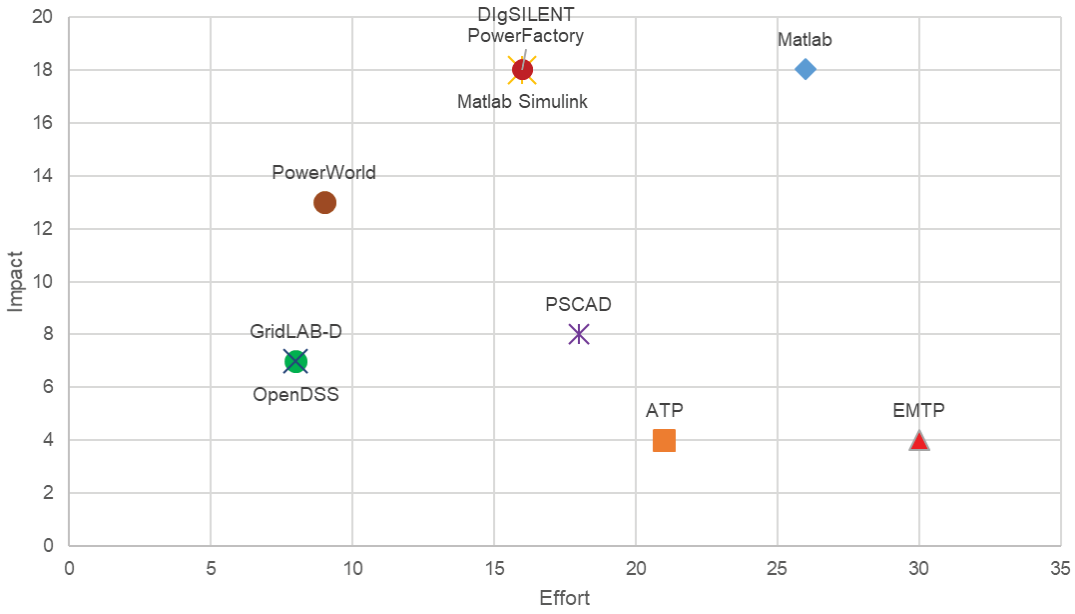

SOURCE: Blasi, Fumagalli, and Pereira (2018).

Considering the possible software to develop the present work OpenDSS was chosen, since it is open-source software and presents predefined models for PV and BESS system, being these ones well consolidated presenting several works in literature. The analysis of power flow simulations with OpenDSS will be discussed in Chapter 5.

4.2 OPTIMUM POWER FLOW

An Optimum Power Flow (OPF) consists of determining the operating state of the power grid, optimizing a given objective, considering the technical and physics constraints. An OPF can be model as an optimization problem, consisting of an objective function and constraints.

The objective function describes the characteristic that should be optimized, being most of the time minimized, such as power system losses, generation costs, load shedding, and others. The constraints, however, are related to operation limits of power grid and equipment, being expressed using equality and inequality expressions.

For the problem studied in the present work, it will be used a multi-period OPF (MPOPF), that realizes the optimization taking into account simultaneously a number of periods for the selected planning horizon.

The classical formulation of a multi-period OPF and an extended formulation developed to optimize the BESS operation under different possible scenarios will be described in the next section.

4.2.1 Multi-Period Optimum Power Flow Classical Formulation

The classical formulation of an OPF has the objective to determinate an optimal operating point for a given instant of time, in order to establish, among other interests, power injections in each bus of the system.

The first fully formulation of OFP model was proposed by Carpentier (1962) defining the OPF problem as an optimization problem, consisting of an objective function and constraints, as presented at eq. (4.1):

$$\min f(u) \tag{4.1}$$

Subject to:

$$g(u) = 0 \tag{4.2}$$

$$h_{min} \leq h(u) \leq h_{max} \tag{4.3}$$

where:

$f(u)$: objective function to be minimized;

$g(u)$: vector of equality constraints;

$h(u)$: vector of inequality constraints;

u: vector of system variables.

In general, the OPF intends to minimize power losses, generation, and operative costs, considering a specific point of operation. Another OPF family deals with the optimization of the network considering a sequence of periods solved simultaneously in order to solve some intertemporal control action, such as the use of energy goals of hydroelectric plants (BORGES; FERNANDES; ALMEIDA, 2011) or charge and discharge of a battery under a study horizon, as the purpose of this work. So, in this way, the multi-period formulation was used in this work.

When the multi-period optimum power flow approach is considered, multiple periods of time operation are considered, requiring the OPF formulation extension.

First applications of MPOPF were related to hydrothermal power system dispatch, considering that the operation at one time affects the operation at the next periods (GILL; KOCKAR; AULT, 2014).

For teaching purposes, a classical multi-period OPF will be initially presented, considering the aim to minimize the power losses, subject to active and reactive power balance restrictions, operational limits of the equipment and related to the adjustment of voltage regulator taps and capacitor bank actuation. In the next section will be presented the insertion of the battery model, based on the approach proposed by Oliveira (2019) in which the MPOPF formulation is used to analyzing battery of electric vehicles behavior and the overture presented by Viola (2017), that proposes a MOPF to the management of a battery energy system and hydrogen storage technology.

The classical formulation of a multi-period OPF that minimizes the electric losses is presented at eq.(4.4) to eq.(4.10) (BORGES; FERNANDES; ALMEIDA, 2011):

$$min \sum_{i=1}^{nb} \sum_{t=1}^{np} P_i^t \tag{4.4}$$

$s.t.$

$$Pg_i^t - Pd_i^t = P_i^t(\dot{V}, a) \tag{4.5}$$

$$Qg_i^t - Qd_i^t + diag\left(\left|\left(\dot{V}_i^t\right)^2\right|.c_i\right) = Q_i^t(\dot{V}, a) \tag{4.6}$$

$$Vmin_i^t \leq \left|\dot{V}_i^t\right| \leq Vmax_i^t \tag{4.7}$$

$$-flmax_j^t \leq fl_j^t \leq flmax_j^t \tag{4.8}$$

$$amin_j^t \leq a_j^t \leq amax_j^t \tag{4.9}$$

$$0 \leq c_i^t \leq cmax_i^t \tag{4.10}$$

j=1,...,nl, i=1,...,nb, t=1,...np

where:

nb: number of buses;

nl: number of branches;

np: number of periods;

P_i^t: injection active power at bus *i* and period t [kW];

Q_i^t: injection reactive power at bus *i* and period *t* [kvar];

Pg_i^t: active power generation at bus *i* and period *t* [kW];

Pd_i^t: active power load at bus *i* and period *t* [kW];

Qg_i^t: reactive power generation at bus *i* and period *t* [kvar];

Qd_i^t: reactive power load at bus *i* and period *t* [kvar];

$\dot{V}_i^t$: phasor of voltage at bus *i* and period *t*;

$Vmax_i^t, Vmin_i^t$: maximum and minimum limit of voltage magnitude at bus *i* and period *t* [V];

fl_j^t: power flow through branch *j* and period *t* [kVA];

$flmax_j^t$: maximum power flow thought branch *j* and period *t* [kVA];

a_j^t: position tap of voltage regulator at branch *j* and period *t;*

$amax_j^t, amin_j^t$: maximum and minimum limit of taps of voltage regulator at branch *j* and period *t;*

c_i^t*:* capacitive susceptance of the bank of capacitors at bus *i* and period *t* [S];

$cmax_i^t$: capacitive susceptance of the bank of capacitors at bus *i* and period *t* [S].

The constraints presented in equations (4.5) and (4.6) are related to the active and reactive power injection at buses, respectively, representing the power balance of the system for each time step. The restriction (4.7) corresponds to the voltage magnitude limits at buses, the constraint (4.8) refers to the power flow limit through the lines, the restriction (4.9) refers to the voltage regulator taps limits, and, at least, the constraint (4.10) refers to the actuation of the capacitor banks.

As an optimization problem, different mathematics methods can be used to solve it. In the present work, the OPF is solved using the interior-points method with a primal-dual version, since it presents a good approach for nonlinear systems allowing to achieve the convergence in a short calculation time. The flowchart presented in FIGURE 21 explains the optimum power flow simulation using interior points primal-dual formulation. In this case, the primal variables are the system parameters, as active and reactive power generation, voltage magnitude and angle, whereas the dual variables are related with the Lagrange multipliers used to problem's solution.

FIGURE 21 - FLOWCHART OF OPTIMUM POWER FLOW SIMULATION USING INTERIOR POINTS PRIMAL-DUAL FORMULATION.

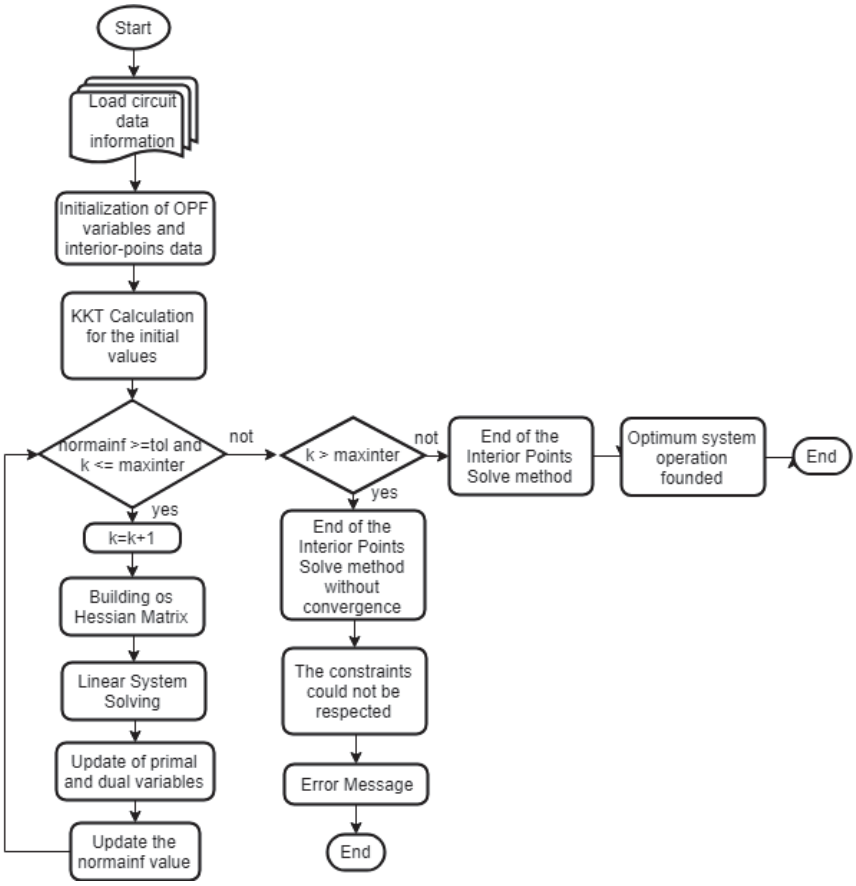

Source: The Author (2019).

The first step consists of load the circuit data information, as buses numbers, lines connection and impedances, equipment connected to the systems, as capacitor banks and voltage regulators, and their corresponding information, and also the characteristics and limits of the generator. In the sequence it is necessary to initialize the OPF variables, considering an estimation of the values. The chosen initial values should be done in order to guarantee that the initial results will fulfill the constraints of the problem, being inside of the feasible solution area.

In the sequence, if the value of the infinity norm (norminf) is higher than the defined tolerance, in this case, defined as 0.001, and the interactions counter (k) does not reach the maximum interaction number (around 200 interactions), the Hessian matrix needs to be built and a linear system should be solved. With the new values of the solution, the variables should be updated and also the new infinity norm should be calculated. This process needs to be done until the infinity norm value is higher than the tolerance or while the number of interactions is lower than the maximum interaction limit.

If the maximum number of interactions is reached, the solution founded is not optimum. However, if the calculation process ended because the infinite norm value is lower than the tolerance and the number of interactions is lower than the maximum, so the optimal solution was founded.

A lot of works were already developed in order to program the OPF formulation considering different grid operations and the connection of different elements. The formulation developed by Borges, Fernandes, and Almeida (2011) will be followed in the present work, in which the BESS characteristics will be inserted. In the present work, the pre-dispatch modeling will be applied to the distribution system, considering the prices of electricity provided by the power utility, the possible photovoltaic generation behavior, and the BESS operation, looking for day-ahead time horizon.

4.2.2 Multi-Period Optimum Power Flow Extended Formulation

Considering an active distribution network operation, it is necessary to insert the distributed generation and battery characteristics in the grid MPOPF formulation. From the generic model presented in section 4.2.1, it is possible to insert the modeling of batteries and solar sources to solve the MPOPF.

The representation of the batteries used in this work is based on the formulation proposed by Oliveira (2019) and Viola (2017). In the present study, the BESS characteristics consist of the power and energy capacity of the system. Some limits of battery operation are also defined, as the depth-of-discharge (DoD), limited in this case to 70%, and the arrival energy ($Ebat\_arrival_i^{t0}$), that corresponds to the energy of the battery system at the period t=0, defined equals to the minimum energy of the storage (30% of the energy capacity for a DoD of 70%).

The active and reactive solar generation value connected at each bus *i* ($Pgsol_i^t$ and $Qgsol_i^t$) is an input parameter that varies according to the period t. These generation values are provided considering discrete solar generation profiles and the installed PV power in each bus.

The new optimization variable inserted in the problem is the charge or discharge power of the battery ($Pbat_i^t$) connected at bus i at the period t. This variable is modeled as a continuous variable, accepting negative and positive values, being defined that positive values ($Pbat_i^t > 0$) corresponds to the battery charge and when

present negative values ($Pbat_i^t < 0$), the battery is discharging. The battery power behavior needs to be inserted into the active and reactive power balance equations (4.2) and (4.3), since they will be demanding or providing power to the system. The reactive power of the battery is defined by the power factor (pf) of the system inverter.

$$Pg_i^t + Pgsol_i^t - Pd_i^t - Pbat_i^t = P_i^t(\dot{V}, a) \quad (4.11)$$

$$Qg_i^t + Qgsol_i^t - Qd_i^t - Pbat_i^t.\tan(\text{acos}(pf)) + diag\left(\left|\left(\dot{V}_i^t\right)^2\right| c_i\right) = Q_i^t(\dot{V}, a) \quad (4.12)$$

i=1,...,nb, and t=1,...,np

The efficiency (eta) of the charge and discharge process is incorporated into the energy battery ($Ebat_i^t$) equation being, for each instant, represented as a function of $Pbat_i^t$, as shown in equation (4.13).

In this case, the power factor and the efficiency of the system will be fixed, considered as parameters, being not optimized variables.

$$Ebat_i^t = [\, Pbat_i^t - (1 - eta).|Pbat_i^t|].\Delta t \quad (4.13)$$

i=1,...,nb, and t=1,...,np

where:

Δt: time interval between two consecutive periods.

The effective amount of the stored energy ($Ebat\_acum_i^t$) depends on the energy values stored in the previous instants, considering since the initial energy on t=0 ($Ebat\_arrival_i^{t0}$). Thus, the total value of the energy stored in the battery at bus *i* to each period *t* is:

$$Ebat\_acum_i^t = \sum_{t=1}^{t}[Pbat_i^t - (1 - eta).|Pbat_i^t|].\Delta t + Ebat\_arrival_i^{t0} \quad (4.14)$$

i=1,...,nb, and t=1,...,np

It is important to highlight that *t* is each one of the periods considered, for example, if the time step is given in hours, *t* is each one of the hours of the total period considered.

These stored energy values must comply with minimum and maximum energy storage limits (4.15) in order to preserve the life of the batteries. These limits are defined by the depth-of-discharge defined to the battery.

$$Ebat\_acum^{\mathbf{min}} \leq Ebat\_acum_i^t \leq Ebat\_acum^{\mathbf{max}} \quad (4.15)$$

Moreover, the maximum values of charge and discharge of the battery shall be taken into account, respecting the equipment limits and also the power limit of the inverter:

$$-Pbat_i^{max} \leq Pbat_i^t \leq Pbat_i^{max} \quad (4.16)$$

In order to improve the battery operation at the distribution system, more optimization criteria can be incorporated. The battery expected behavior consists of charging during the solar generation period, avoiding reverse power flow into the substation and the impacts of PV into the grid, and discharging of the BESS during the peak load times, developing a peak-shaving and allowing to postpone grid investments.

For thus, hourly cost values ($cost^t$) for the power provided by the substation must be considered (substation located at bus 1 - Figure 52), representing the cost of demand for the DSO. The cost of energy was applied following the white tariff behavior (represented by the variable $cost^t$), that increases the cost during the peak times, as a way of penalizing demand growth at this time.

The cost of the total power supplied by the substation bus is given by (4.17).

$$Cost_{total} = \sum_{\boldsymbol{t=1}}^{\boldsymbol{np}} Pg_1^t . cost^t \, \Delta t \quad (4.17)$$

Considering a realistic scenario, the price of battery operation was also modeled based on the battery cost of degradation ($cost_{degradation}$), defined on equation (2.1), since every time that the system operates doing a charge or discharge, the lifetime of the system is reduced. In this way, the battery operation cost is also a variable that should be minimized.

$$Cost_{bat} = \sum_{\boldsymbol{i=1}}^{\boldsymbol{nb}} \sum_{\boldsymbol{t=1}}^{\boldsymbol{np}} Pbat_i^t . cost_{degradation} . \Delta t \quad (4.18)$$

Thus, the complete final formulation of the optimization problem of optimum power flow considering battery energy storage operation becomes:

$$
\begin{aligned}
min\ \ wp.\sum_{i=1}^{nb}\sum_{t=1}^{np}\left(Pg_i^t + Pgsol_i^t - Pd_i^t - Pbat_i^t\right).cost^t \\
+ wc.\sum_{t=1}^{np} Pg_1^t.cost^t + wbat\sum_{i=1}^{nb}\sum_{t=1}^{np}|Pbat_i^t|.cost_{degradation}.\Delta t \\
s.t \\
Pg_i^t + Pgsol_i^t - Pd_i^t - Pbat_i^t = P_i^t(\dot{\mathrm{V}}, a) \\
Qg_i^t + Qgsol_i^t - Qd_i^t - Pbat_i^t.\tan(\mathrm{acos}(pf)) + diag\left(\left|\left(\dot{V}_i^t\right)^2\right| c_i\right) = Q_i^t(\dot{\mathrm{V}}, a) \\
Vmin_i^t \le \left|\dot{V}_i^t\right| \le Vmax_i^t \\
-flmax_j^t \le fl_j^t \le flmax_j^t \\
amin_i^t \le a_i^t \le amax_i^t \\
-Pbat_i^{max} \le Pbat_i^t \le Pbat_i^{max} \\
Ebat\_acum^{\mathbf{min}} \le \sum_{t=1}^{np}[Pbat_i^t - (1-eta).|Pbat_i^t|].\Delta\mathrm{t} + Ebat\_arrival_i^{t0} \\
\le Ebat\_acum^{\mathbf{max}} \\
j=1,...,nl,\ \ i=1,...,nb,\ \text{and}\ t=1,...,np
\end{aligned}
\tag{4.19}
$$

where: *wp*, *wc*, and *wbat* are weights related to each of one the functions that compose the objective function, being the minimization of losses, generation costs, and battery cost, respectively. With these weights, it is possible to disregard one of the objectives, without the need to change the problem formulation, as well to control the levels of importance of each of the portions of the objective function by assigning higher and lower weights to each other is also possible. For the interior-points-method the control variables are the power provided by the subestation bus (Pg) and the power that flows though the battery system ($Pbat$). Power provided by solar system, power demand and also the costs are parameters previous defined for each time step considered for simulations. In addition, it is important to mention that in the proposed method all the variables are continuous, as well the parameters.

In the present work, the MPOPF proposed was solved using the interior-points using primal-dual formulation, implemented at Matlab. In this case, all the implementation happened by scripts development, requiring the definition of vectors

and matrixes in order to allow the problem dimension compatibility and the derivatives representation, following the steps presented on the flowchart at Figure 21.

4.3 CHAPTER FINAL CONSIDERATIONS

Power system analysis can be performed in different ways. For steady state analysis, the most used is power flow simulation, which consists of calculating voltage magnitude and angle for all buses, considering a defined grid scenario. In this case, the evaluation of the results is looking for a predefined grid state, does not allow to change variables along the time of analysis.

In this way, when the grid operation wants to be optimized, the approach needs to move to optimum power flow, in which the variables can be optimized during the interactions process, changing the scenario in order to reach the objective function.

Thus, the optimum power flow approach defined for the present work consisted of a multiperiod problem, since it will calculate at each interaction all the period considered for simulation, for example, all the 24-hours in a day.

In the case of the MOPF approach, some optimization variables need to be defined, being those ones calculated during the simulation in order to improve the objective function and at the same time respecting the constraints. For the present study, the variables considered are the power provided by the substation bus (Pg) and the power provided or absorbed by the battery system ($Pbat$), in all defined scenarios.

With the formulation of the problem in different approaches, it is necessary to evaluate the best analysis scenarios and the results obtained from simulations.

5 EVALUATION OF PHOTOVOLTAIC SYSTEMS AND BATTERY ENERGY STORAGE SYSTEMS INTO THE POWER GRID

This chapter describes the methodology to evaluate the insertion of photovoltaic systems and battery energy storage systems into the distribution power grid.

In this way, a power flow analysis using OpenDSS was simulated to evaluate grid behavior during one day, allowing to observe the impacts of these elements to distribution power grid operation.

First, the analyses performed will be detailed and then the results for the simulation will be presented, considering an IEEE 13 tests Node Test Feeder.

5.1 POWER FLOW SIMULATIONS

For power flow simulations the OpenDSS software was chosen, as mentioned in chapter 4.

This computational tool model the three-phase power grid, the photovoltaic system, and the BESS, as well as different simulation scenarios, can be established. For these elements, curves that represent their behavior during the simulation period can be provided, in addition to their nominal power values and power factors.

5.1.1 OpenDSS

The electric power distribution system simulator (DSS) was developed by EPRI in 1997, with the proposal to evaluating the impacts of DERs integration with power grids. The software is capable to solve unbalanced and multi-phase power flow, quasi-static time-series (QSTS), fault analysis, harmonic analysis, flicker analysis, multi-period analysis, and linear and non-linear analysis. Moreover, it allows implementing some control strategies for line regulator and capacitor banks, smart inverters, energy storage dispatch, price modeling, distribution management systems and protective devices (EPRI, 2019).

The power flow simulation in OpenDSS does not use a common power flow solution methodology, once it was a consequence of harmonics analysis, owing to the software had been designed to perform distribution system aspects, that included

harmonics studies. The power flow can execute different solution modes including Snapshot, daily or yearly mode, Monte Carlo mode and others because the time period can be defined by the user, depending on the studies it is intending to do. Power flow supports radial or meshed distribution systems simulations, presenting the results of losses, voltages, currents, and flows of each element (DUGAN; MONTENEGRO, 2018).

5.1.2 IEEE 13 Buses Distribution System

For power flow simulations, it was chosen the IEEE 13 Node Test Feeder, which corresponds to a distribution feeder. The schematic draw of the circuit is presented at FIGURE 22**,** in which is possible to notice the existence of a low voltage bus (bus 634) and also part of the system that can be disconnected from the main grid (buses 692 and 675).

FIGURE 22 - IEEE 13 BUSES TEST FEEDER.

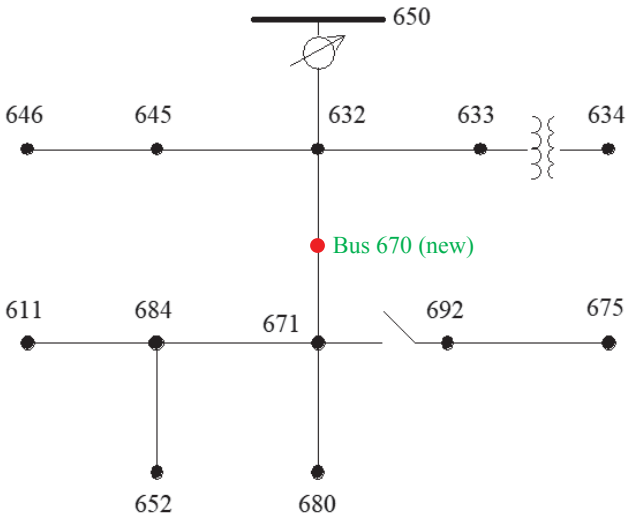

SOURCE: IEEE POWER ENGINEERING SOCIETY (1992).

The corresponding information of circuit elements is provided by the IEEE Power Engineering Society (1992). This circuit represents a radial distribution system with some interesting characteristics:

1) nominal voltage of 4.16kV, that in Brazil, for example, is not a typical voltage level for distribution feeders;
2) presents overhead and underground lines;
3) unbalance spot and distributed load;

4) a voltage regulator on the substation bus.

As there are distributed loads between buses 632 and 671, therefore, to allow the system implementation in a simulation tool, a new bus (670) was added between the buses. This equivalent load was placed in the middle distance between both buses (632 and 671), corresponding to an average of the distributed load effect.

The first simulations developed is a static power flow using OpenDSS, software tool. This simulation was performed to check the modeling of the system since the results could be compared with the ones presented by the IEEE 13 bus system documentation.

In order to enable time serious simulations, load profiles were applied for all loads, based on Yamakawa (2007) measurements realized.

These profiles are split into residential and commercial consumers. For residential consumers, there is another division according to the social classes, presenting different behaviors for low-income, middle incomes, and high incomes consumers. The profiles of each group are presented in FIGURE 23, in which is possible to verify the different behaviors during one day according to each group of consumers. It is important to highlight that the maximum power value can be higher than one, since the load is not normalized but it is in *per unit* (p.u.), being calculated considering a voltage base 13.8 kV and an apparent power base of 70 kVA.

Visualizing the load profiles presented, it is curious that in the peak load of low income profile are higher than the peak of high income profile. This happens since the low income presents a concentrated demand between 7 p.m. and 9 p.m. caused by the intense use of the electric shower. However, the total energy consumption during the day from high income consumers group is higher than the low income ones.

Using the p.u. profile it is possible to keep the installed power of the loads, being the peak of the demand with the same values of the static simulation performed previously.

In this way, four profiles were defined, considering different combinations of consumers percentages, as presented in TABLE 12.

TABLE 12 - DEFINED LOAD PROFILES COMPOSITION.

Load Profiles	Residential			Commercial
	Low Incomes	Middle Incomes	High Incomes	
Profile 1	35%	55%	10%	0%
Profile 2	10%	80%	10%	0%
Profile 3	35%	30%	5%	30%
Profile 4	10%	50%	10%	30%

SOURCE: The Author (2018).

FIGURE 23 - LOAD PROFILES FOR RESIDENTIAL AND COMMERCIAL CONSUMERS IN PU WITH SAME BASE POWER.

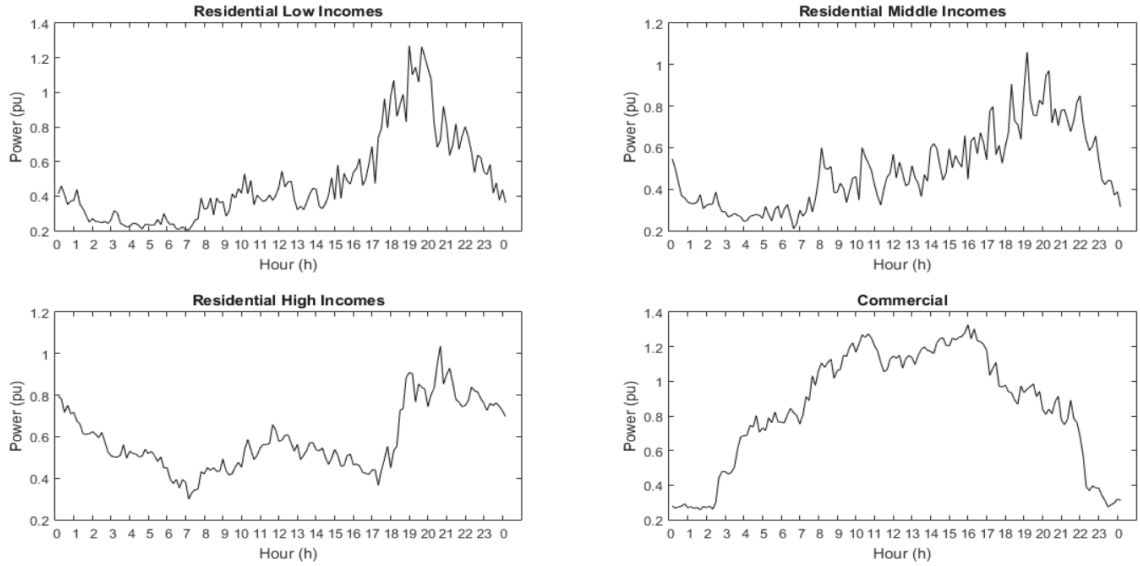

SOURCE: Adapted from Yamakawa (2007).

The four proposed profiles were plotted on FIGURE 24, is possible to notice the differences between them. Profiles 3 and 4 have an increase in the load during the afternoon since it presents the contribution of commercial consumers' behavior. However, all profiles present the peak of the load in the same period, between the 18h and 21h, coinciding with the peak period founded by the majority of distribution players in Brazil.

FIGURE 24 - DEFINED LOAD PROFILE ACCORDING TO EACH COMPOSITION.

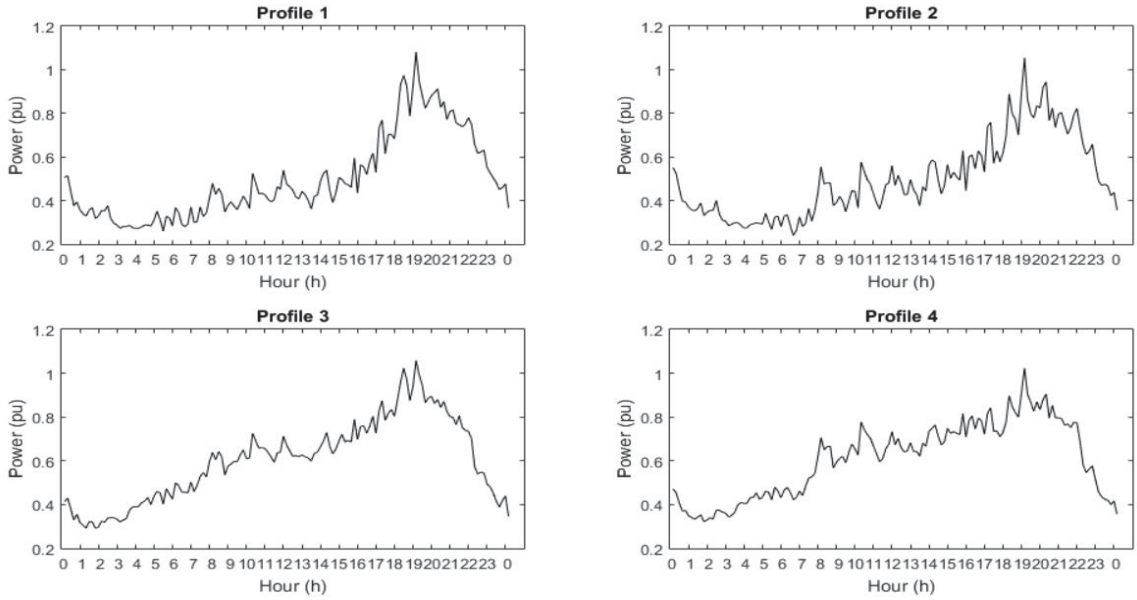

SOURCE: The Author (2019).

5.1.3 Photovoltaic Modeling in OpenDSS

In OpenDSS a photovoltaic system can be defined using the predefined device model PV System, that integrated the PV module and the PV inverter specification.

At FIGURE 25 the PV System model is illustrated. The inputs of the model are irradiance, temperature and power curve dependency between power output and temperature, besides the curve of efficiency and power output relation used to represent the PV inverter behavior.

The output of the complete module presents the active and reactive power from the system, being this last one defined by the information of the power factor (PF) of inverter system operation. However, it is also possible to define a profile of reactive power supplied by the PV system, being in this case, calculated by the power factor of the system inverter (EPRI, 2011a).

For the present work, the PV System receives the irradiation curve obtained from real data acquisition realized on a PV Power Plant installed on Lactec in Curitiba. The measurements were realized from October to December of 2017 and the data obtained corresponds to the output of active power.

FIGURE 25 - BLOCK DIAGRAM REPRESENTATION OF PV SYSTEM ELEMENT ON OPENDSS.

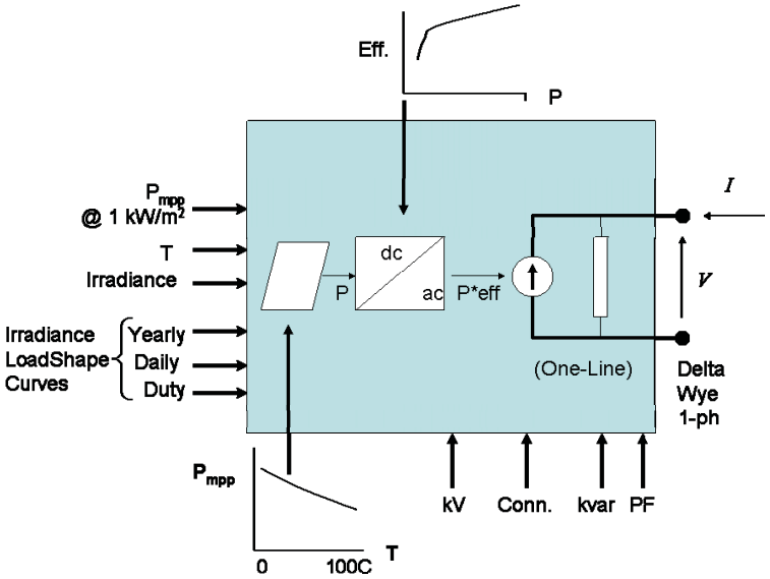

SOURCE: EPRI (2011).

As the output power presents the same behavior of the irradiation in the PV modules, the data was normalized, allowing them to get irradiation behavior. For the simulations, it was considered two different possible irradiations profiles, one corresponding to a clear sky day and another for a cloudy day, as shown in FIGURE 26. In this case the temperature behavior applied at OpenDSS were the same for both situations, considering just the fluctuation due to clouds move in the cloudy sky day scenario.

Another important parameter that was required to insert the PV System element in OpenDSS simulation was PV installed power as well as the nominal power of the PV inverter. This information changes according to the simulations that are planned to be done and how much PV will be considered. One example of PV System parametrization in OpenDSS is given in TABLE 13.

From the implementation at the PV system in OpenDSS, the Pmpp parameter refers to the photovoltaic system installed power, given in kWp, in order that the kVA parameter refers to the PV inverter power, being always higher than the power of the generation system.

FIGURE 26 - IRRADIATION BEHAVIOR FOR A CLEAN SKY AND FOR A CLOUDY DAY.

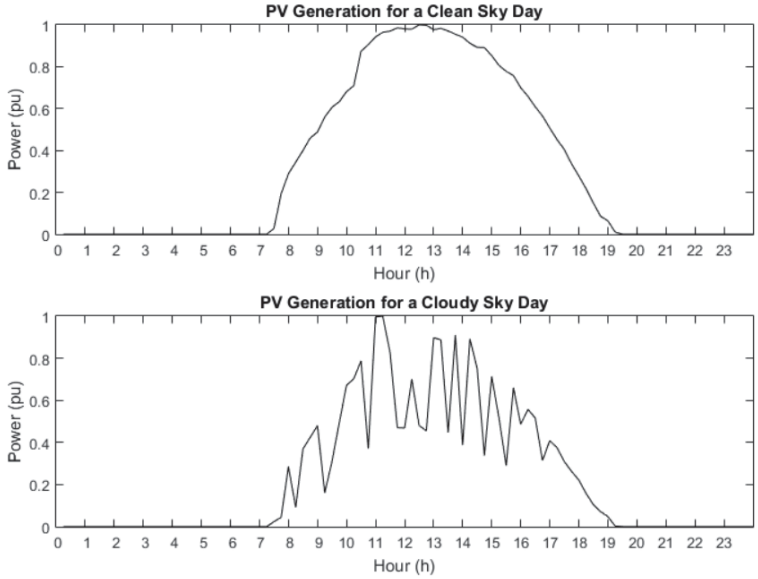

SOURCE: The Author (2019).

In this work, different penetration levels of photovoltaic generation in the distribution feeder was proposed, taking into account different calculation criteria.

TABLE 13 - EXAMPLE OF PV SYSTEM PARAMETRIZATION AT OPENDSS.

```
//-------------------- DECLARING the PV System-----------------------------------------------------------------------
-

// This one is for a Pmpp stated at 25 deg
New XYCurve.MyPvsT npts=4  xarray=[0  25  75  100]  yarray=[1.2 1.0 0.8  0.6]

// efficiency curve is per unit efficiency vs per unit power
New XYCurve.MyEff npts=4  xarray=[0.1  0.2  0.4  1.0]  yarray=[0.86  0.9  0.93  0.97]

// per unit irradiance curve
New Loadshape.MyIrrad npts=96 minterval=15 mult=[File=PV_gen_clean_sky.txt]   // Irradiance for
a clean sky day
!New Loadshape.MyIrrad npts=96 minterval=15 mult=[File=PV_gen_cloud_sky.txt] // Irradiance for
a cloudy sky day

// 24-hr temperature in PV module curve
New Tshape.MyTemp npts=24 interval=1 temp=[25 25 25 25 25 25 25 25 35 40 45 50  60 60  55 40
35  30  25 25 25 25 25 25]

// PV power installed
New PVSystem.PV671 phases=3 bus1=671.1.2.3 kV=4.16  kVA=970  irrad=0.98  Pmpp=808
temperature=25 PF=0.95 %cutin=0.1 %cutout=0.1  effcurve=Myeff  P-TCurve=MyPvsT
Daily=MyIrrad  TDaily=MyTemp
```

Source: The Author (2019).

5.1.4 Photovoltaic Penetration Levels

The amount of penetration of photovoltaic generation in a distribution system can be calculated using different components. In this way, two different criteria were defined based on different parameters: one frequently used in Brazil (called Criteria 1) and other adopted worldwide, for example in Germany (named Criteria 2).

5.1.4.1 Criteria 1 for Photovoltaic Penetration Levels

The Criteria 1 used to calculate the distributed generation penetration level into the power grid is based on percentages of the total load ($\boldsymbol{P_{load}}$) installed on the feeder. Hence, it is needed to define how much can be considered a high or a low level of DG penetration.

In this case, three different levels ($DG_{\boldsymbol{penetration}}$) were defined: 10% (low penetration), 35% (medium penetration) and 70% (high penetration). So, it was possible to calculate the total amount of PV power installed ($P_{generation}$) in the circuit considering each case, using the equation (5.1).

$$DG_{penetration} = \frac{P_{generation}}{P_{load}} * 100\% \quad (5.1)$$

The total load installed on the three phases of the IEEE 13 bus system, corresponds to 3117 kW.

Since this circuit is unbalanced, the amount of power installed in each phase is not the same. Thus, to define the total amount per phase, the values of installed power in each phase were added, resulting in the values presented on TABLE 15, in which is possible to visualize that the lowest load phase corresponds to phase 2.

Using this constraint, 70% of the total load (high penetration scenario) will correspond to 2181.9 kW, being this value, the amount of DG power installed. In this scenario, the total power is equivalent to 61.89% of Phase 1 load, 70% of Phase 2 load and 58.09% of Phase 3 load. The amount of power correspondent to each level of penetration defined is presented in TABLE 14.

TABLE 14 - PV GENERATION POWER LEVELS.

PV Penetration Levels		Distributed Installed Power (kW)
10%	Low	311.7
35%	Medium	1090.95
70%	High	2181.9
Total Installed Load (kW)		3117

SOURCE: The Author (2018).

The PVs generation along the feeder was placed near to the consumer's buses with higher loads, representing the behavior of an urban feeder.

Another constraint defined was that the maximum power generation installed in a bus should not be higher than 70% of the total load existent in the same node (PV Power Max - TABLE 15). So, when 70% of the load power in a certain bus is installed (PV Allocation - TABLE 15), and the sum of the total installed generation does not reach the total amount specified for the penetration level considered, more PV systems should be installed in next bus that presents more load. At the collum named “To be allocated” at TABLE 15 is presented the difference between the total amount that will be allocated and the sum of the total power already allocated on previous buses. This process should be done until all the DG generation power is allocated.

TABLE 15 - PV ALLOCATION TABLE CONSIDERING 70% OF PV PENETRATION.

	Load							PV Power		
Node	**Phase 1**		**Phase 2**		**Phase 3**		**Total 3Phase Bus Power**	**Maximum**	**Alocated (kW)**	**To be alocated**
	kW	kvar	kW	kvar	kW	kvar	kW	kW	**Total = 2181,9 kW**	kW
671	385	220	385	220	385	220	1155	808,5	**808,5**	1373,4
675	485	190	68	60	290	212	843	590,1	**590,1**	783,3
634	160	110	120	90	120	90	400	280	**280**	503,3
670	17	10	66	38	117	68	200	140	**140**	363,3
646	0	0	230	132	0	0	230	161	**161**	202,3
692	0	0	0	0	170	151	170	119	**119**	83,3
645	0	0	170	125	0	0	170	119	**83,3**	0
611	0	0	0	0	170	80	170	119	**0**	0
652	128	86	0	0	0	0	128	89,6	**0**	0
TOTAL	1175	616	1039	665	1252	821	3466	2426,2		

SOURCE: The Author (2018).

5.1.4.2 Criteria 2 for Photovoltaic Penetration Levels

The Criteria 2 is based on a technical characteristic of the distribution feeders. This calculation considers the limit of distributed generation that is supported by the

distribution feeder, evaluating how strong it is, based on the short circuit power (S_{SC}) at the substation bus (CIGRE, 2016).

Considering the short circuit power, it is possible to verify if the grid is strong enough to support the insertion of generation. For this, a relation is defined ($\mathrm{R_{SC}}$), representing the ratio between the short circuit power and the generation installed power.

$$R_{SC} = \frac{S_{SC}}{P_{generation}} \qquad \% \, S_{SC} = \frac{100}{R_{SC}} \tag{5.2}$$

If $\mathrm{R_{SC}} \geq 20$, it means that the grid is strong and can support the amount of $\mathrm{P_{generation}}$. If $20 > \mathrm{R_{SC}} \geq 10$, means that the generation system should be adapted to do not disturbs and affect significantly the grid at the point of connection, and at least, if $\mathrm{R_{SC}} < 10$, the installation is not recommended.

In this way, the maximum penetration of PV for the IEEE 13 bus test feeder was calculated, considering the short circuit power at the substation of 113 MVA. For maximizing the penetration on the distribution system, it was considered $\mathrm{R_{SC}} = 20$, that means 5% of S_{SC}, resulting in 5.65 MW. This value is bigger than the highest PV power calculated when Criteria 1 is considered and also bigger than the total load of the circuit (in this case 81% higher than the installed load).

In this case, a low penetration scenario is not relevant to be simulated, since it will not make any impact on feeder supportability, by the way, that it is strong enough to support more power.

For the allocation of the PV power was not possible to use the same strategy of Criteria 1, since the amount of distributed generation power is higher than the load. Thus, the PV allocation process, in this case, considered that all buses that present load will receive PV generation. The amount of PV in each bus will correspond to the same percentage of load that is installed on the bus in reference to the total load. These percentages values (Percentages of Load in Each Bus – TABLE 16) are applied to the amount of total PV generation, being possible to define the PV power in each bus.

TABLE 16 - PV ALLOCATION FOR CRITERIA 2.

Node	Load					PV Power for each bus (5% Scc)
	Ph-1	Ph-2	Ph-3	Total 3F Bus Power	Percentage of Load in Each Bus (%)	
	kW	kW	kW	kW		kW
671	385	385	385	1155	33,32	**1882,79**
675	485	68	290	843	24,32	**1374,19**
634	160	120	120	400	11,54	**652,05**
670	17	66	117	200	5,77	**326,02**
646	0	230	0	230	6,64	**374,93**
692	0	0	170	170	4,90	**277,12**
645	0	170	0	170	4,90	**277,12**
611	0	0	170	170	4,90	**277,12**
652	128	0	0	128	3,69	**208,66**
TOTAL	1175	**1039**	1252	**3466**	**100%**	**5650**

SOURCE: The Author (2019).

5.1.5 Battery Energy Storage System Modelling in OpenDSS

The storage element is modeled in OpenDSS as a dispatchable generator, that can produce (discharge) or consume (charge) power from the grid (FIGURE 27). Its operation can be done considering a pre-defined profile, in which the power flow is informed for each instant of time, presenting positive values for discharge and negative values for the charge (EPRI, 2011b).

FIGURE 27 - SCHEMATIC OF STORAGE ELEMENT IN OPENDSS.

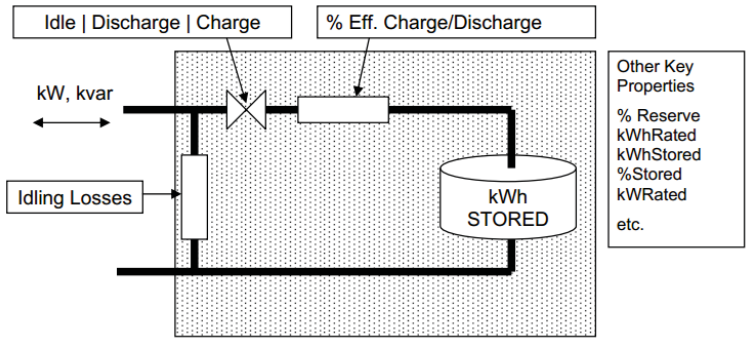

Source: EPRI (2011b).

For the Storage element is possible to include the information of the charge and discharge efficiency, idling losses, depth-of-discharge, internal impedance and reserve of energy. One example of how to configure a storage element in OpenDSS was presented in TABLE 17. Similarly, to what happens with the PV system, the information of “kwrated” and “kwhrated” consists, respectively, on the power and energy of the battery system. The “kW” parameter consists of the nominal power of the

battery inverter. The variable “%stored = 0” needs to be defined in order to define the energy of the battery in t=0.

TABLE 17 - EXAMPLE OF STORAGE PARAMETRIZATION AT OPENDSS.

```
//Loadshape Battery – presents the battery behavior of charge and discharges
New Loadshape.storage npts=24 interval=1 mult=(-0.8 -0.8 -0.8 -0.8 -0.8 -0.8 0 0 0 0 0 0 0 0 0 0 0 0 1
1 1 1 0 0 0)

//Defining the storage element
New Storage.BAT phases=3 Bus1=632.1.2.3 kv=4.16 kW=1000 kwrated=500 kwhrated=2000
pf=0.95  %stored=0 %reserve=0 dispmode=follow daily=storage
```

Source: The Author (2019).

The BESS installed in the present work was considered with 500 kW and 2 MWh.

The battery charge and discharge periods (FIGURE 28) were defined based on some premises:

- the charge of the system will happen during the night period (0h30 to 6h), corresponding to the period with low load. The charge was not considered during the PV generation moment, because the idea is to reduce the load of the feeder during this time;
- the discharge period will happen during the peak load period (18h to 21h), in order to reduce the feeder peak, allowing to postpone investments of the feeder.

FIGURE 28 - BATTERY ENERGY STORAGE BEHAVIOR AT OPENDSS SIMULATIONS.

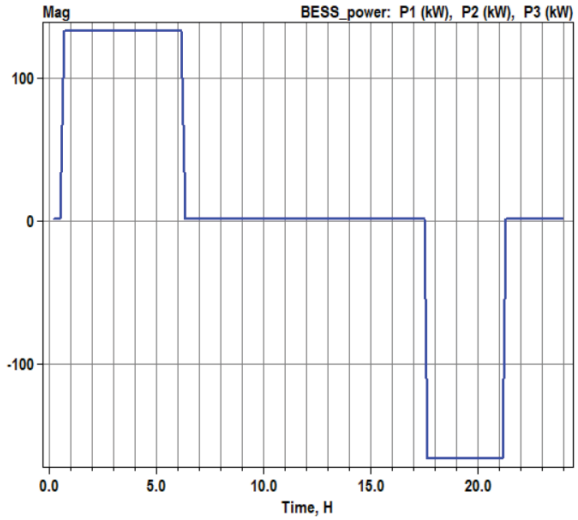

SOURCE: The Author (2019).

5.2 VOLTAGE STABILITY INDEX

Voltage stability is related to the ability of the power system to keep the voltage levels inside of acceptable values (TABLE 3) in all nodes, considering the normal operation and also when it is subject to a disturbance. With the increase of complexity and uncertainties of the power system, the possibility of instability also grows (REIS; BARBOSA, 2006).

The voltage stability analysis can be performed in different approaches considering multi-period analysis or steady-state operation. Most of the time the instability occurs when the circuit is overloaded and the system could not supply enough reactive power.

Considering the insertion of new elements into the power grid, the operation changes constantly, and a voltage stability analysis is recommended, preventing the network from collapsing. In this way, the results of the power flow simulation in OpenDSS were used to calculate the voltage stability index, bespeaking the buses of the grid that present more probability of voltage collapse.

To developed this analysis were used in the formulation presented by Lebid (2017) in his master thesis. In his work, it is detailed the mathematical formulation to calculate the voltage stability index applying two different techniques: index L (SUBRAMANI; DASH; BHASKAR, 2009) and index SI (CHAKRAVORTY; DAS, 2001).

For the present work, the Stability Index (SI) formulation was chosen since this criterion is more recommended for radial distribution systems and requires only the power flow results to the calculation and definition of each bus are more prone to voltage instability (CHAKRAVORTY; DAS, 2001).

Considering the notation of the buses K and M, presented in FIGURE 29, the equation for SI calculation is presented in Eq. (5.3), is calculated for all system buses.

FIGURE 29 - BUSES NOTATION AT THE DISTRIBUTION SYSTEM.

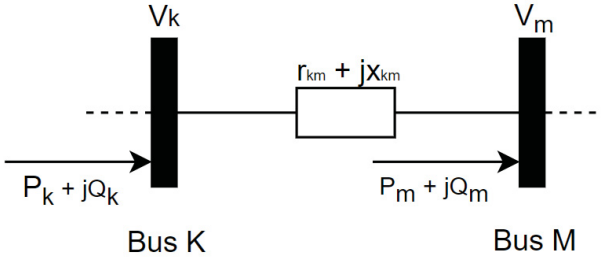

Source: Adapted from Lebid (2017).

$$SI_m = V_k^4 - 4\,V_k^2\,(P_m\,r_{km} + Q_m\,x_{km}) - 4(P_m\,r_{km} + Q_m\,x_{km})^2 \quad (5.3)$$

It is important to highlight that buses that present lower SI are more subject to voltage collapse, and as much closer to zero, more prone it is (CHAKRAVORTY; DAS, 2001).

The SI was calculated for each step of time of power flow simulations, presenting the values of stability index for all buses all day. However, to perform the analysis just the lowest values of each bus during the day should be considered, since they represent the most critical point.

5.3 POWER FLOW SIMULATION SCENARIOS

Some scenarios were defined to analyze different technical impacts using power flow simulations. The scenarios consider different possibilities of penetration levels and criteria of calculation, followed by the insertion of a storage system.

The first step consists of simulating the IEEE 13 bus system with the original system configuration, inserting the four different load curves shown in chapter 5.1.2. In the sequence, the Criteria 1 of penetration level calculation was considered and the system was simulated for low, medium and high PV penetration levels, considering also a clean and a cloudy day of generation. The next step consists in perform the same simulations considering the Criteria 2 of penetration calculation. For both PV criteria cases, the simulations were the same, changing the total amount of PV power generation installed and the placement of the systems. Finally, the battery energy storage system was inserted in different points of the system, in order to evaluate the impacts on grid operation, considering the allocation on substation bus and in the bus with more load. All simulation possibilities are illustrated in FIGURE 30, being chosen one of the load profiles, one of the PV possibilities and one of the possibilities for battery scenarios.

FIGURE 30 - SIMULATIONS POSSIBILITIES.

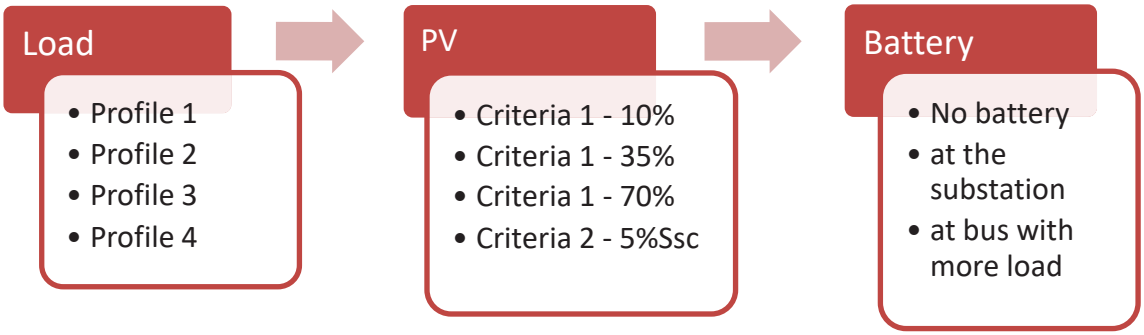

SOURCE: The Author (2019).

After performing the power flow simulations, the electrical technical impacts were evaluated. It was verified the impacts on voltage profile with and without PV and BESS allocation, number of TAP changes, power losses and the total energy that needs to be provided by the utility as well if there is reverse power flow at the substation. Moreover, the results of power flow simulations were used to calculate the voltage stability index of all buses, allowing them to analyze the voltage stability of the system under different operation conditions.

5.4 ANALYZES OF ELECTRICAL TECHNICAL IMPACTS

Considering, initially, the original IEEE 13 buses circuit, that means, without DG and BESS insertion, the application of the load profiles were done in different scenarios, being applied one profile each time.

The active power flow at the substation bus is presented at FIGURE 31, in which is possible to visualize the unbalancing of system loading (black line – phase 1, red line – phase 2 and blue line – phase 3), as well the peak of load at 19h.

The power flow results are presented at TABLE 18, which compared the results of voltage levels, tap changes, total losses and the total energy of the circuit during one day.

FIGURE 31 – INJECTION OF ACTIVE POWER FLOW FROM SUBSTATION CONSIDERING LOAD PROFILE 4.

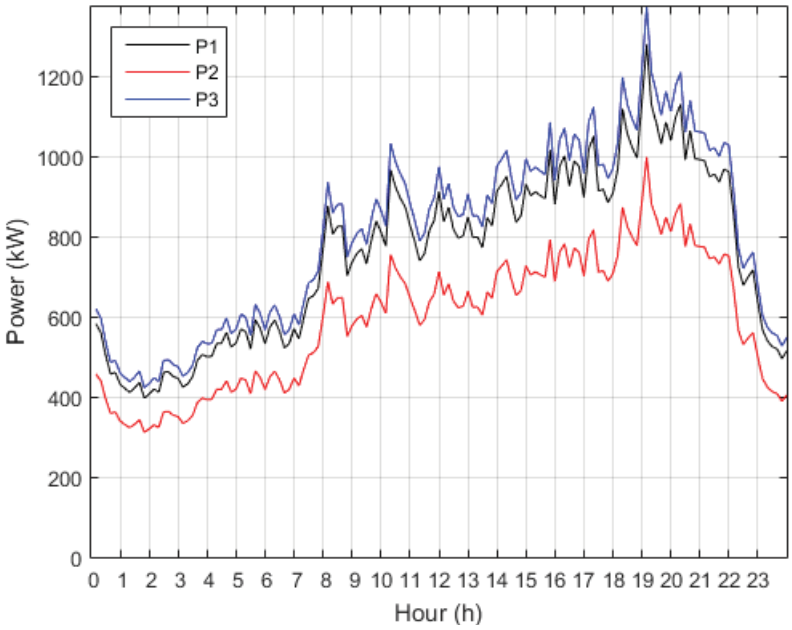

SOURCE: The Author (2019).

Looking at the results is possible to conclude that voltage levels do not present significant variations, once it happens only after the third decimal place. The minimum voltage of 0.94 pu happens at 680 bus, that corresponds to a bus without any load and at the end of the main feeder, otherwise, in all other buses, the minimum voltage level corresponds to 0.96 pu, being over the acceptable values for appropriate voltage level (over 0.93 pu).

TABLE 18 - RESULTS WHEN APPLIED THE DIFFERENT LOAD PROFILES COMPOSITIONS.

Analysis	**Results**			
	Profile 1	**Profile 2**	**Profile 3**	**Profile 4**
Voltage				
Max PU Voltage (pu)	1,048	1,047	1,048	1,047
Min PU Voltage (pu)	0,947	0,948	0,944	0,948
TAP Changes				
Phase 1 - Number of Changes	10	12	10	9
Phase 2 - Number of Changes	5	5	6	5
Phase 3 - Number of Changes	11	12	11	11
Losses				
Total Power Losses (kWh)	715	723	1029	1034
Total Energy (kWh)	42042	42222	50963	51541
Total Reactive Energy (kvarh)	10500	10580	16765	17124

SOURCE: The Author (2018).

Related to the tap changes of the voltage regulator installed at the substation, it is possible to see that the number of changes does not change significantly between the different profile scenarios. For each case, the time when the changes happen is noted the same, mainly in the period during the day (6h to 17h). From 17h to midnight almost all the profiles present the same tap changes behavior since the load increase to the peak time presents the same characteristics.

When profile 4 is considered, the number of tap changes does not change more than in other cases, even presenting the highest load demand. This happens because in this profile the load increases slowly during the day, do not presenting so abrupt variations.

Analyzing the power losses it is possible to verify that it is lower for profile 1 since it presents low energy consumption during the day. This happens due to the fact that this profile presents the lowest energy consumption during the day.

Considering these results as a base case, since it represents the original system composition, the results of the next scenarios will be compared with these ones, in order to evaluate the grid operation behavior incorporating the insertion of new elements.

5.4.1 Impacts in Number of Tap Changes

Considering the criteria 1 of PV penetration levels, the number of OLTC TAP changes varies according to the amount of PV, and also with the load profile that is being considered. Characteristics as weather behavior, that impacts on PV generation, will also change the number of TAP changes performed by the OLTC transformer, being higher when a cloudy sky is considered in comparison with a clear sky day of generation.

For the analysis, all the PV generators were considered with the same phases that exist in the point of the connection, is not considered three phases in all cases, since changes on circuit configuration are not considered. Another important information for the analysis is that all PV generators were considered with unit power factor, injecting the maximum active power, corresponding to the worst scenario for grid operation, due to the increase of power losses and none reactive power supply.

Therefore, applying all possible PV penetration levels and the clean and cloudy sky day of generation profiles, the changes in the number of tap changes increased as much increased the penetration level.

At TABLE 19 is presented the number of tap changes considering three different scenarios: initially without distributed generation and after the scenarios with high penetration considering criteria 1. The PV penetration considered corresponds to 70% of the total installed load, being this one divided into two cases with a clean and cloudy radiation profile. This divided was used, in order to evaluate the impacts of a more fluctuating generation in the number of tap changes.

The scenarios of 10 and 35% of penetration do not present significant changes in the number of tap changes, mainly when 10% is considered, presenting, in this case, the same values of the scenario without DG.

TABLE 19 - NUMBER OF TAP CHANGES WITHOUT DG AND WITH HIGH PENETRATION SCENARIO.

Number of TAP Changes	without DG	70% Clean Generation	70% Cloudy Generation
Profile 1 - Phase A	13	14	15
Profile 1 - Phase B	7	9	11
Profile 1 - Phase C	13	15	15
Profile 2 - Phase A	15	15	16
Profile 2 - Phase B	6	11	15
Profile 2 - Phase C	14	18	19
Profile 3 - Phase A	10	10	14
Profile 3 - Phase B	6	8	10
Profile 3 - Phase C	11	13	15
Profile 4 - Phase A	11	11	15
Profile 4 - Phase B	5	7	9
Profile 4 - Phase C	9	13	17

Source: The Author (2019).

The tap changes behavior illustrated in FIGURE 32, FIGURE 33 and FIGURE 34 consider the load profile 2, to each phase, respectively. The analysis will be realized considering load profile 2 that presented the highest total number of tap changes. In those figures are illustrated the tap changes in the scenario without distributed generation for each phase, and when 70% of penetration is considered for clean and cloudy sky day. Additionally, the scenario with a 5% Ssc of PV penetration for a clear sky day is also showed.

For the representation of tap changes behavior, the output voltage of the OLTC is monitored. In this case, the voltage steps represent the tap changing for each phase.

From the graphics, it is possible to visualize the increase of the number of TAP changes in all phases, in comparison with the case without distributed generation, as much higher is the PV penetration and also when a cloudy sky day of generation is considered.

FIGURE 32 - TAP CHANGES OF VOLTAGE REGULATOR ON PHASE 1 WHEN PROFILE 2 IS APPLIED WITHOUT DISTRIBUTED GENERATOR AND WITH 70% OF PV AND 5% OF SHORT CIRCUIT POWER.

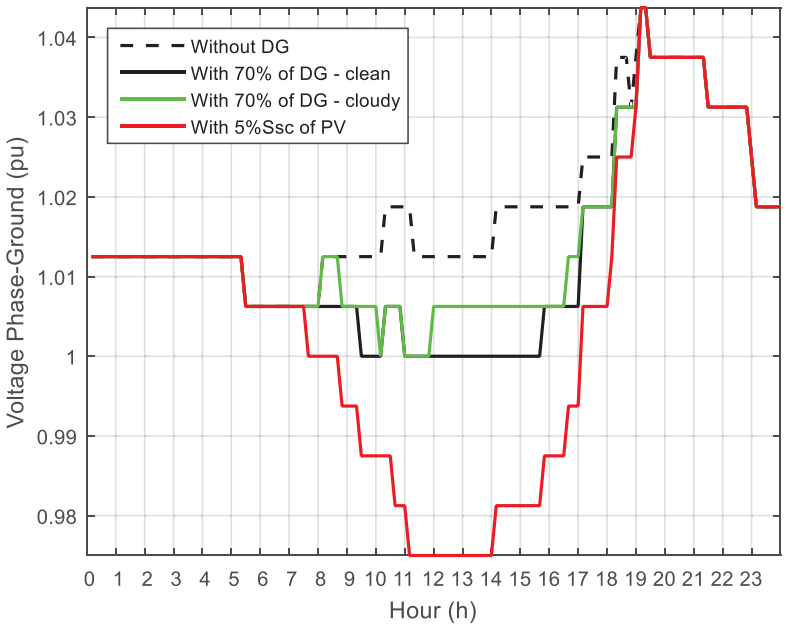

SOURCE: The Author (2019).

FIGURE 33 - TAP CHANGES OF VOLTAGE REGULATOR ON PHASE 2 WHEN PROFILE 2 IS APPLIED WITHOUT DISTRIBUTED GENERATOR AND WITH 70% OF PV AND 5% OF SHORT CIRCUIT POWER.

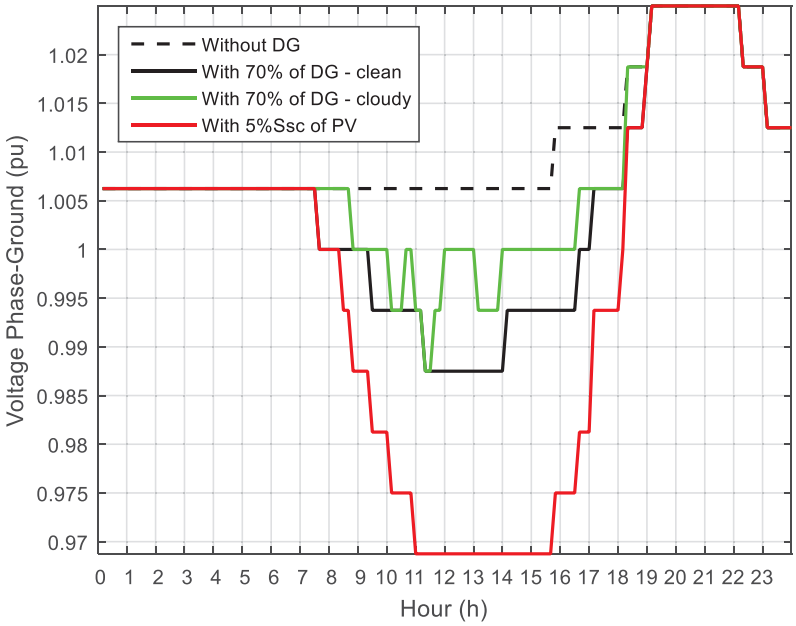

SOURCE: The Author (2019).

FIGURE 34 - TAP CHANGES OF VOLTAGE REGULATOR ON PHASE 3 WHEN PROFILE 2 IS APPLIED WITHOUT DISTRIBUTED GENERATOR AND WITH 70% OF PV AND 5% OF SHORT CIRCUIT POWER.

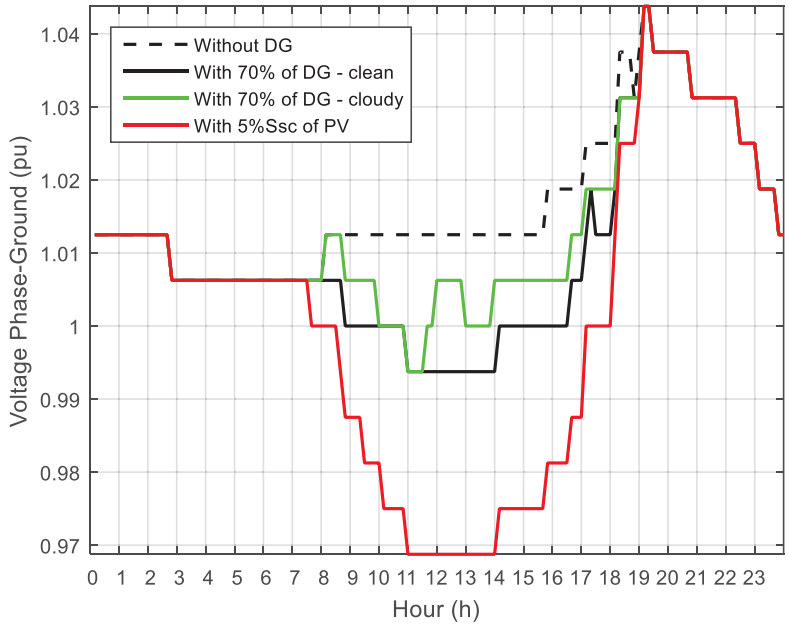

SOURCE: The Author (2019).

The number of TAP changes varies also if a cloudy or clean radiation profile is considered. When there is a cloudy sky day of generation, the number of TAP changes increase in comparison to the scenario with clean sky generation, considering the same penetration level. This happens due to generation fluctuation that forces the

voltage regulator to actuate more times in order to keep the voltages levels inside the limits.

In the scenario with the highest penetration level (5% of Short Circuit Power) and a cloudy sky day of generation, the highest number of tap changes is founded (FIGURE 35). In this scenario, when load profile 2 is considered, it was registered 33 tap changes on phase 1, 33 on phase 2 and 47 on phase 3, in contrast to 20 on phase 1, 17 on phase 2 and 24 for phase 3, when a clean sky is considered for same PV penetration level.

FIGURE 35 - TAP CHANGES OF VOLTAGE REGULATOR ON PHASE 3 WHEN PROFILE 2 IS APPLIED CONSIDERING DIFFERENT PENETRATION LEVELS AND GENERATION PROFILES.

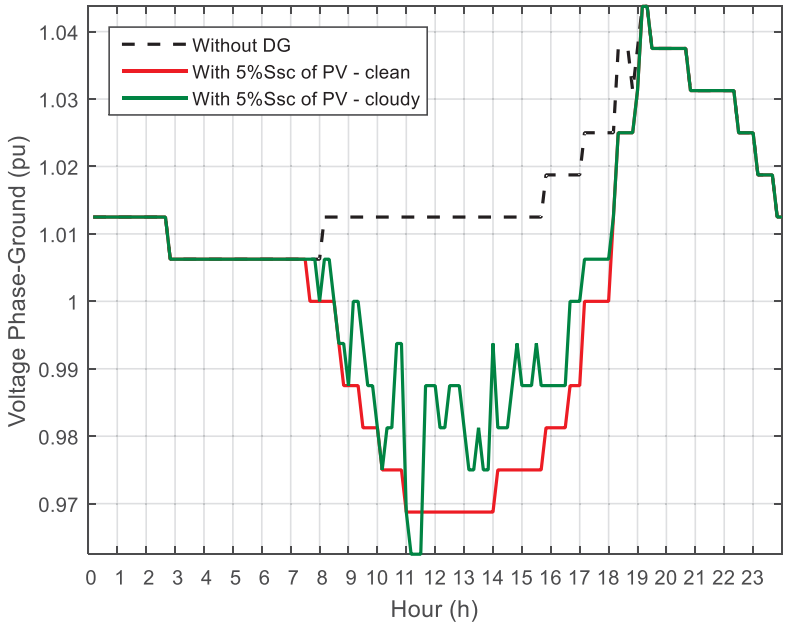

SOURCE: The Author (2019).

When high levels of PV penetration are considered, reverse power flow at the substation level starts to happen. Considering Criteria 1 of penetration level, just in the case of 70% of PV, reverse power flow at substation level starts to happen, even in a cloudy sky day of generation (FIGURE 36). However, when 5% of Ssc of PV is considered (FIGURE 37), the reverse power flow at the substation bus is higher and fluctuates significantly in a cloudy sky day of generation.

It is important to highlight that the OLTC is placed at the substation bus and each TAP change corresponds to a change of 0.005 pu (0.5%).

In the sequence, the same analysis was developed considering also the insertion of the battery energy storage system. In the first moment, the BESS was

placed at the substation bus (bus 632), being in the sequence placed at the bus with more load connected (bus 671).

FIGURE 36 - THREE PHASE POWER INJECTION AT SUBSTATION WITH 70% OF PV PENETRATION FOR A CLOUDY SKY DAY, CONSIDERING LOAD PROFILE 2.

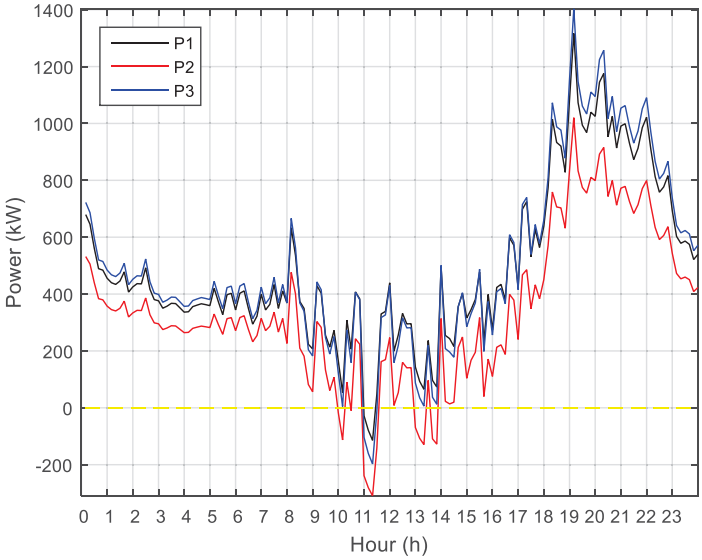

SOURCE: The Author (2019).

FIGURE 37 - THREE PHASE POWER INJECTION AT SUBSTATION WITH 5% Ssc OF PV PENETRATION FOR A CLOUDY SKY DAY, CONSIDERING LOAD PROFILE 2.

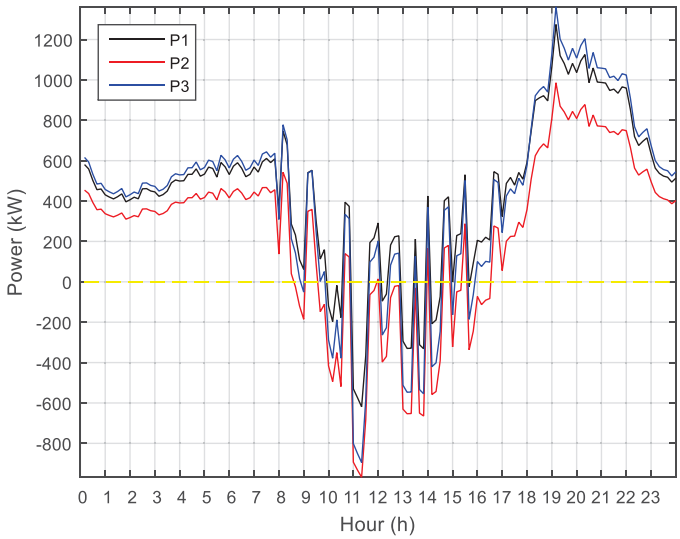

SOURCE: The Author (2019).

When the Battery Energy Storage System is installed at substation bus (bus 632), the battery will be charging during the night, from midnight to 6:00 a.m. and will discharge during the peak time, from 7:00 p.m. to 9:00 p.m, so as not to influence the impact of solar generation during the day, allowing the analysis of a more critical scenario. In this way, at FIGURE 38, FIGURE 39 and FIGURE 40 it is represented the

power injection from substation for each phase, considering three different scenarios: without distributed generation and battery system, in the sequence, inserting only the battery system and later, the insertion of 70% of PV penetration in addition to the battery system.

FIGURE 38 - POWER INJECTION AT PHASE 1 FROM BUS 632 CONSIDERING LOAD PROFILE 2 AND THREE DIFFERENT SCENARIOS WITH AND WITHOUT PV AND BESS AT BUS 632.

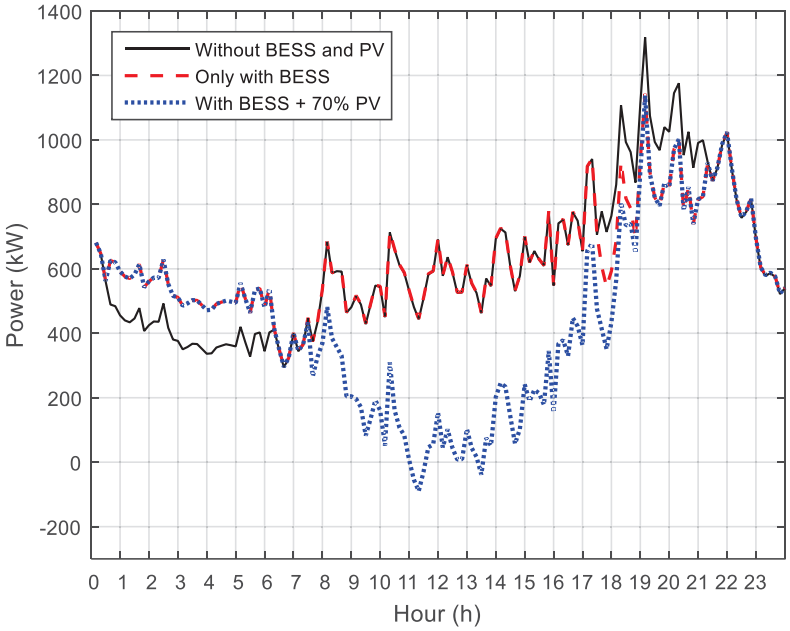

SOURCE: The Author (2019).

FIGURE 39 - POWER INJECTION AT PHASE 2 FROM BUS 632 CONSIDERING LOAD PROFILE 2 AND THREE DIFFERENT SCENARIOS WITH AND WITHOUT PV AND BESS AT BUS 632.

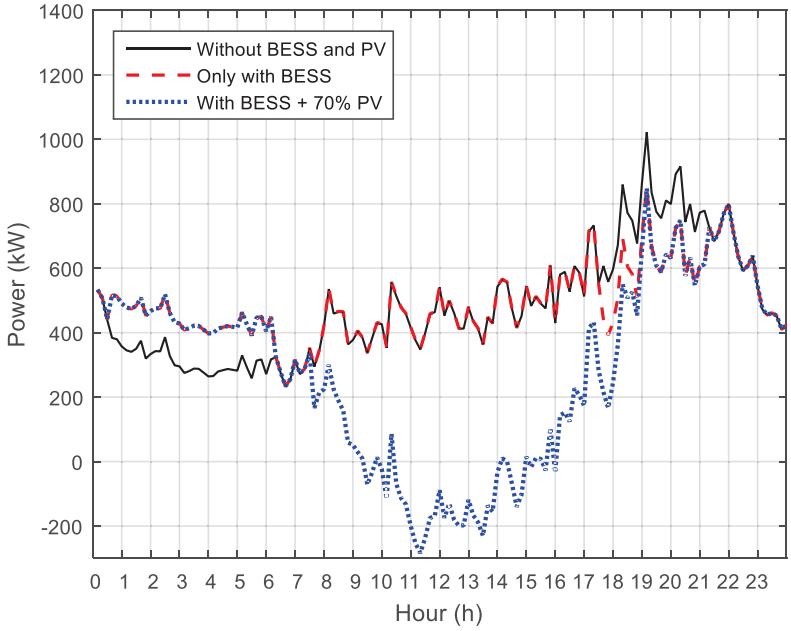

SOURCE: The Author (2019).

FIGURE 40 - POWER INJECTION AT PHASE 3 FROM BUS 632 CONSIDERING LOAD PROFILE 2 AND THREE DIFFERENT SCENARIOS WITH AND WITHOUT PV AND BESS AT BUS 632.

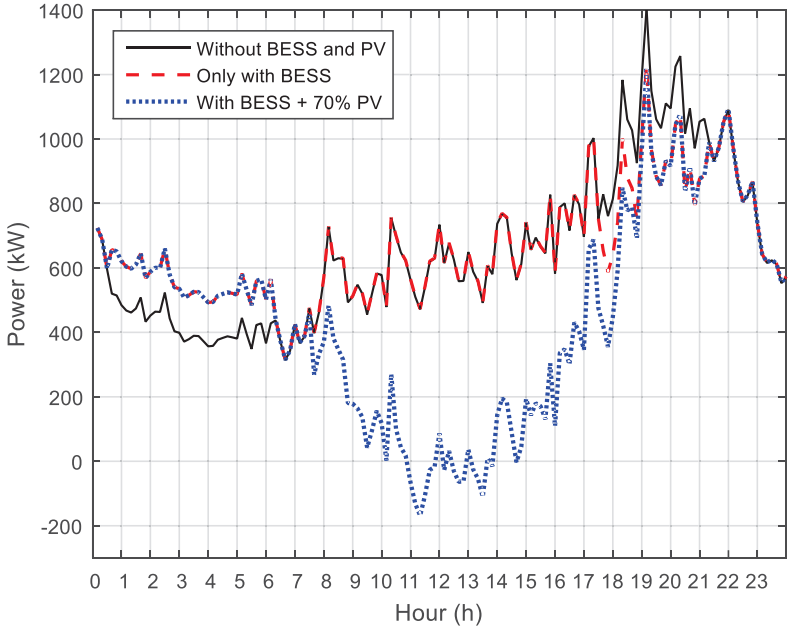

SOURCE: The Author (2019).

From FIGURE 38, FIGURE 39 and FIGURE 40 it is possible to visualize the load increase during the night due to the charge of the battery and the reduce of load peak demand during the peak time attributable to the discharge of the BESS. In these periods it possible to verify the changes on tap caused by the battery operation. At FIGURE 41, FIGURE 42 and FIGURE 43 are presented the voltage regulator tap changes behavior for the cases without PV and BESS, placed at BUS 632, just with PV penetration and only with BESS, for phases 1, 2 and 3 respectively.

Considering the BESS operation, it is possible to verify that the tap changes during the night (midnight to 6:00 a.m.) for phases 1 and 3 happen lately, passing from the middle of this period to happen after 6:00 a.m. This happened due to the increase of load during this period, reducing load variation in subsequent moments. During the PV generation time, it is possible to see that, as the BESS is not operating, the tap changes behavior was not affected.

However, during the peak load time, the tap changes in low levels in comparison with the cases without the storage system, reducing the number of tap positions changes. This happens since part of the load demand is supplied by the BESS, relieving the load provided by the substation, as well as providing a portion of reactive power, since the BESS is operating at a power factor of 0.95, thus contributing to raising the voltage on the substation bus. When BESS is placed at the substation bus, the location of the system is downstream to the voltage regulator. Due to this

position, the BESS can contribute to peak time, reducing the tap changes of the voltage regulator.

FIGURE 41 - TAP CHANGES OF VOLTAGE REGULATOR ON PHASE 1 WHEN PROFILE 2 IS APPLIED CONSIDERING THE INSERTION OF PV AND BESS AT BUS 632.

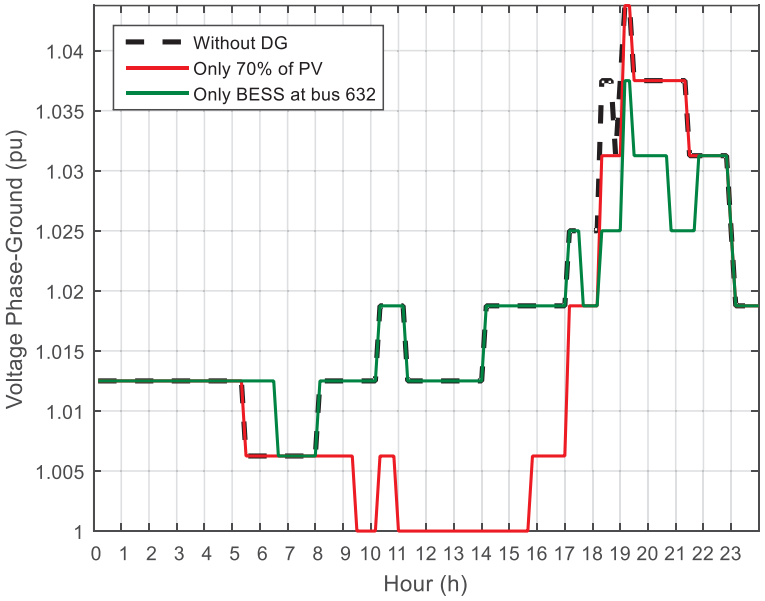

SOURCE: The Author (2019).

FIGURE 42 - TAP CHANGES OF VOLTAGE REGULATOR ON PHASE 2 WHEN PROFILE 2 IS APPLIED CONSIDERING THE INSERTION OF PV AND BESS AT BUS 632.

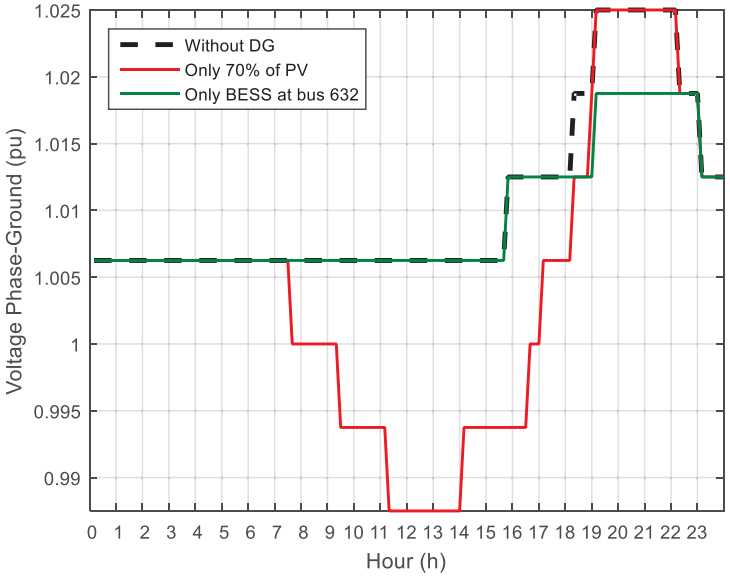

SOURCE: The Author (2019).

FIGURE 43 - TAP CHANGES OF VOLTAGE REGULATOR ON PHASE 3 WHEN PROFILE 2 IS APPLIED CONSIDERING THE INSERTION OF PV AND BESS AT BUS 632.

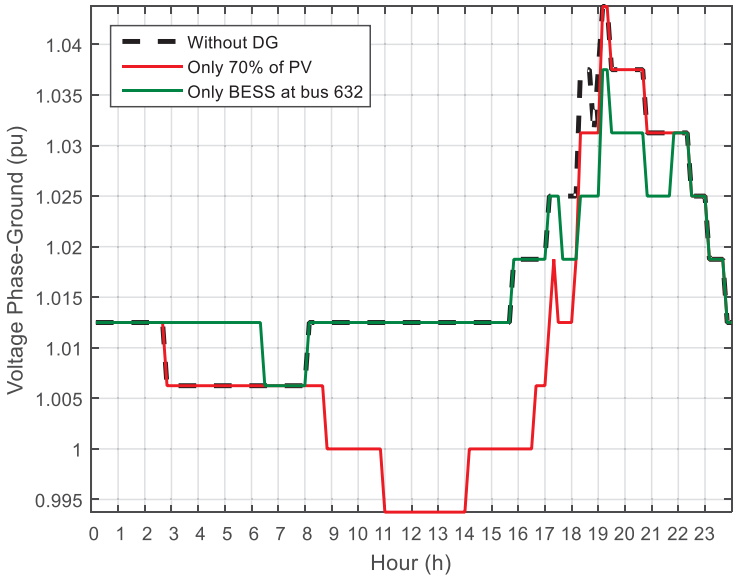

SOURCE: The Author (2019).

In order to compare the tap changes behavior considering the insertion of the storage in addition to different penetration levels of photovoltaic generation, FIGURE 44 compares all the possible cases. It is possible to verify that the battery changes the number of tap changes during the peak time, does not affecting the number of tap changes during the PV generation time since in this period the BESS will be in standby mode.

Performing the simulation with the BESS placed close to the bus with more load (bus 671), it was verified that in terms of the number of tap changes there were no changes in comparison with the case in which the BESS is placed on substation bus.

For all previous simulations, the power factor of BESS was defined as 0.95 for charge and discharge. Changing the BESS at the bus 632 power factor during the discharge it is possible to verify how the provision of reactive power can affect the tap positions of the voltage regulator during peak time.

FIGURE 44 - TAP CHANGES OF VOLTAGE REGULATOR ON PHASE 1 WHEN PROFILE 2 IS APPLIED CONSIDERING DIFFERENT PV PENETRATION IN ADDITION TO BESS AT BUS 632.

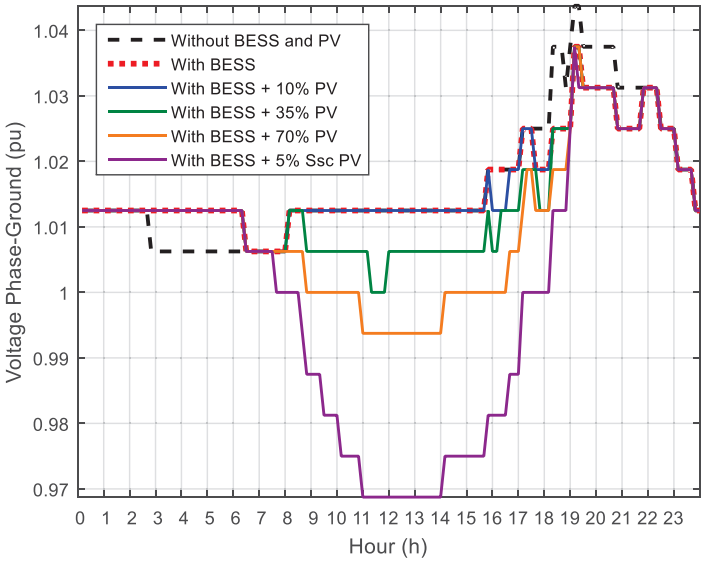

SOURCE: The Author (2019).

At FIGURE 45 the tap changes behavior of the voltage regulator is presented considering the power factor values of 0.5, 0.7, 0.9 and 0.95 for the BESS during the discharge (highlighted at FIGURE 45) and the power factor of 0.95 during the charge period. It is possible to visualize that as much reactive power is supplied by the storage system, the tap of the voltage regulator starts to present lower positions since part of voltage support to the grid is being provided by the reactive power from the BESS. In this way, it is visible that applying a power factor control would be possible to reduce the number of tap changes.

FIGURE 45 - TAP CHANGES OF VOLTAGE REGULATOR ON PHASE 3 WHEN PROFILE 2 IS APPLIED CONSIDERING DIFFERENT BESS POWER FACTORS.

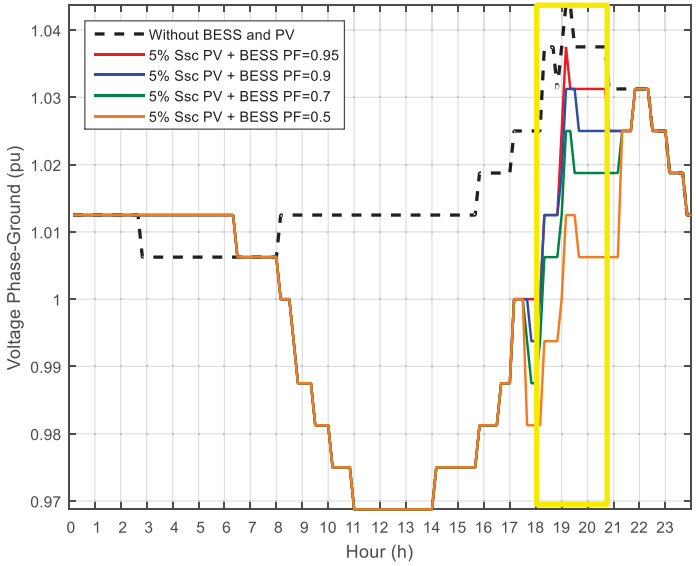

SOURCE: The Author (2019).

5.4.2 Impacts on Power Losses

For the analysis of power losses on the system during the entire day of the simulation, different scenario compositions were defined, in order to verify the power losses behavior in different conditions.

The results of the simulations are shown in TABLE 20. They were considered: the initial scenario, without PV and BESS, and after different PV penetration levels followed by the insertion of the storage system considering two different positions, at the substation bus (bus 632) and close to the bus with more load (bus 671).

From the results, it is possible to verify that the minimum power losses values for all load profiles happened when there are 70% of PV penetration and BESS placed at bus 671. The reason why this happens is because of the local load supply, since much of the demand is being attended locally and, with the battery located near the highest concentration of load, it contributes more effectively to reduce the peak load on the system, thus reducing the power flow from the substation to the loads.

TABLE 20 - POWER LOSSES CONSIDERING DIFFERENT PV PENETRATIONS AND BATTERY ALLOCATIONS FOR ALL THE LOAD PROFILES.

			Energy Losses (kWh)			
Scenario Composition			Profile 1	Profile 2	Profile 3	Profile 4
Without GD and BESS			735	723	1029	1034
Only PV	Clean Sky	10% GD	697	683	971	973
		35% GD	603	581	804	798
		70% GD	555	525	681	666
		5%Ssc GD	835	780	724	683
	Cloudy Sky	10% GD	708	694	987	990
		35% GD	633	614	861	859
		70% GD	582	558	757	748
		5%Ssc GD	664	623	669	642
BESS at 632 bus	Clean Sky	10% GD	709	706	987	1004
		35% GD	617	606	822	830
		70% GD	571	551	702	704
		5%Ssc GD	858	813	752	725
BESS at 671 bus	Clean Sky	10% GD	655	651	934	948
		35% GD	564	551	769	774
		70% GD	517	496	648	645
		5%Ssc GD	803	758	698	667

SOURCE: The Author (2019).

However, when the PV generation is higher, 5% Ssc, the total power loss increases rather than decreases. This happens due to the reverse power flow during the time of solar generation, increasing the flow of energy through the lines, and consequently, increasing power losses.

In order to enable a better comparison of the losses when different scenarios are considered, the graphic presented in FIGURE 46 shows the behavior when load profile 1 is considered. In the graphic is possible to verify the decrease of total power loss as much the PV penetration increases considering criteria 1 of calculation. Yet, when the PV generation increase to 5% of Ssc the total power loss also increases, present for most of the scenarios the highest values.

Yet, when load profile 4 is considered, the total power loss with 5% Ssc of PV presents values lower than when 10% or 35% of PV are considered, as presented on FIGURE 47. This happens because of the load profile behavior. Looking again for the load curves presented in FIGURE 24 is possible to see the differences related to the increase of the load during the solar generation period. As much load there is in the period, lower is the reverse power flow, and hence, lower are the power losses.

FIGURE 46 - ENERGY LOSSES FOR DIFFERENT SCENARIOS WHEN LOAD PROFILE 1 IS CONSIDERED.

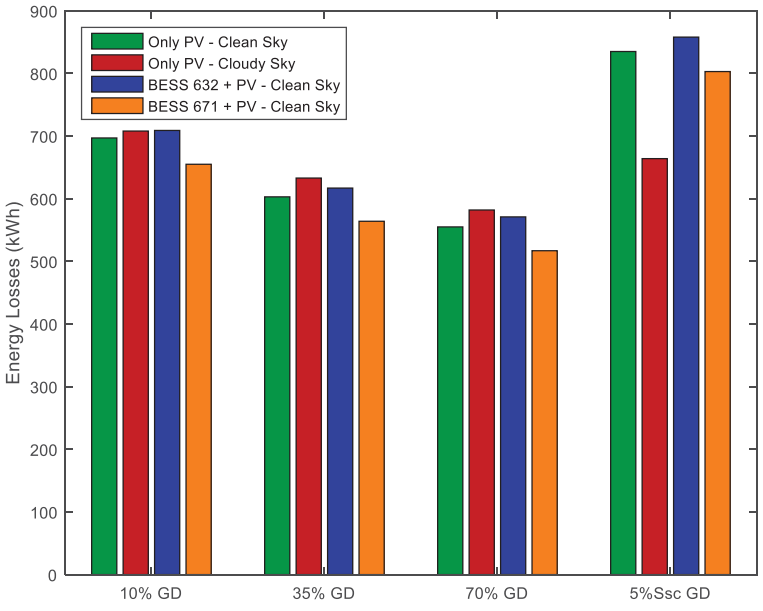

SOURCE: The Author (2019).

FIGURE 47 - ENERGY LOSSES FOR DIFFERENT SCENARIOS WHEN LOAD PROFILE 4 IS CONSIDERED.

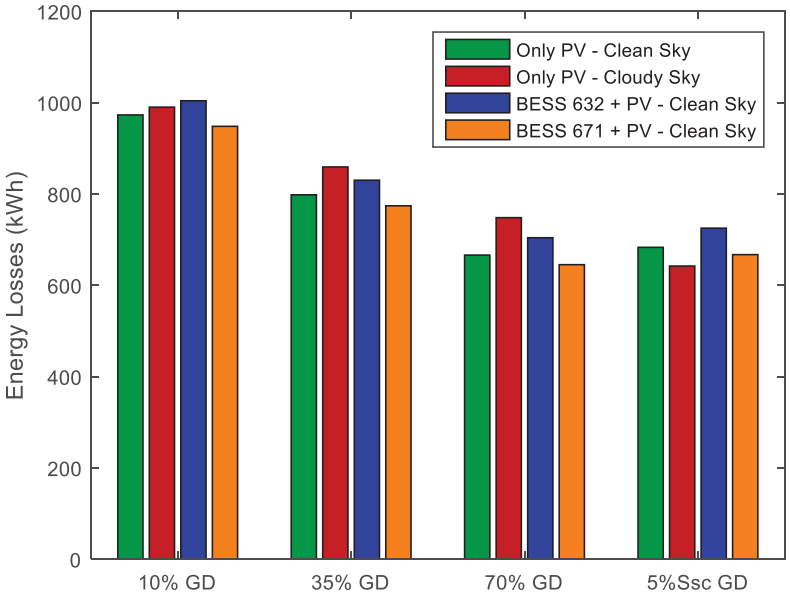

SOURCE: The Author (2019).

From the results is also possible to verify the influence of the cloudy sky day of generation in power losses, increasing the power losses in comparison with a day with a clear sky. This occurs because the generation is lower and thus low part of the load can be supplied locally, in cases when criteria 1 of PV is considered.

Another point from the results to be highlighted is the influence of battery position on power losses. In case the battery is placed outside of the substation and be close to the most loaded bus, the power losses are lower than in case when the battery is placed at the substation bus. The reason is the same from the reverse power flow, as low power will be flowing on the system.

5.4.3 Impacts on Voltage Behavior and Voltage Stability

The voltage behavior was analyzed for all buses of the IEEE 13 bus system. In this case, the most important information consisted in check if the voltage limits were reached.

Analyzing all buses, none of them reaches the limits, considering all the different simulations scenarios. This happens due to voltage regulator actuation (OLTC), which presents the tap changes during the day, as presented before.

The voltage varies at a maximum of 0.72% between all maximum values and the same percentage was found for minimum voltage values comparison.

During the moments that have provisioning of power, either by the PV or by the battery discharge, the voltage profile tends to increase and, when there is an increase in load, due to the battery's charge, the voltage profile tends to decrease.

Considering all possible scenarios, the voltage stability index was calculated, for all buses and for all time steps.

As the voltage stability concept used to calculate the index considers that as much close to zero, more unstable is the bus, for the analysis, it was looked for the minimum values presented by each bus during the entire day.

The comparison between some scenarios will be presented in FIGURE 48. Profile 4 was considered to illustrate because it does not present significant changes in comparison with the results founded when other profiles were considered.

FIGURE 48 is presented the stability index of all buses when different penetration levels of PV are considered, using criteria 1 for the calculation. In this graphic is possible to visualize that as much increase the PV penetration, better is the stability index for some buses, as 680 and 684, by the way, that some buses had present no changes.

FIGURE 48 – STABILITY INDEX WHEN DIFFERENT PENETRATION LEVELS ARE CONSIDERED PROFILE 4.

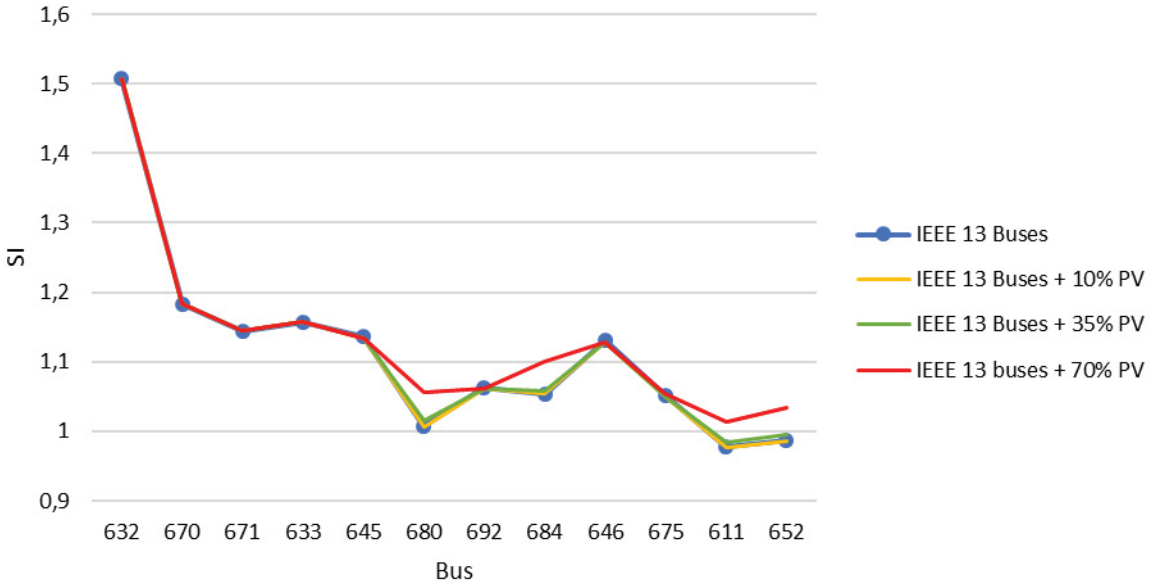

SOURCE: The Author (2019).

In order to compare the voltage stability with the insertion of the BESS in different positions, the indexes were plotted at FIGURE 49. When the battery is placed at the bus with more load (bus 671), the index increases for the buses downstream,

but for the buses upstream, the index decreases. However, even the buses that decrease the stability index, they do not present problems of instability.

FIGURE 49 - STABILITY INDEX WHEN THE BESS IS CONSIDERED WITH AND WITHOUT THE PV PENETRATION - PROFILE 4.

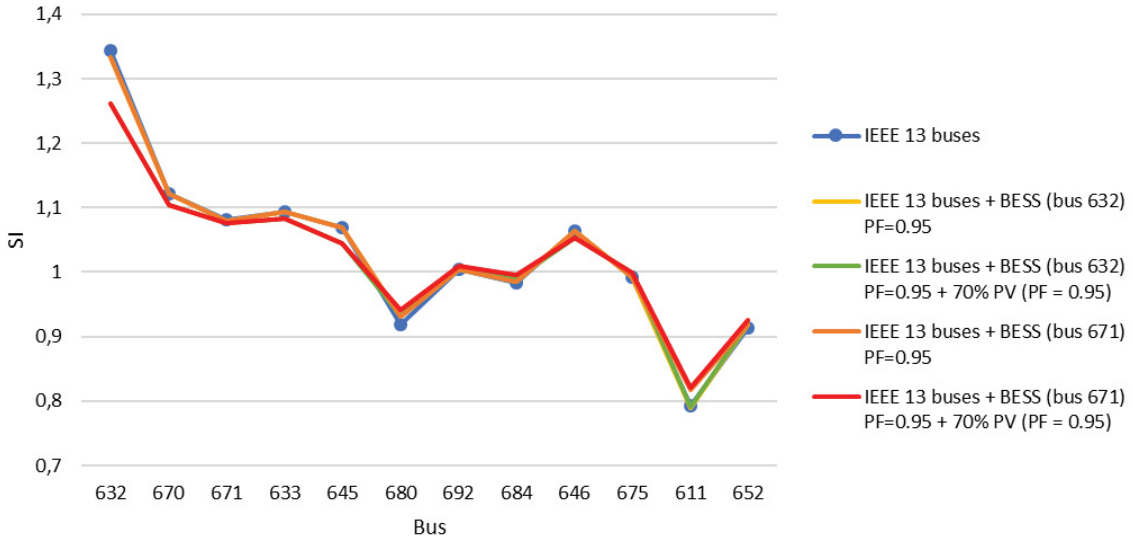

SOURCE: The Author (2019).

Considering the highest PV penetration level of 5% of Ssc, the voltage stability indexes are presented in FIGURE 50, with and without the allocation of the BESS. In this case, is clearly seen that the indexes of the buses downstream of the BESS location present better results than in the case without BESS. Yet, the values of the indexes on buses close to the substation are worse than in the case without PV and BESS.

FIGURE 50 - STABILITY INDEX WHEN 5% OF PV PENETRATION LEVEL IS CONSIDERED.

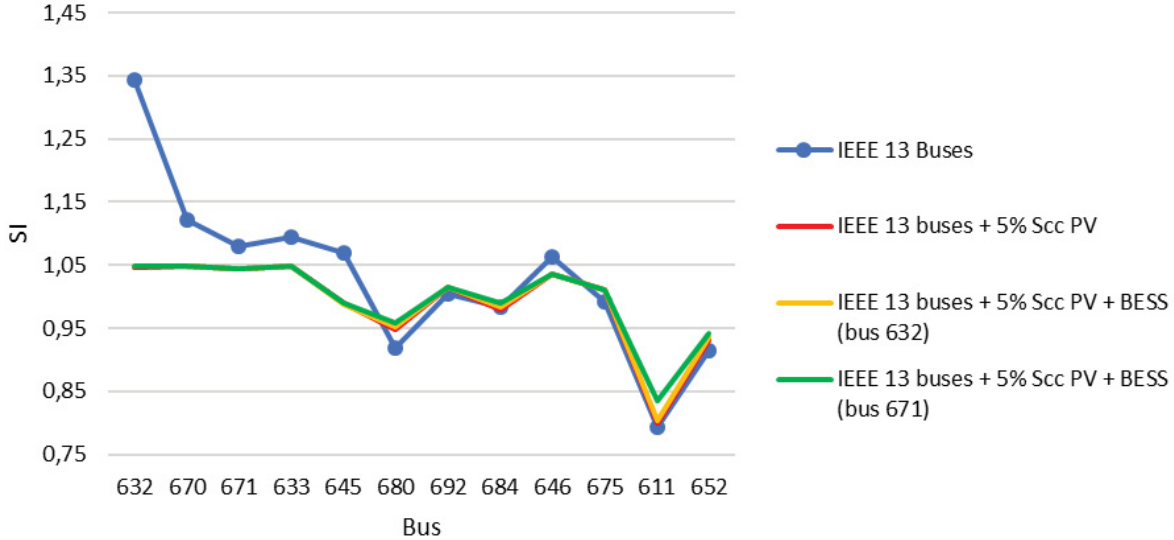

SOURCE: The Author (2019).

Calculating the voltage stability indexes in cases with and without the voltage regulator operation, it is possible to verify how much the actuation of the OLTC can contribute to increasing the stability indexes at all buses, as shown at FIGURE 51. This happens because the equipment guarantees that voltage limits will be respected. Without the operation of the OLTC, none of the buses reaches the instability, however, in this case, the buses begin more prone to instability.

In all cases, the bus nearer to the instability is the bus 611. This bus is connected just in a single phase in the middle of the feeder, while the rest of the circuits are connected by a two or three-phase connection. On the other hand, the strongest bus is 632, placed very close to the output of the substation, being directly affected by the voltage regulator operation.

FIGURE 51 - STABILITY INDEX IN CASES WITH PV AND BESS WITH AND WITHOUT THE OLTC OPERATION.

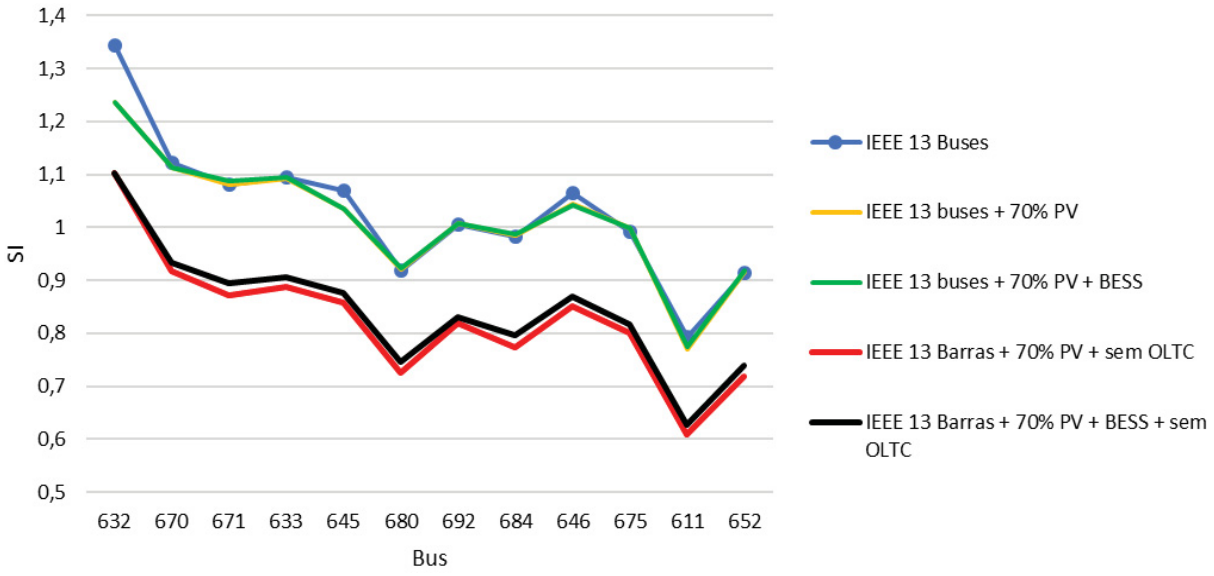

SOURCE: The Author (2019).

5.5 DISCUSSION OF THE RESULTS

Looking at the different criteria of distributed generation penetration levels it is possible to see that the Brazilian criterion is more restrictive that German criteria, because for this case the generation will not reach the load value. However, if the feeder can support the insertion of more generation, it is possible to present high levels of PV generation, information that is considered when the German criterion is applied, once it is not based on the load but based on short circuit power of the feeder.

In this way, different scenarios of photovoltaic generation can be defined and analyzed. Moreover, not only the penetration level can change the grid operation, but the amount of power generated from the system according to weather conditions can causes interferences on grid operation. This can be visible in the number of tap changes and in cases of power losses values comparison.

In the cases when reverse power flow exists into the substation the grid needs to be prepared to receive the power flow in a non-conventional way. For this, studies of protection coordination should be done by the DSOs, in order to prevent blackouts and equipment damage.

In different system compositions, the number of tap changes increases in order that, if the equipment operates in these levels every day, the equipment life-cycle will be reduced significantly.

From the simulations, it was also possible to visualize the problems of reverse power flow with the increase in power system losses and an increase in the number of tap changes.

The results presented show the behavior of an urban distribution feeder, with load and generation distributed along the feeder. In the case of rural system representation, the load would be centralized and due to high remote consumption, the reverse power flow would be higher.

The results from voltage stability analysis show that distribution system operation is affected by the insertion of active systems as distributed generators and storage systems. From the analyzed of minimum stability index values is possible to verify that as much higher is the penetration of PV systems, worst is the values given for the stability analyses. None of the buses present instability, once the minimum values founded are around 0.8. This happened because of the voltage regulator tap changes, contributing significantly to keep an adequate voltage profile.

6 SIMULATIONS AND RESULTS WITH MULTI-PERIOD OPF

In order to solve a problem using the MOPF formulation developed, a distribution system was chosen, considering in this, the allocation of photovoltaic distributed generation and the placement of a battery energy storage system.

Moreover, some operation conditions and equipment characteristics were defined allowing the calculation of the planning of grid operation considering different scenarios for the day-ahead horizon.

Besides different scenarios, different grid configurations were considered, as the operation or not of the voltage regulator, as well the battery placement that was first considered at the substation and in a further scenario, placed along the feeder.

6.1 MULTI-PERIOD OPF SIMULATION SCENARIOS

To test the MPOPF proposed in Chapter 4.2.2, it was considered a system of 90 buses (The BESS location in the system change during simulations scenarios, in a similar way that was done in Chapter 5, being placed first at the substation bus and later in a bus that presents downstream a high percentage of the total system load.

FIGURE 52) adapted from Godoi (2009) and Lachovicz (2018). This system is based on the Baran and Wu (1989) system of 69 buses, to which were added 20 buses of low voltage (GODOI, 2009) and also added 16 distributed equivalent solar generators, allocated at buses 7, 15, 20, 25, 30, 35, 38, 40, 45, 51, 53, 55, 60, 65, 68 and 70 (LACHOVICZ, 2018). All photovoltaic systems present the same installed power.

The simulation system was changed compared with the one chosen to the analysis done in Chapter 5, once it was intended to verify the planning of operation of a more complex system, with more load and generation points spread into the feeder.

In the system there are five fixed capacitor banks, placed on buses 13, 23, 37, 57 and 62, that will stay connected all the time to the distribution system. Moreover, there is a voltage regulator, placed between buses 59 and 60, since the buses with the lowest voltage are buses 88, 87 and 86. Detailed information about the system configuration, system loads and PV system power and locations into the system are placed at APPENDIX B.

The BESS location in the system change during simulations scenarios, in a similar way that was done in Chapter 5, being placed first at the substation bus and later in a bus that presents downstream a high percentage of the total system load.

FIGURE 52 - IEEE 90 BUS SCHEMATIC DRAW.

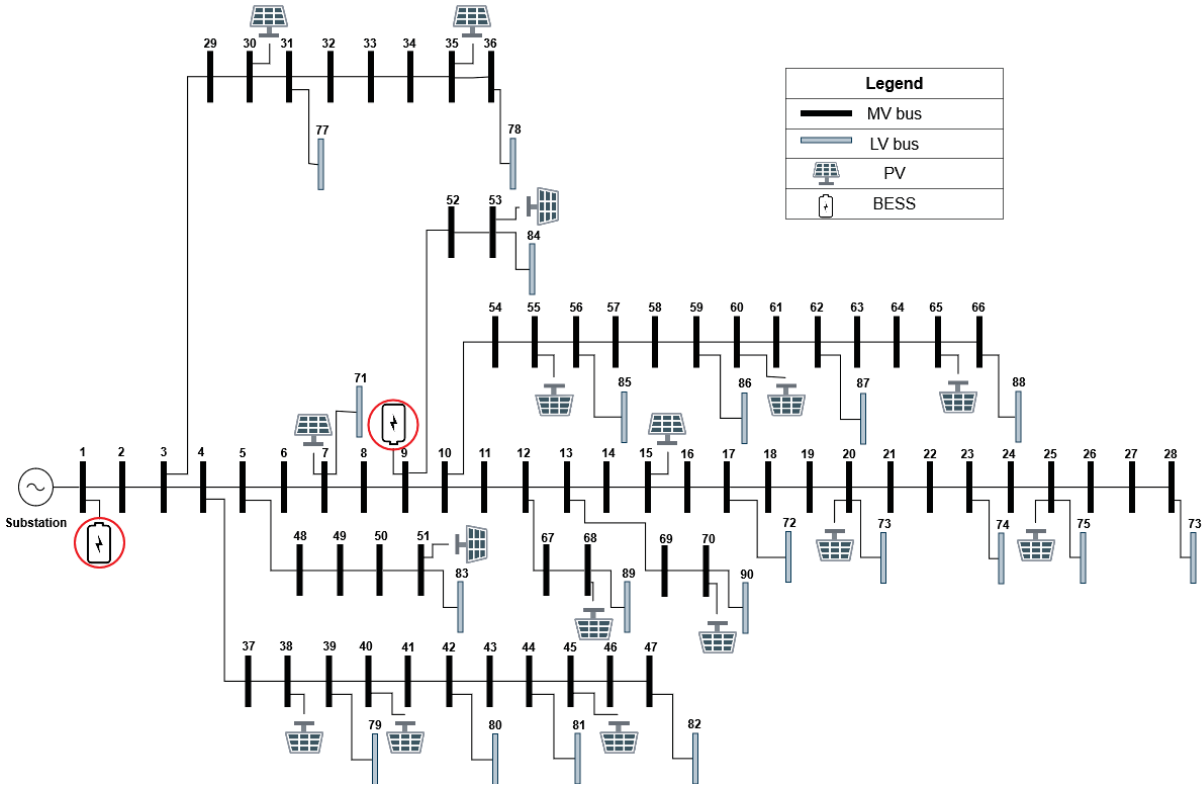

Source: The Author (2019).

From the 90 system buses, 69 are load buses that totalized 4.575 MW of installed load. The insertion of distributed generation, in this case photovoltaic, was considered in 16 buses, being connected at all in medium voltage (MV), representing an equivalent of PV systems that can also be installed at low voltage (LV) buses. The PV installed power totalize 3,2025 MW, corresponding in this case to a penetration level of 70% calculated according to criteria 1 of penetration levels, corresponding to the same percentage that was considered a high penetration in the analysis performed on Chapter 5. The horizon of studied is a day-ahead with 24 periods of 1 hour each.

Different generation profiles were considered, in order to evaluate how it can affect the grid operation. As the day-ahead horizon is being considered, the PV generation profile consists of a forecast of the generation profile of the next day. For this estimation there are a lot of different probability techniques that can be considered, but that it is not the aim of the present work. Thus, six different possibilities of solar

behavior were defined at FIGURE 53, obtained from INMET (Brazilian National Institute of Meteorology) data for Curitiba, during one week of January 2019, in which is represented the profile of maximum (first curve), and the lowest generation of the month (sixth curve).

It is interesting to consider these possible profiles, since they present different generation characteristics, as high intermittence or shifted time of peak generation. However, it is important to highlight that this information is considering the “summer time” application in Brazil, that until 2019 corresponded to increase one hour on Brazillian timezone during the summer season.

FIGURE 53 – DIFFERENT SOLAR GENERATION BEHAVIORS TO BE SIMULATED.

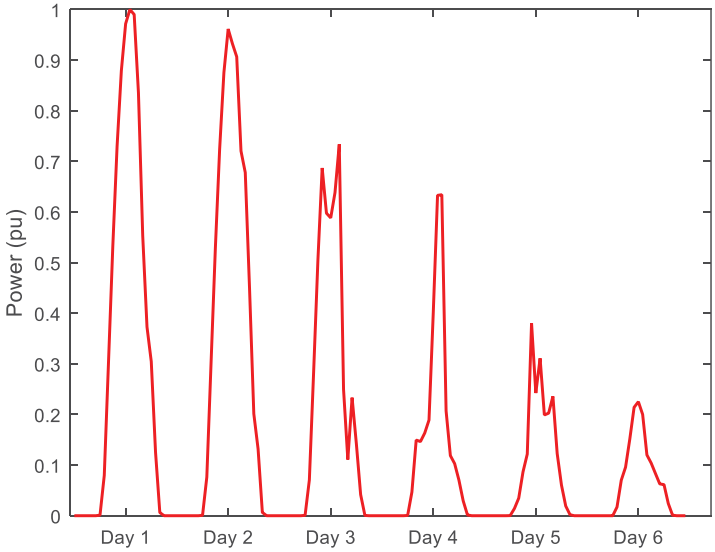

SOURCE: The Author (2019).

As explained in Chapter 4.2.2, a function of generation cost, provided by the substation, needs to be defined. In the present work, it was adopted the white tariff, which presents different costs of electricity according to the time of the day, penalizing the peak time attributing a higher price of the kWh.

This tariff started to be implemented in Brazil in January, 1st 2018, is regulated by the NR 414/2010 and NR 733/2016. The behavior of white tariff prices is presented at FIGURE 54, which is divided into three groups of hours: outside the peak (hours in green), intermediary (yellow) and peak hours (orange). In 2019, the prices adopted by COPEL (distribution utility in Paraná State - Brazil) are R$0.43568/kWh for the outside peak period, R$0.5969/kWh during the intermediary period and R$0.91974/kWh for peak hours, being these values applicable for residential consumers. The conventional

tariff presents the constant price of R$0.50752/kWh. All the values presented are without taxes (COPEL, 2019).

FIGURE 54 - WHITE TARIFF PRICES OF ELECTRICITY.

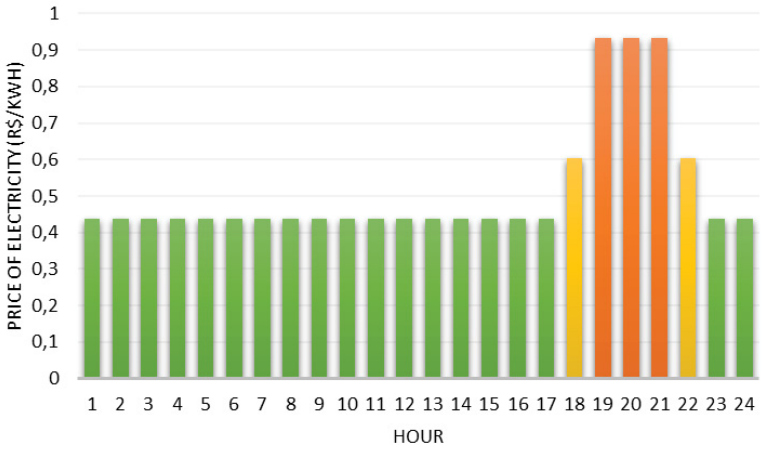

SOURCE: Adapted from COPEL (2019).

In this distribution system, it was placed the BESS presenting 1MW/2MWh, with a DoD maximum of 70%.

The battery operation cost is dependent on the battery degradation cost, which was previously defined in chapter 2, in equation 2.1.

For the lithium-ion BESS size considered, the estimated cost in the market nowadays is around R$12 million. Moreover, considering a Dod of 70%, the number of cycles to failure is around 4000 cycles, for a lithium-ion battery. In this way, the cost of degradation can be estimated at R$ 2,140.00/MWh.

To characterize the voltage at the substation output bus, it was included the parametrization of the voltage substation bus for all periods, considering different load stages of the system, divided in low, intermediate and heavy load stage. According to COPEL (2017) technical norm NTC 905100, the voltage levels at steady state for load buses should follow the values presented at TABLE 21. For the substation bus, the minimum voltage values were considered in all periods. The periods' division was done based on CEPEL (2018).

TABLE 21 - SUBSTATION VOLTAGE LIMITS ACCORDING TO LOAD LEVELING

Load Stage	Minimum Voltage (pu)	Maximum Voltage (pu)	Period
Heavy	0.9927	1.00	18h00 – 22h00
Intermediate	0.9783	0.9927	08h00 – 17h00 23h00 – 00h00
Low	0.9565	0.9783	00h00 – 07h00

SOURCE: Adapted from COPEL (2017).

For this analysis, two load profiles were considered, presented at FIGURE 55, were both obtained from typical load curves from the Brazilian Nacional Interconnected System (SIN). Load curve 1 presents the classical load behavior, in which the peak hours happen in the evening, representing the load profile of the SIN during the winter months, for weekdays. However, the load curve 2 represents a common load profile of the SIN for summer days, in which the peak load happens in the middle of the day, mainly due to the use of air conditioner equipment.

FIGURE 55 - LOAD CURVE PROFILE FOR DFPO SIMULATIONS.

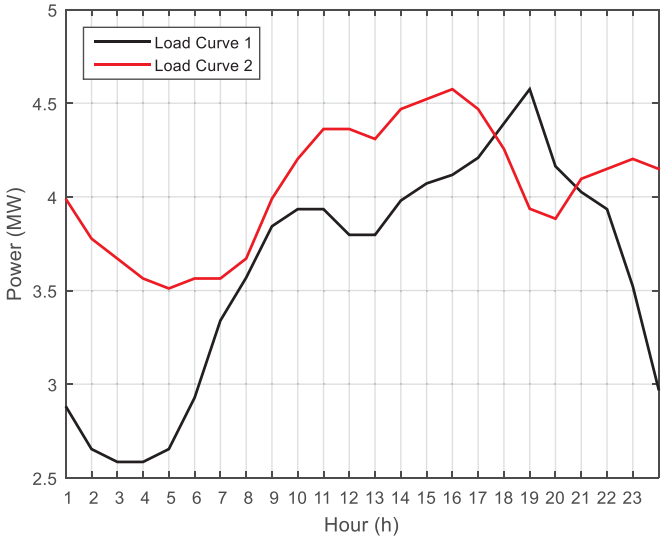

SOURCE: Adapted from ONS (2019b).

Considering the characteristics of the system and of the equipment, it is possible to solve the MPOPF for different scenarios. Three different scenarios were defined to evaluate grid planning as presented in FIGURE 56. In all scenarios, the first moment were considered the operation of the voltage regulators and of the capacity banks, being the voltage regulators turned off in some moments in order to evaluate the grid operation without this equipment.

FIGURE 56 - SIMULATION SCENARIOS FOR MPOPF SIMULATIONS.

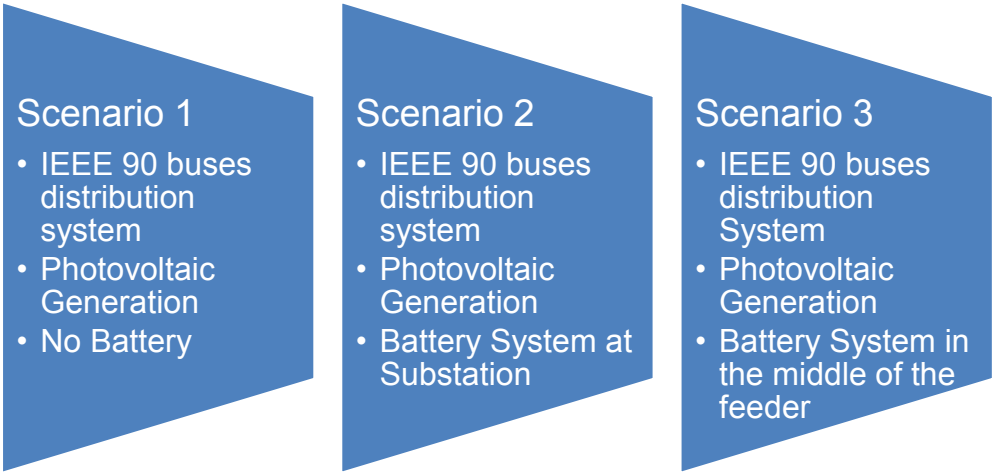

SOURCE: The Author (2019).

6.2 MPOPF SCENARIO 1

In the first scenario, the PV penetration was considered and both load curves were applied, presenting the power flow results shown in FIGURE 57 (with maximum solar radiation). The power flow results are the energy provided by the substation (Pgh 1) and the total solar generation (Solar Generation) necessary to supply the total load (Load) for each period. The power losses could be visualized by the difference between the total power supplied to the grid and the total load.

FIGURE 57 - POWER FLOW BALANCE WITH SOLAR GENERATION CONSIDERING LOAD CURVE 1 (a) AND LOAD CURVE 2 (b) – SCENARIO 1.

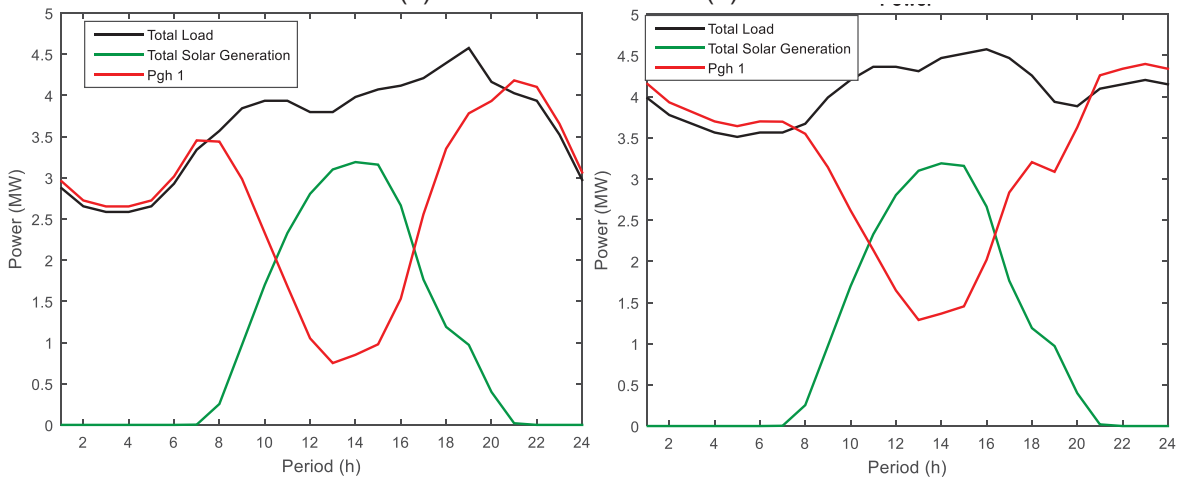

Source: The Author (2019).

It is important to highlight that the solar irradiation, in this case, is considering the Brazilian "summer time", as mentioned before, in which, until 2019, during the summer season the official timezone used to be increased in one hour.

When the minimum solar radiation is considered (FIGURE 58), the load supply by the PV generation reduces significantly, in order that the peak needs to be fully supplied by the substation power when load curve 1 is considered. Yet, when load curve 2 is applied, the peak power provided by the substation is lower, since the solar generation contributes during the peak time.

FIGURE 58 - POWER FLOW BALANCE WITH SOLAR GENERATION CONSIDERING LOAD CURVE 1 (a) AND LOAD CURVE 2 (b) – SCENARIO 1- AND WITH MINIMUM SOLAR RADIATION

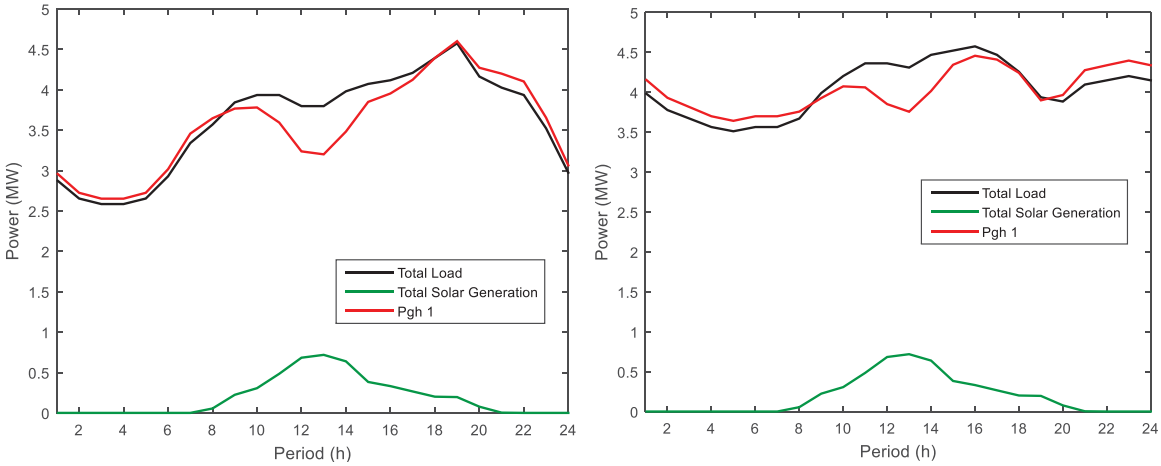

SOURCE: The Author (2019).

It is verified that, for these cases, there is no reverse power flow at the substation bus, since the solar generation is not higher enough to supply all the load during the generation period, even when the maximum radiation is considered. However, there is reverse power flow within the system, since the local generation surplus is absorbed by the load buses along the feeder, not reaching the substation bus.

Considering the maximum solar radiation, there is reverse power flow within the system from 08h00 a.m. to 06h00 p.m. when both load profiles are considered. Meanwhile, considering the minimum solar radiation, there is reverse power flow only at buses 51 and 52 in a short period of time, from 10h00 a.m to 01h00 p.m. with load profile 1 and from 11h00 a.m. also until 01h00 p.m. considering load profile 2.

At FIGURE 59 it is presented the buses with reverse power flow at 01h00 p.m. applying load curves 1 and 2. Both cases considered the maximum radiation of the

solar. For the case with load profile 1, there is reverse power flow in 35 buses, whereas when load profile 2 is applied this happens on 32 buses.

FIGURE 59 - REVERSE POWER FLOW BUSES AT 01H00 P.M WHEN (a) LOAD CURVE 1 AND (b) LOAD CURVE 2 IS CONSIDERED AND WITH MAXIMUM SOLAR RADIATION – SCENARIO 1.

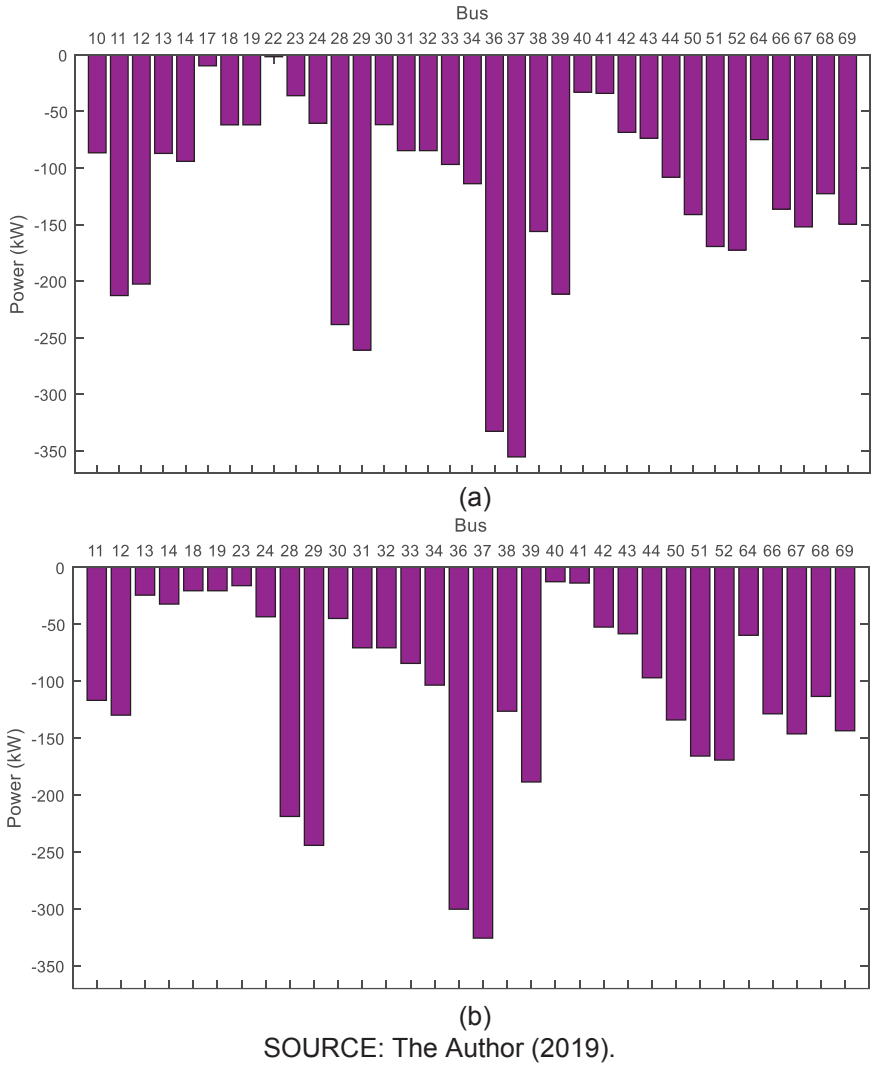

SOURCE: The Author (2019).

Looking at the power losses and the operational costs, the results for maximum and minimum radiation, applying both load curves, are presented at TABLE 22. In case that there is low solar generation the power losses of the system are higher than in a sunny day, because there is low load being supplied locally, so the substation needs to provide more power, increasing the energy flowing through the lines. When load curve 2 is applied, the power losses are higher since the power demand is higher than in profile 1 during almost all periods. In this way, the total load to be supplied is higher and hence, the total power losses are also higher.

TABLE 22 - RESULTS OF POWER LOSSES AND OPERATIONAL COSTS – SCENARIO 1.

	Maximum Radiation		**Minimum Radiation**	
	Load Curve 1	Load Curve 2	Load Curve 1	Load Curve 2
Power Losses (MW)	2.46	3.22	3.21	4.08
Operational Costs(R$)	35,339.2	39,953.86	45,165.27	49,821.92

SOURCE: The Author (2019).

About the operational costs, as much power needs to be provided by the substation, higher are the operational costs, being always higher for profile 2 in comparison with profile 1.

Analyzing, in the sequence, the load profile of all the buses of the system with the insertion of the distributed generation and different load profiles, the voltage behavior of each bus is presented at FIGURE 60 (with maximum solar radiation) and FIGURE 61(with minimum solar radiation), is possible to visualize that in all cases the minimum voltage value happens at bus 86. Moreover, when the maximum solar radiation is considered (FIGURE 60), the voltage level of the buses increases during the generation period and the limits of 1.05 and 0.93 pu for adequate voltage level (TABLE 3) were not reached. However, when the minimum radiation is considered (FIGURE 61), the minimum limit is violated in peak load instant.

FIGURE 60 - VOLTAGE IN ALL BUSES WITH MAXIMUM RADIATION WHEN LOAD (a) PROFILE 1 (b) PROFILE 2 ARE CONSIDERED WITH VOLTAGE REGULATOR OPERATION - SCENARIO 1.

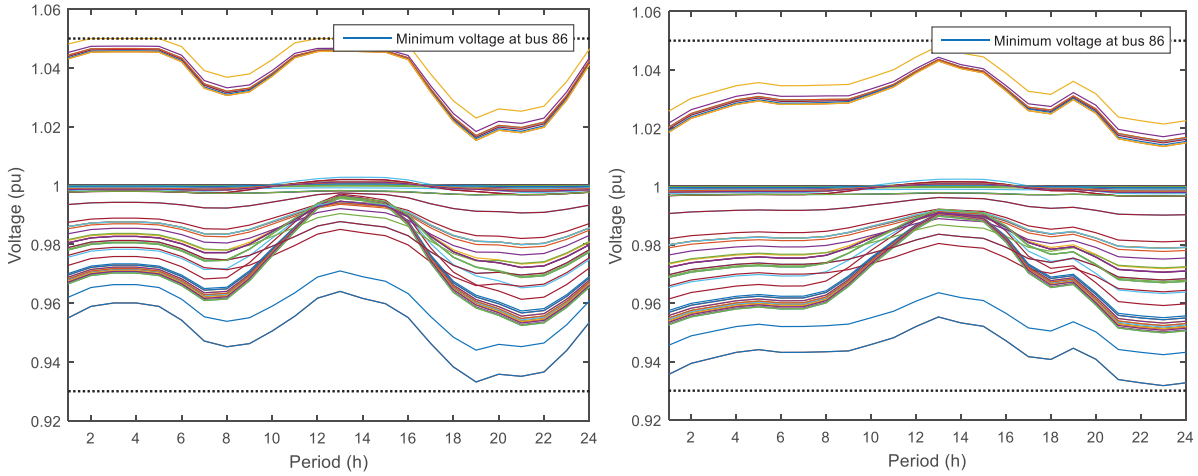

(a) (b)

SOURCE: The Author (2019).

FIGURE 61 - VOLTAGE IN ALL BUSES WITH MINIMUM RADIATION WHEN LOAD (A) PROFILE 1 (B) PROFILE 2 ARE CONSIDERED WITH VOLTAGE REGULATOR OPERATION - SCENARIO 1.

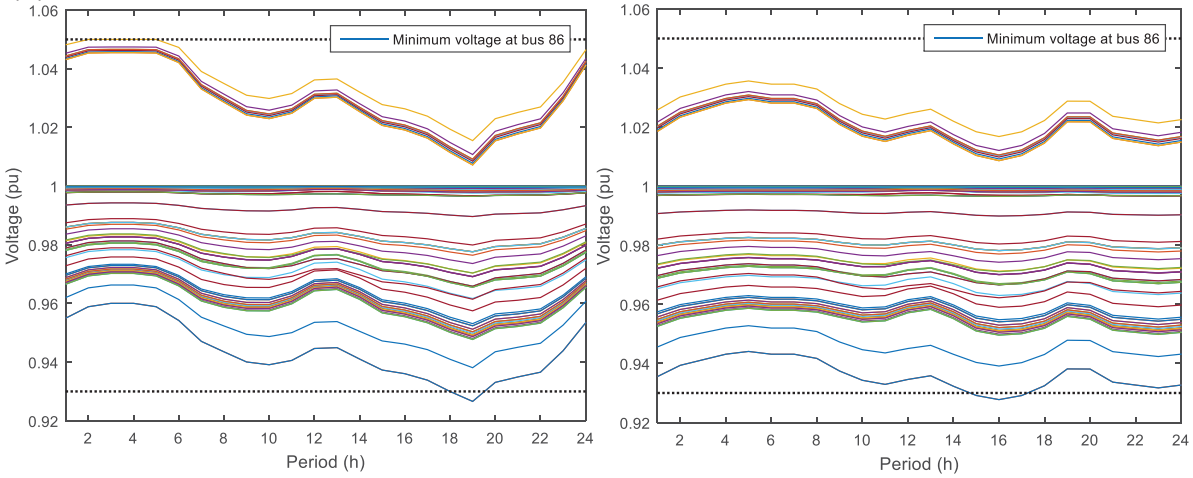

(a) (b)

SOURCE: The Author (2019).

The tap behavior of the OLTC at the substation bus during the daily operation is presented in FIGURE 62, in which is possible to compare the tap positions during the day, for different load profiles. It can be observed that when there is more PV generation in moments with low load, that is the case with load profile 1, the voltage regulator needs to actuate in order to avoid an overvoltage in the system, reducing the positions. However, when load profile 2 is applied, the changes in voltage values are not so expressive, since there is high load demand during solar generation, contributing to avoid overvoltage in the system. In this way, with load profile 2, tap changes were not performed.

FIGURE 62 - TAP CHANGES BEHAVIOR WITH MAXIMUM RADIATION WHEN LOAD (a) PROFILE 1 (b) PROFILE 2 ARE CONSIDERED WITH VOLTAGE REGULATOR OPERATION - SCENARIO 1.

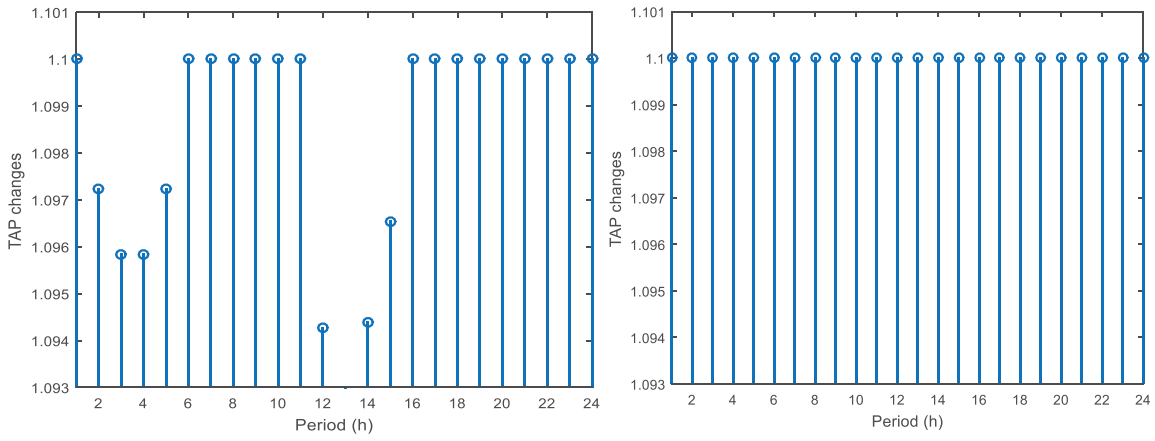

(a) (b)

SOURCE: The Author (2019).

If the voltage regulator is disabled (FIGURE 63), the minimum voltage values are lower than when the OLTC is operating, being founded buses that violate the voltage limits, presenting undervoltage (under 0.93 pu).

FIGURE 63 - VOLTAGE PROFILES IN ALL BUSES WITH MAXIMUM RADIATION AND WHEN LOAD (a) PROFILE 1 (b) PROFILE 2 ARE CONSIDERED WITH VOLTAGE REGULATOR DISABLE – SCENARIO 1.

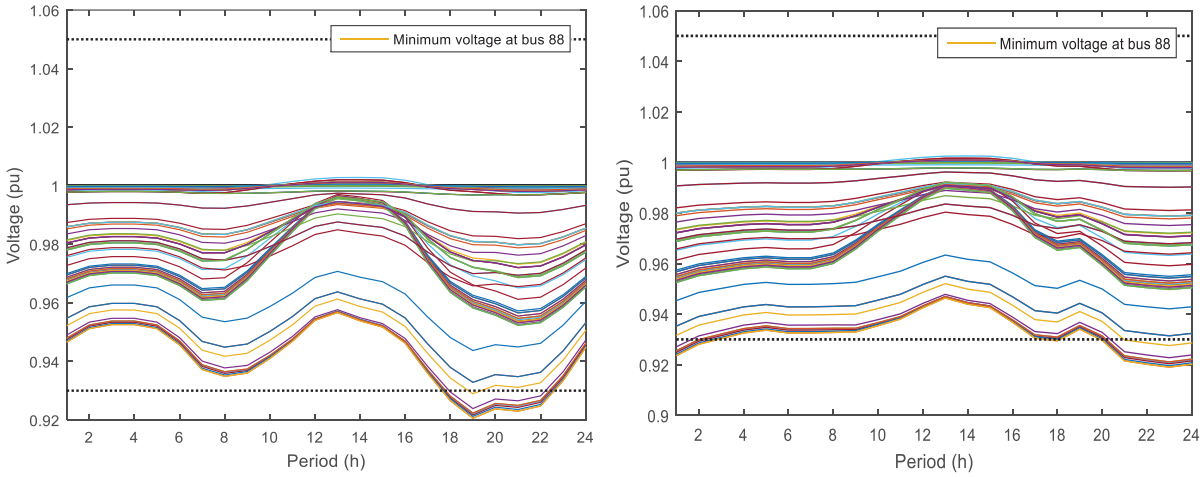

(a) (b)

SOURCE: The Author (2019).

As the maximum impact of the distributed generation happens when the maximum solar radiation is considered, this will be the PV generation profile choose for the next simulation scenarios.

The convergence of the MPOPF solution took around 26.84 seconds to be solved with minimum radiation and around 34.17 seconds when the maximum solar radiation was considered, both in addition to voltage regulator operation. The evolution of the infinite norm for the convergence of the problem in each case simulated is shown in FIGURE 64.

FIGURE 64 – CONVERGENCE OF OPTIMIZATION METHOD WITH LOAD CURVES 1 AND 2, BESIDES MINIMUM AND MAXIMUM SOLAR RADIATION – SCENARIO 1.

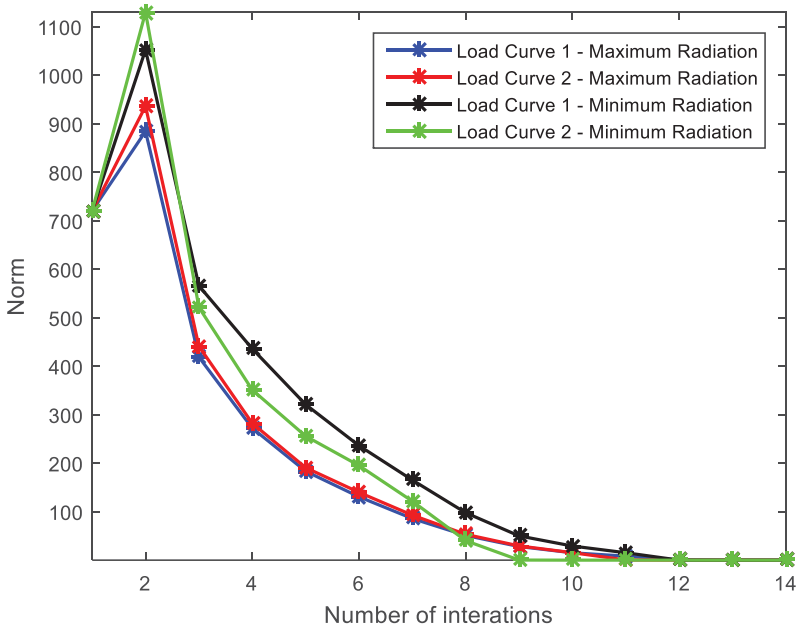

SOURCE: The Author (2019).

6.3 MPOPF SCENARIO 2

Following the same approach of scenario 1, the battery was added to the circuit, being placed at the substation bus (bus 1). The battery operation is also an objective of the optimization problem, as previously detailed in chapter 4.2.2 and which characteristics of the equipment and limits of operation are defined in chapter 6.1.

In this way, the MPOPF will propose an optimum charge and discharge behavior of the BESS, finding the optimum solution for the entire system operation, considering all the optimization objectives.

In this case, the active power balance is presented in FIGURE 65, which is considered the maximum solar power radiation and the battery operation, for both load profiles. It is important to highlight that when the battery power is positive, it means that the BESS is charging, and when the value is negative, the battery is discharging.

FIGURE 65 - POWER BALANCE OF THE SYSTEM WITH BESS AT THE SUBSTATION BUS WHEN LOAD (a) PROFILE 1 (b) PROFILE 2 ARE CONSIDERED – SCENARIO 2.

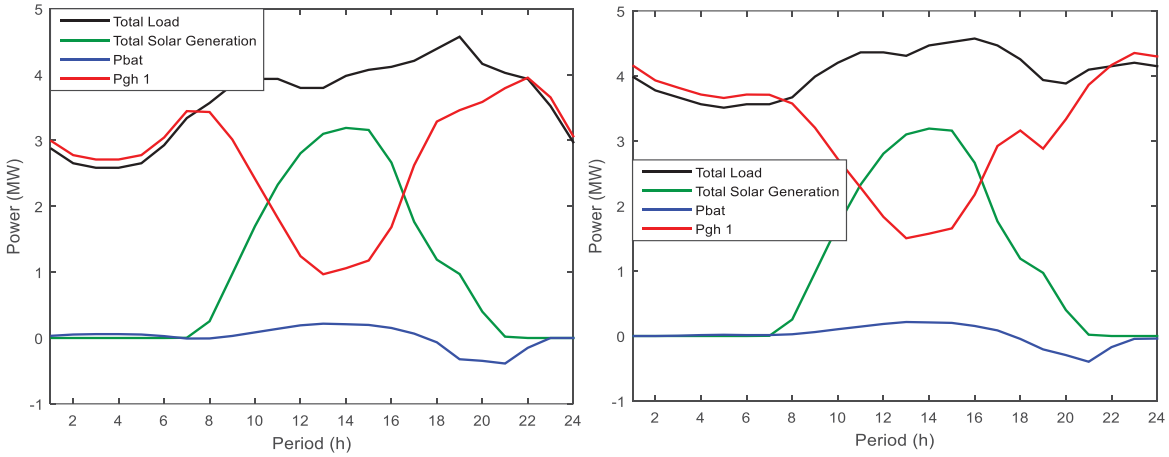

SOURCE: The Author (2019).

With the battery operation, the total power losses at the distribution system do not change in comparison with the case simulated under the same conditions in scenario 1 as shown in TABLE 24. In this case, the power losses do not change since the BESS is located at the substation bus, so the power flowing thought the power lines is the same then the case without the BESS, in which the power is provided by the substation. For the same reason, when evaluating the reverse power flow behavior, the results obtained were the same as in scenario 1.

Nevertheless, the operational cost reduce, since part of the power is provided to the system by the BESS reducing the demand from the substation, mainly during the peak time of the load, since the white tariff is being considered and the discharge of the BESS is happening during the most expensive price of the energy period. It is important to emphasize that the cost of the BESS operation is not paid during the operation since the utility will buy the entire system and this price corresponds to the depreciation caused by each cycling of the battery.

TABLE 23 - RESULTS OF POWER LOSSES AND OPERATIONAL COSTS CONSIDERING THE MAXIMUM SOLAR RADIATION – SCENARIO 2.

	Scenario 1		**Scenario 2**	
	Load Curve 1	**Load Curve 2**	**Load Curve 1**	**Load Curve 2**
Power Losses (MW)	2.46	3.22	2.46	3.22
Operational Costs(R$)	35,339.2	39,953.86	34,909.30	39,592.35
Cost of the BESS (R$)	-	-	6,124.81	5,669.45

SOURCE: The Author (2019).

Analyzing the BESS operation is possible to visualize that it started the day with the minimum energy storage, being in this case 30% of the energy storage capacity of the system, considering the system discharged. At the end of the day, after the operation, the battery presents the same value, being discharged until the limited value target. This happens because the operation cost of the BESS is also being optimized. The power and energy values obtained for each hour of the day are presented in TABLE 24 and the energy and power profiles are shown in FIGURE 66 for load profile 1.

TABLE 24 - BATTERY ENERGY AND POWER VALUES WHEN LOCATED AT THE SUBSTATION CONSIDERING BOTH POSSIBILITIES OF LOAD CURVE, PROFILES 1 AND 2 – SCENARIO 2.

Battery Operation Behavior				
hour	**Considering Load Curve 1**		**Considering Load Curve 2**	
	Energy (MWh)	Power (MW)	Energy (MWh)	Power (MW)
1	0.6314	0.0314	0.6	0.0
2	0.6852	0.0539	0.6	0.0
3	0.7459	0.0606	0.6043	0.0047
4	0.8065	0.0606	0.6172	0.0144
5	0.8604	0.0539	0.6345	0.0192
6	0.8872	0.0268	0.6474	0.0144
7	0.8733	-0.0139	0.6606	0.0147
8	0.8579	-0.0155	0.6848	0.0269
9	0.8761	0.0182	0.7396	0.0608
10	0,9466	0.0704	0.8337	0.1046
11	1.0699	0.1233	0.9639	0.1446
12	1.2466	0.1767	1.1309	0.1856
13	1.4478	0.2012	1.3248	0.2155
14	1.6386	0.1908	1.5130	0.2091
15	1.8179	0.1793	1.6945	0.2017
16	1.9514	0.1335	1.8337	0.1546
17	2.0000	0.0486	1.9114	0.0846
18	1.9198	-0.0802	1.8626	-0.0444
19	1,5522	-0.3675	1.6364	-0.2056
20	1.1711	-0.3811	1.3140	-0.2931
21	0.7541	-0.417	0.8789	-0.3956
22	0.6	-0.1541	0.6910	-0.1708
23	0.6	0	0.6428	-0.0438
24	0.6	0	0.6	-0.0389

SOURCE: The Author (2019).

FIGURE 66 - BATTERY BEHAVIOR (a) POWER (b) ENERGY CONSIDERING THE MAXIMUM SOLAR RADIATION AND LOAD PROFILE 1 – SCENARIO 2.

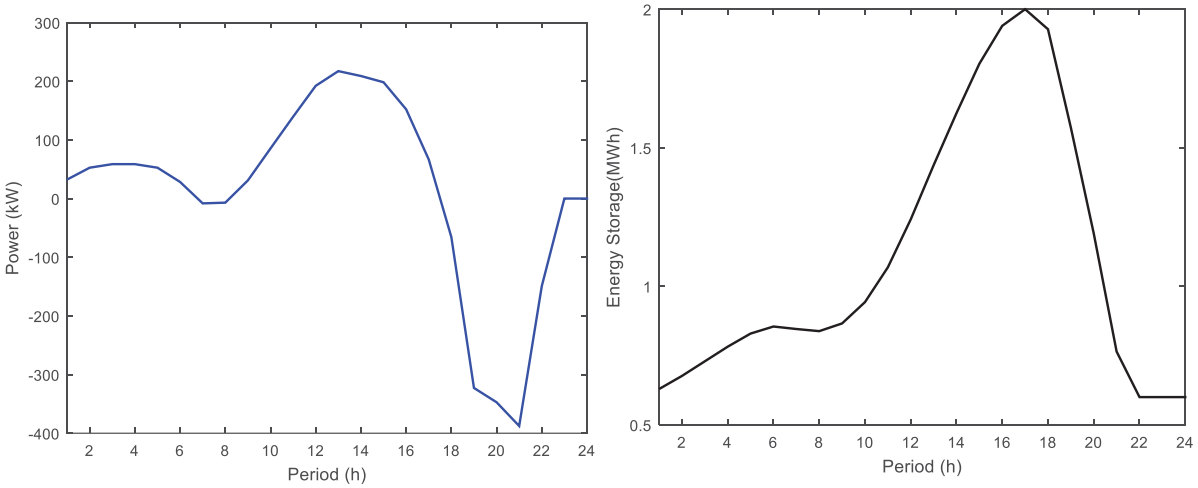

(a) (b)

SOURCE: The Author (2019).

When load profile 2 is considered, the behavior of the battery does not change significantly. A comparison between the state-of-charge (SOC) of the BESS when different load curves are applied is present on FIGURE 67, in which it is possible to visualize that if load profile 2 is considered, the charge of the system happens only in solar generation moments. As well, then the load curve 1 is considered, the battery discharge faster during the peak time hours since it matches the peak of the load.

FIGURE 67 – SOC BATTERY BEHAVIOR CONSIDERING THE MAXIMUM SOLAR RADIATION AND LOAD PROFILE 1 AND 2 – SCENARIO 2.

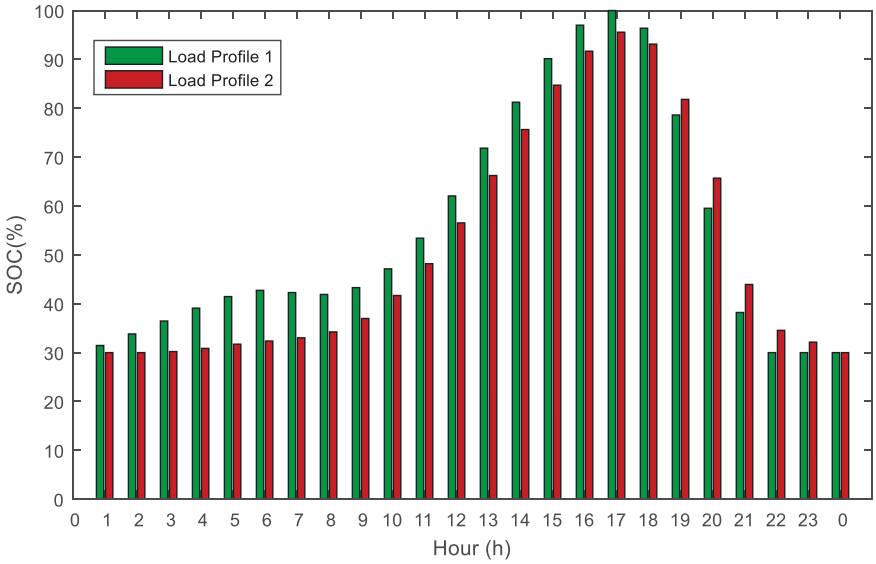

SOURCE: The Author (2019).

For this operational scenario, the voltage profile of all buses and the voltage regulator behavior is the same as the one present for the simulation without BESS.

This happens because the voltage at the substation bus is fixed according to the load level, fluctuating following the load behavior, so as the BESS is connected at substation bus, the voltage of the BESS presents the same values and the voltage of all buses are not affected.

If the operation of the BESS is considered to a minimum solar radiation day, the behavior of BESS power and energy changes significantly, as presented in FIGURE 68, as well the BESS state-of-charge that presents different behavior, as shown at FIGURE 69.

FIGURE 68 – POWER BATTERY BEHAVIOR POWER THE LOAD CURVE 1 AND MINIMUM AND MAXIMUM SOLAR RADIATION – SCENARIO 2.

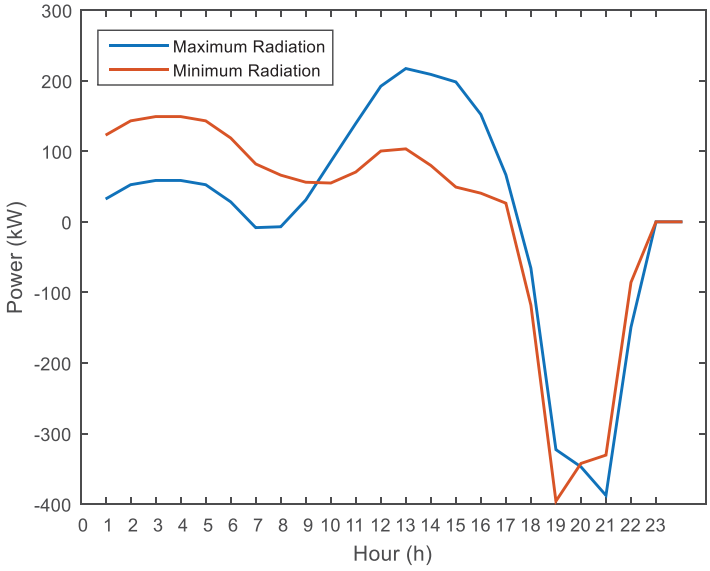

SOURCE: The Author (2019).

In the case with minimum radiation, the battery charging happens during the first hours of the day in a way to ensure sufficient load to be discharged in the peak period. So, it is important to know the radiation forecast for the day, in order to guarantee the storage of energy in the most appropriate period of the day. In this situation, the operational cost of the system is R$44,727.25, also lower than in a similar scenario without BESS considering load curve 1.

FIGURE 69 - SOC BATTERY BEHAVIOR CONSIDERING THE MAXIMUM AND MINIMUM SOLAR RADIATION AND LOAD PROFILE 1 – SCENARIO 2

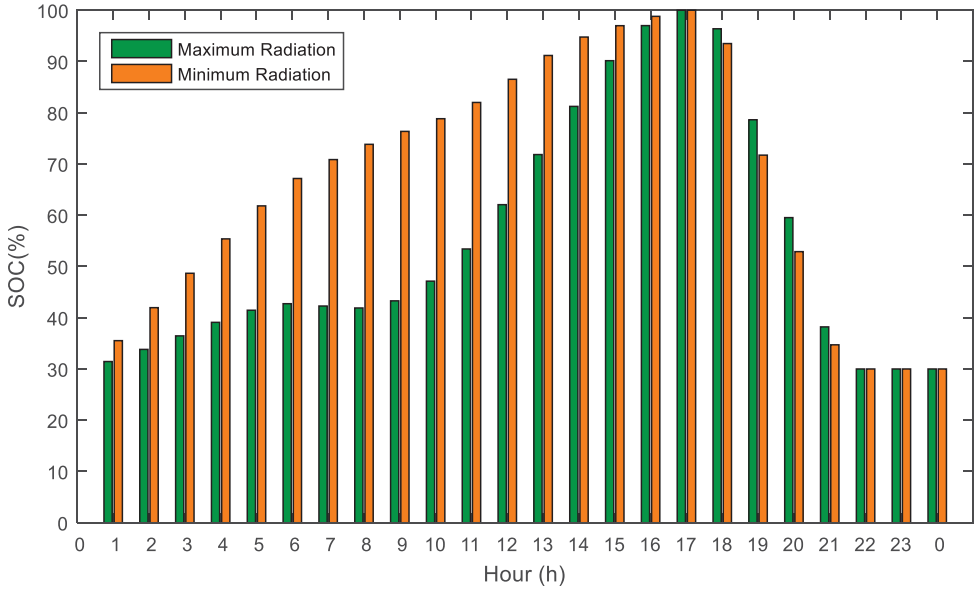

SOURCE: The Author (2019).

6.4 MPOPF SCENARIO 3

For this scenario, the placement of the battery system was changed into the distribution feeder, is now placed outside of the substation. The new location chosen in the first moment was on bus 9 since 66.15% of the installed load is located downstream of this bus. In the sequence, other positions were analyzed, as bus 22, since in the middle of the main part of the feeder and bus 64, that is a position downstream of the OLTC.

Considering this new system configuration, the power balance is present in FIGURE 70, with the maximum solar radiation, the BESS placed at bus 9 and both possible load curves.

In this case, the reverse power flow presents the same values of scenario 1. This happened since the BESS keep being placed upstream of the buses in which happened reverse power flow. So, if the battery was connected, for example, at bus 22, there will not have reverse power flow on buses upstream, since the PV generation surplus from downstream will be stored at this point of the circuit.

FIGURE 70 - POWER BALANCE OF THE SYSTEM WITH THE BESS AT BUS 9 WHEN LOAD (a) PROFILE 1 (b) PROFILE 2 ARE CONSIDERED – SCENARIO 3.

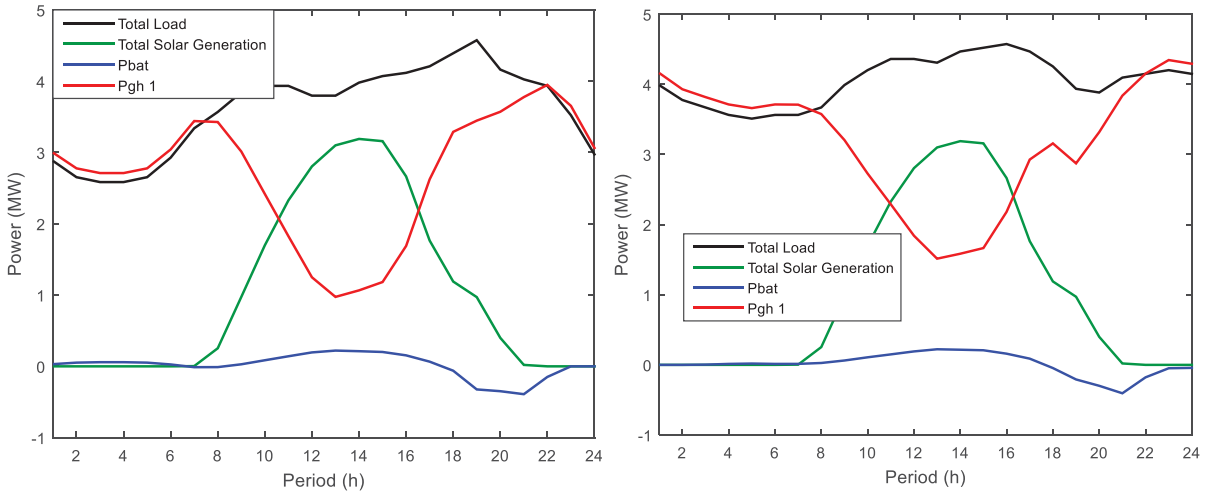

SOURCE: The Author (2019).

FIGURE 71 - REVERSE POWER FLOW BUSES AT 01H00 P.M WHEN THE BESS IS PLACED AT BUS 22 CONSIDERING LOAD PROFILE 1 AND MAXIMUM RADIATION.

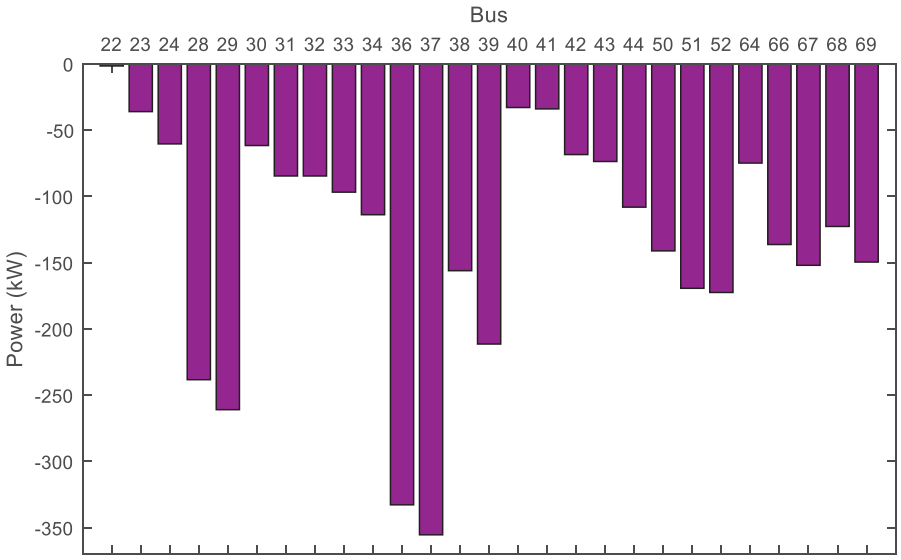

SOURCE: The Author (2019).

At TABLE 25 is presented a comparison of the losses and costs considering different placements of the BESS along the feeder. Looking at the total power loss, it reduces just a few, as well the price of the system operation that was being reduced as much far is located the BESS. This happens due to the local load supply and the reduction of power losses. In the same way, the BESS needs to operate more and the cost of battery degradation increases.

TABLE 25 - RESULTS OF POWER LOSSES AND OPERATIONAL COSTS CONSIDERING THE MAXIMUM SOLAR RADIATION AND LOAD PROFILE 1– SCENARIO 3.

	BESS Location			
	Bus 1	**Bus 9**	**Bus 22**	**Bus 64**
Power Losses (MW)	2.46	2.45	2.42	2.44
Operational Costs (R$)	35,339.20	34,878.70	34,850.62	34,811.25
Cost of the BESS (R$)	6,124.81	6,160.52	6,216.76	6,250.40

SOURCE: The Author (2019).

The battery operation behavior can be better understood at FIGURE 72, being similar to the behavior obtained when the BESS is placed at the substation since the total load profile of the system is the same at the substation or in the middle of the feeder. For the present simulations, the same load profile was considered for all loads, in addition, the white tariff was considered in all cases.

FIGURE 72 - BATTERY BEHAVIOR POWER CONSIDERING (a) MAXIMUM AND (b) MINIMUM SOLAR RADIATION FOR BESS PLACED IN DIFFERENT LOCATIONS – SCENARIO 3.

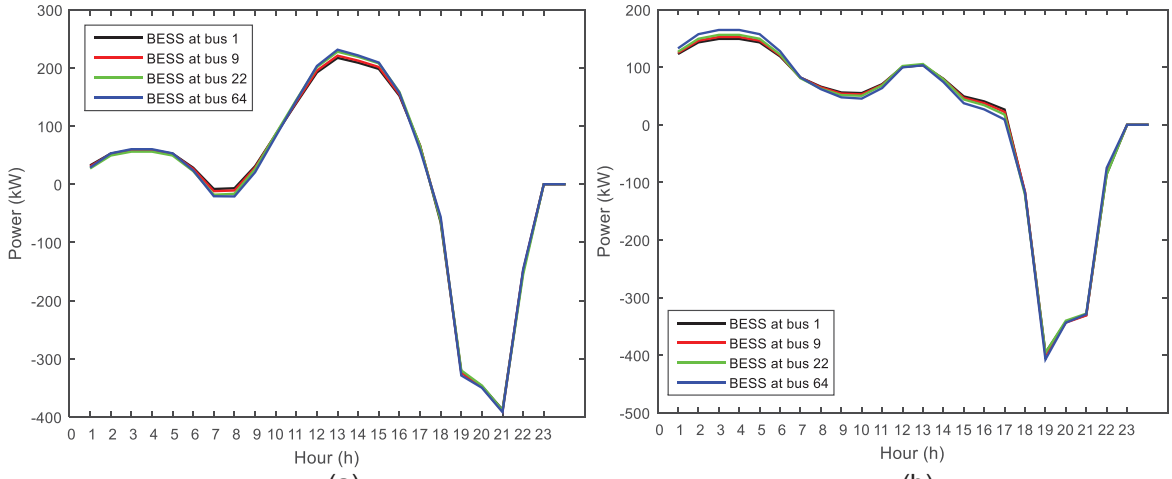

SOURCE: The Author (2019).

Aiming to analyze the voltage behavior, FIGURE 73 shows the results when both possible load profiles are considered and the BESS is placed at bus 9, considering maximum solar radiation. In this case, none of the buses reached the limits. When the BESS is placed downstream of the OLTC, at bus 64, the voltage profile of the bus 86, that is the bus with lowest voltage values in all scenarios, increases in a day with maximum or even with minimum solar radiation, as shown at FIGURE 74. It is important to highlight that the BESS is operating with a power factor of 0.95, contributing to the supply of a small portion of reactive to the system.

FIGURE 73 - VOLTAGE PROFILES IN ALL BUSES WITH BESS AT BUS 9 MAXIMUM SOLAR RADIATION AND LOAD (a) PROFILE 1 AND (b) PROFILE 2.

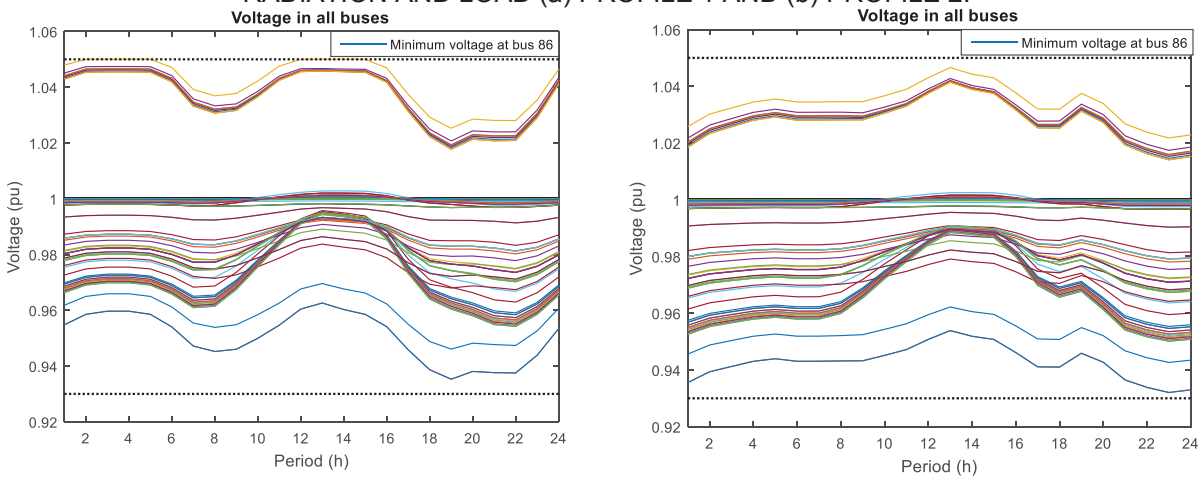

(a) (b)

SOURCE: The Author (2019).

FIGURE 74 - VOLTAGE PROFILES IN ALL BUSES WITH BESS AT BUS 64 WITH LOAD PROFILE 1 AND (a) MAXIMUM AND (b) MINIMUM SOLAR RADIATION.

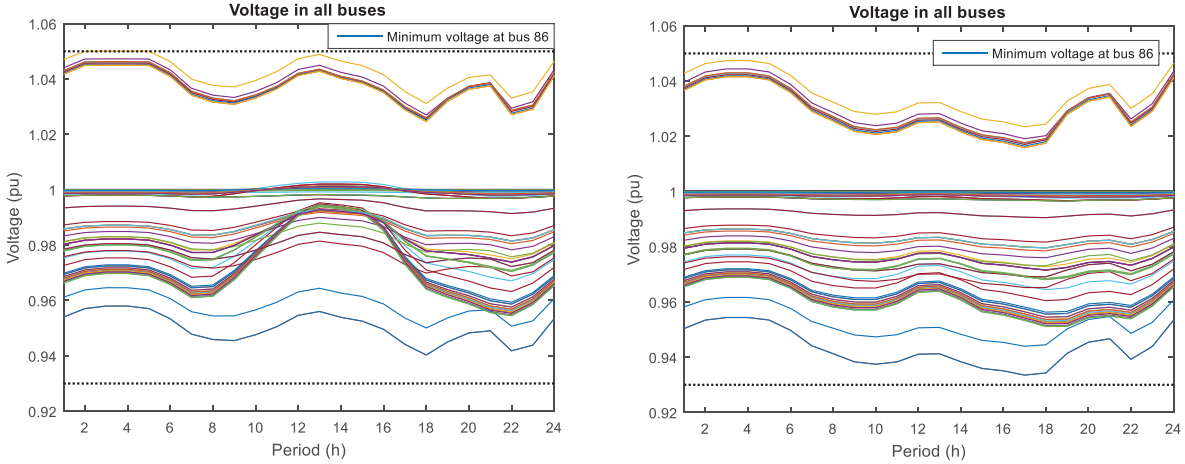

(a) (b)

SOURCE: The Author (2019).

Nevertheless, as no power factor control is implemented, as well as voltage control by the BESS, when the voltage regulator is disabled and there is minimum solar radiation, there is undervoltage in some buses, mainly when the BESS is placed at the end of the circuit, as shown at FIGURE 75.

FIGURE 75 - VOLTAGE PROFILES IN ALL BUSES WITH MINIMUM RADIATION AND LOAD PROFILE 1 CONSIDERIN BESS AT (A) BUS 9 AND (B) BUS 64 WITH VOLTAGE REGULATOR DISABLE

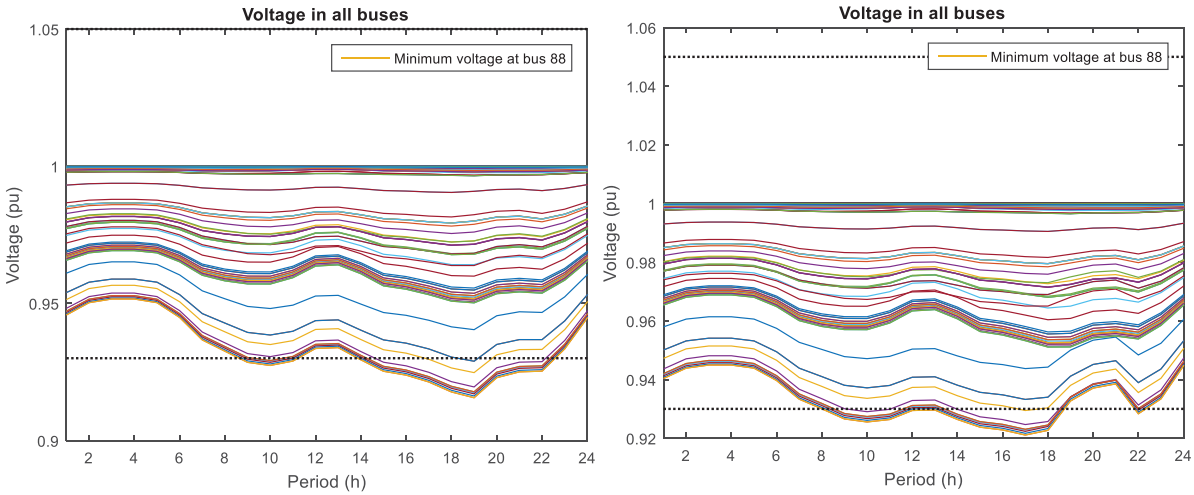

SOURCE: The Author (2019).

With the BESS located outside of the distribution feeder, the tap position also changes, presenting high positions as much far from the substation it is placed. Moreover, in days with minimum solar radiation, the tap position used to be higher, since there is more load into the system. All this behavior is presented in FIGURE 76.

FIGURE 76 - TAP VOLTAGE POSITIONS OF VOLTAGE REGULATOR LOCATED BETWEEN BUS 59 AND 60 WHEN BESS IS LOCATED AT (a) BUS 9 WITH MAXIMUM SOLAR, (b) BUS 9 WITH MINIMUM SOLAR, (c) BUS 64 WITH MAXIMUM SOLAR AND (d) BUS 64 WITH MINIMUM SOLAR.

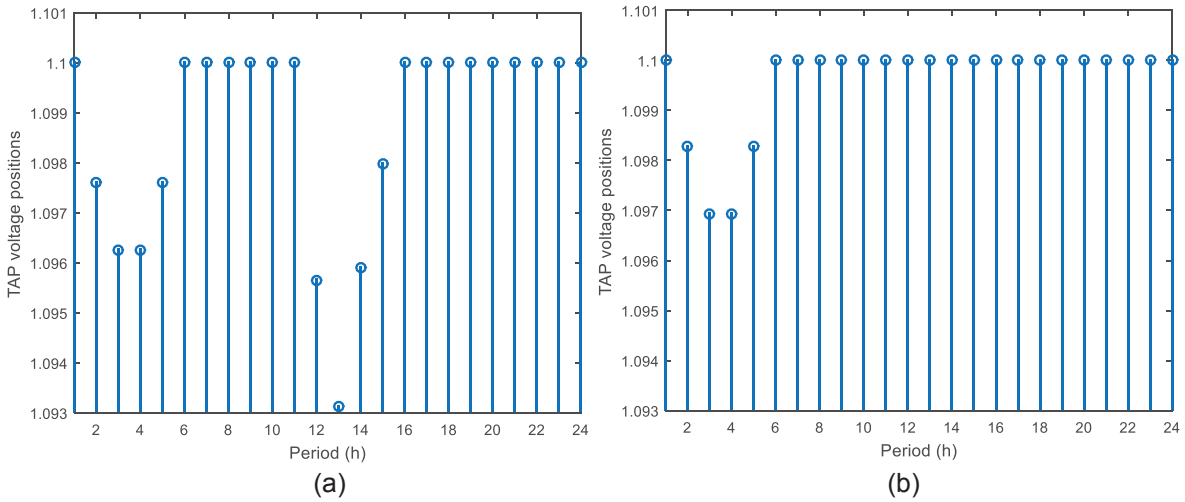

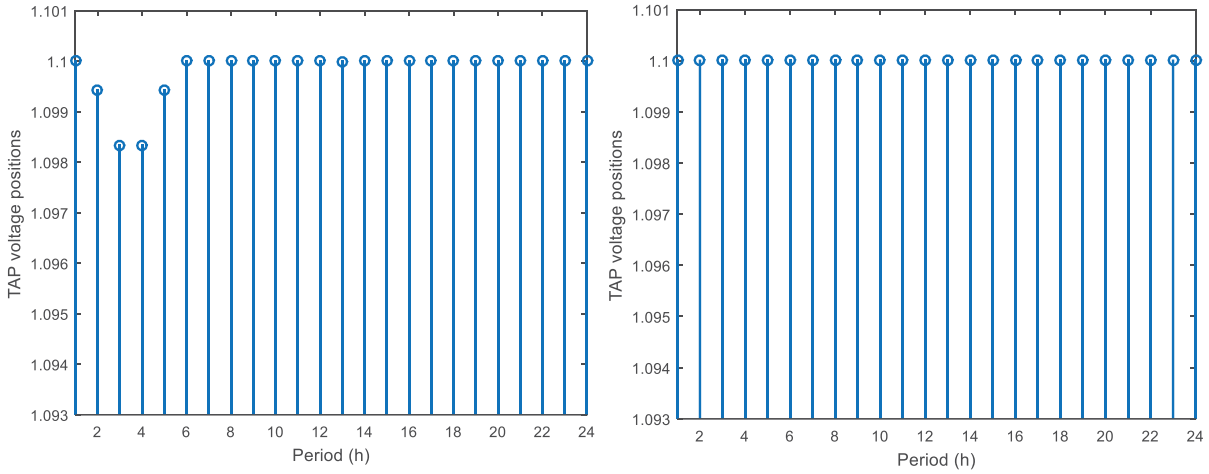

SOURCE: The Author (2019).

6.5 PLANNING OPERATION CONSIDERING DIFFERENT PHOTOVOLTAIC GENERATION SCENARIOS

Considering the different photovoltaic generation scenarios proposed at FIGURE 53 the planning of system operation was developed, fixing the battery placement at bus 9 and the load profile 1, for each photovoltaic generation profile, being organized all of them in sequence, in order to simulate the operation of the distribution system during the week. The planning of day-ahead is always done in the previous day, allowing to pre-defined the BESS charge periods, based also in the solar generation forecast.

The results of power balance are presented in FIGURE 77, in which is possible to verify how the solar generation profile affect the battery operation, considering the same load profile in all cases.

FIGURE 77 - SYSTEM BALANCE CONSIDERING DIFFERENT SOLAR GENERATIONS AND CONSEQUENTLY DIFFERENT BATTERY OPERATIONS.

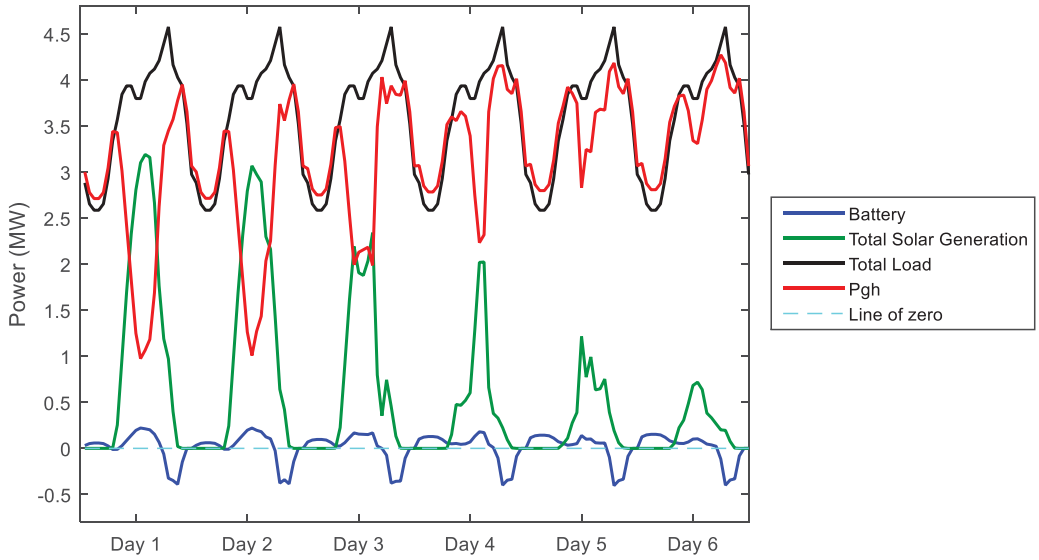

SOURCE: The Author (2019).

Analyzing the battery behavior shown at FIGURE 78, it is possible to verify that the discharge of the systems happens always during the peak time since the cost of substation energy is higher during this time, considering the white tariff. Charge behavior changes according to the photovoltaic generation availability. For the days with more solar radiance, the charge of the battery happens during the solar generation time, by the way, that when low solar generation is considered, the battery charge happens during the lowest load period, in this case in the first hours of the day.

FIGURE 78 - BATTERY BEHAVIOR (a) POWER (b) ENERGY AT BUS 9 CONSIDERING DIFFERENT SOLAR GENERATION SCENARIOS.

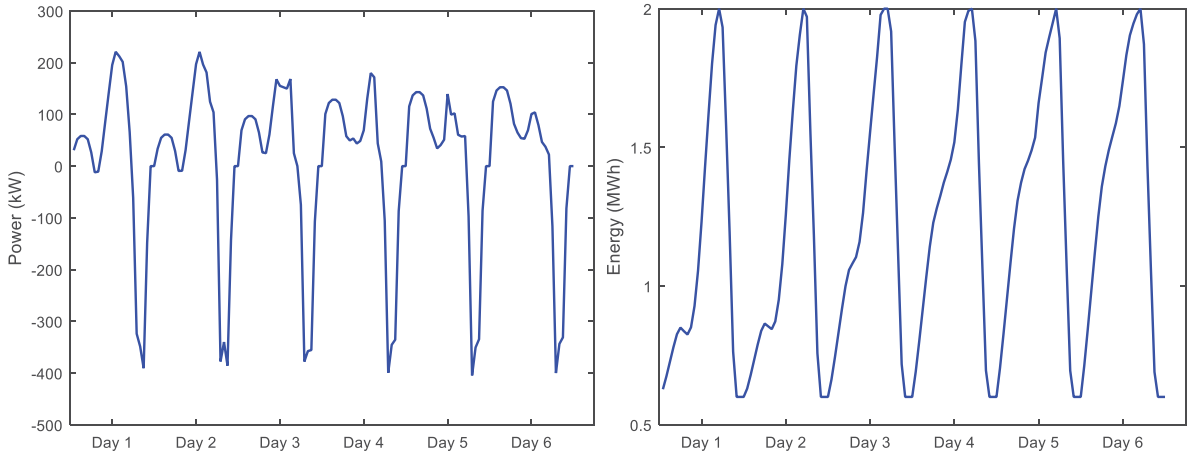

SOURCE: The Author (2019).

A comparison of system and battery operational cost was also developed, in which it is possible to visualize that as much solar generation, lower is the operational cost of the system, once the higher amount of load can be supplied by PV systems (FIGURE 79). On the other hand, the battery cost of operation does not change significantly, but the lowest values are founded when solar generation is also lower. This happens because, in this case, the power flowing into the battery to charge presented low values, charging the system smoothly, and consequently degrading less the battery.

It is important to highlight that the PV generation does not present any cost for the DSO since the systems correspond to distributed generation spread along the feeder, built by the prosumers. Therefore, the cost for the DSO corresponds to the storage system degradation cost, related to the cost and life-cycle of the BESS, as well as the cost of providing power from the substation to supply the load demand.

FIGURE 79 - COSTS OF SYSTEM AND BATTERY OPERATION UNDER DIFFERENT PHOTOVOLTAIC GENERATION SCENARIOS.

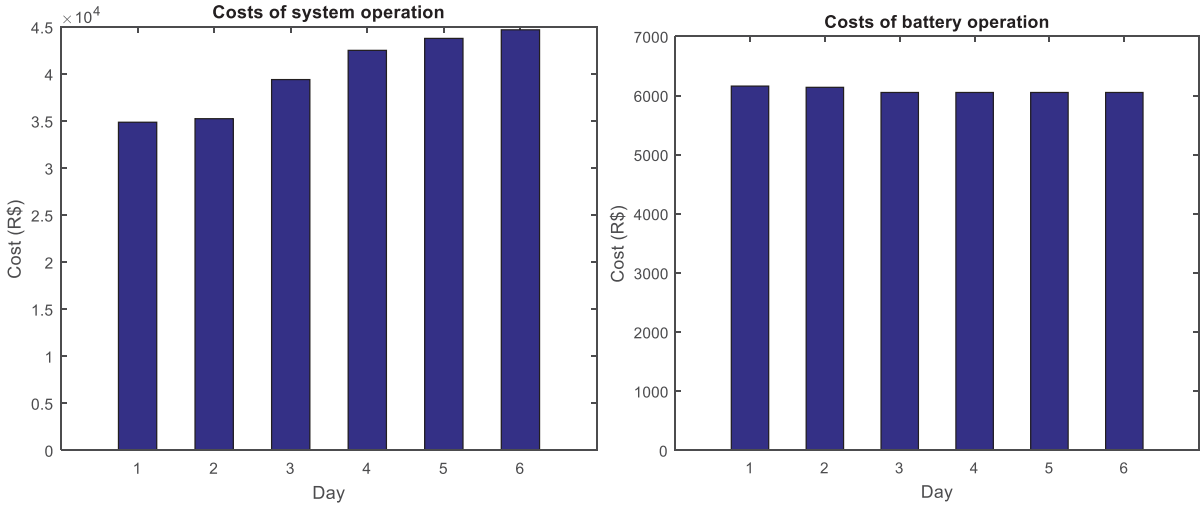

SOURCE: The Author (2019).

6.6 DISCUSSION OF THE RESULTS

The insertion of distributed energy resources changed the grid operation, as well when an energy storage system was placed to operate into the feeder. This operation needs to be optimized in order to allow the DSO, to use the new systems as a tool to improve grid operation.

In this way, multi-period optimal power flow can be a good approach to minimize the operational costs of the system in addition to reduce the power losses.

Aiming to get reliable results, a precision forecast of irradiation is required, in order to allow the planning of the system looking for the photovoltaic generation behavior in the day-ahead horizon.

The owner of the battery system is the DSO, so the operation of the system is defined according to the operator necessity. Moreover, the location of the BESS can be chosen inside of the substation or in an appropriate location in the middle of the distribution feeder in a way to improve the voltage profile of the system and reduce power losses.

Developing the simulations for allocations at the substation and outside, it is possible to verify that when the BESS are placed along the feeder, the operational results of the distribution systems are better, since the reverse power flow is reduced as well the prices of system operatio are improved. In this way, it is important to develop a study about how to define the best placement of a battery system inside of a distribution feeder in a similar way that there are studies about the best placement of capacitor banks and voltage regulators.

When different radiation profiles are considered, it is visible the impact of the distributed generation on battery system operation planning, since if there is not enough solar generation, the storage system needs to be fed by the power grid during the charging time which should happen at the moment with low load in the feeder.

7 CONCLUSIONS AND FUTURE WORKS

The active distribution networks are a reality that is growing in the power systems. The insertion of distributed generation is increasing significantly in the distribution systems. In this way, it is necessary to better understand the system operation, avoiding problems as voltage profile outside the standard limits, voltage instability, and guarantee system reliability.

Moreover, storage systems are new elements that are being inserted on distribution systems. These systems can be placed at the prosumers systems in order to improve the consumer load management or even can be owned by the power utility, being placed at the substation or in the middle of the distribution feeder. In this case, the battery system can develop different grid applications in order to provide support to the grid operation.

The impacts of the distributed generation could be verified by the power flow simulation developed, since a fixed grid operation scenario was defined and none of the characteristics are optimized. The simulations were developed for different distributed generation penetration levels, allowing to verify how the growth of DG can impact the grid.

The penetration levels were calculated using two different criteria: one used in Brazil and another used worldwide. The first criteria consider the relation between the installed power of load and of the distributed generation. Yet, the second criterion is based on the feeder supportability to generation, which is calculated as a percentage of the short-circuit power, corresponding to more technical criteria.

Voltage limits, power losses, and a number of tap changes were monitored for different scenarios of generation and also with or without the battery energy storage system placement. From the results was verified that as much higher is the DG penetration levels, lower are the power losses of the system since a greater amount of load is supplied locally, reducing the amount of power flowing through the lines. On the other hand, the number of tap changes increases as much more photovoltaic generation is considered since the amount of power generated can results in overvoltage if the voltage regulator does not actuate.

When the power flow simulations were executed, the battery behavior was fixed to develop a peak shaving and to charge during the night, once it is the period

with low load. With the peak shaving, it was possible to verify that the number of tap changes reduced as well as the total power losses of the system.

From the voltage stability analysis, it was verified that in none of the simulated scenarios the voltage collapse happens at any buses. As much higher is the distributed generation penetration, higher were the voltage stabilities indexes, due to the increase of voltage levels when existing solar generation. From the results of the stability, index was also possible to prove the contribution of the voltage regulation to improve voltage values and stability indexes.

To optimize the battery operation in a distribution network, a multi-period optimum power flow was proposed, considering the complete modeling of the grid, with the operation of a voltage regulator and capacitor banks. Furthermore, the photovoltaic generation was considered in different points of the distribution feeder and once again, different generation profiles were considered to the planning of the system operation.

The proposed Multi-Period Optimum Power Flow presented as a differential the insertion of the battery operation modeling and its degradation cost. Its operation was characterized by the inequality constraints that set the power limits that can flow through the battery, as well as the energy levels that can be stored, which were limited from 30 to 100% of the state-of-charge.

The formulation proposed minimized the total power losses as well as system and battery operational costs. To model, the system cost was used the white tariff, introduced in the Brazilian sector in January 2018. With this tariff, the price of energy varies according to the time of the day, presenting low costs for periods in which the load is lower and higher-priced in the peak time when the system demand is higher (corresponding to the period from 7 p.m. to 9 p.m).

The multi-period problem was resolved via the interior-points method implemented on Matlab, and the analysis was realized considering a day-ahead time horizon sampling for each hour.

The analysis of the multi-period OPF monitored the power balancing of the system, the voltage behavior at all buses as well as the tap positions of the voltage regulator placed. The power and energy behaviors of battery operation were also verified, allowing to check the moments of charge and discharge of it that varied according to the solar generation behavior forecast.

The same system operation characteristics were monitored when the placement of the BESS was allocated at the substation bus and in the middle of the feeder.

Considering different battery positions is was observed low changes on load losses and operational costs, which isolated can do not represent an expressive value, but during along the time of the system, the operation can result in a great different for the DSO.

In the present work, it was not considered the possibility of the storage system provides ancillary services to the system operation, as voltage support. In this way, the operation of the voltage regulator is very important to keep voltage levels inside of the acceptable limits, being not enough in some cases.

Some suggestions for future works are presented:

- Application of battery systems for ancillary services in the distribution networks, using these systems to improve grid reliability and power quality levels;
- Improve the battery model for dynamic studies, considering the dynamic input and output of photovoltaic generation;
- Include a load modeling considering different kinds of consumer behaviour spread along the feeder, presenting a scenario of real systems;
- Implement a power factor control of the photovoltaic generation and of the storage system, improving the voltage levels of the system reducing the dependency of the voltage regulator and capacitor banks for such a function.

REFERENCES

ADB. **Handbook on Battery Energy Storage System**. Manila, Philippines: [s.n.]. Available in: <https://www.adb.org/publications/battery-energy-storage-system-handbook>.

ALI, A. F.; EID, A.; ABDEL-AKHER, M. Online Voltage Instability Detection of Distribution Systems for Smart-Grid Applications. **International Journal of Automation and Power Engineering.**, p. 75–80, 2012.

ANEEL. **Resolução Normativa Nº482/2012**, 2012. Available in: <http://www2.aneel.gov.br/cedoc/ren2012482.pdf>

ANEEL. **Resolução Normativa Nº687/2015**, 2015. Available in: <http://www2.aneel.gov.br/cedoc/ren2015687.pdf>

ANEEL. **Procedimentos de Distribuição de Energia Elétrica no Sistema Elétrico Nacional - PRODIST Módulo 1 - Introdução**. [s.l: s.n.]. Available in: <http://www.aneel.gov.br/documents/656827/14866914/Módulo1_Revisão10/f6c63d9a-62e9-af35-591e-5fb020b84c13>.

ANEEL. **Procedimentos de Distribuição de Energia Elétrica no Sistema Elétrico Nacional - PRODIST Módulo 8 - Qualidade de Energia Elétrica**. [s.l: s.n.]. Available in: <http://www.aneel.gov.br/documents/656827/14866914/Módulo_8-Revisão_10/2f7cb862-e9d7-3295-729a-b619ac6baab9>.

ANEEL. **Geração Distribuída Aneel - informações compiladas e mapa**. Available in: <https://app.powerbi.com/view?r=eyJrIjoiZjM4NjM0OWYtN2IwZS00YjViLTllMjItN2E5MzBkN2ZlMzVkIiwidCI6IjQwZDZmOWI4LWVjYTctNDZhMi05MmQ0LWVhNGU5YzAxNzNlBlMSIsImMiOjR9>. Acesso em: 29 ago. 2019a.

ANEEL. **Banco de Informações de Geração**. Available in: <http://www2.aneel.gov.br/aplicacoes/capacidadebrasil/capacidadebrasil.cfm>.

AZIZ, T.; KETJOY, N. PV Penetration Limits in Low Voltage Networks and Voltage Variations. **IEEE Access**, v. 5, 2017.

BARAN, M. E.; WU, F. . Optimal capacitor placement on radial distribution systems.

IEEE Transactions on Power Delivery, v. 4, n. 1, p. 725–734, 1989.

BATTERY UNIVERSITY. **BU-205: Types of Lithium-ion**. Available in: <https://batteryuniversity.com/learn/article/types_of_lithium_ion>.

BATTERY UNIVERSITY. **BU-203: Nickel based Batteries**. Available in: <https://batteryuniversity.com/learn/article/nickel_based_batteries>.

BATTERY UNIVERSITY. **BU-808: How to Prolong Lithium-based Batteries**. Available in: <https://batteryuniversity.com/learn/article/how_to_prolong_lithium_based_batteries>. Acesso em: 22 set. 2019c.

BEAUDIN, M., ZAREIPOUR, H. SCHELLENBERGLABE, A.ROSEHART, W. Energy storage for mitigating the variability of renewable electricity sources: An updated review. Energy for Sustainable Development, v. 14, n. 4, p. 302–314, dez. 2010.

BERNARDS, R., VERWEIJ, R., COSTER, E., MORREN, J., SLOOTWEG, H.. Application and evaluation of a probabilistic forecasting model for expected local PV penetration levels. 24th International Conference & Exhibition on Electricity Distribution (CIRED), v. Session 5:, 2017.

BLASI, T. M.; FUMAGALLI, J. P.; PEREIRA, G. M. DO. S. **Evaluation of simulation tools for energy storage system in power system**. IEEE 2018 9th Power Instrumentation and Measurment Meeting Proceedings. **Anais**...2018 Available in: <http://epim2018.org/>

BORGES, S.; FERNANDES, T. S. P.; ALMEIDA, K. C. Pré-despacho hidrotérmico de potência ativa e reativa via Método dos Pontos Interiores e Coordenadas Retangulares. **Revista Controle & Automação**, v. 22, n. 5, p. 479–494, 2011.

BURATTI, R. P. **Reguladores de Tensão em Redes Elétricas com Alta Penetração de Cargas Não Lineares**. [s.l.] UNESP, 2016.

BURGER, B., Kiefer, K., Kost, C., Nold, S., Philipps, S., Preu, R., Rentsch, J., Schlegl, T., Stry-Hipp, G., Willeke, G., Wirth, H., Warmuth, W.. **Photovoltaics report**. [s.l: s.n.]. Available in: <https://www.ise.fraunhofer.de/content/dam/ise/de/documents/publications/studies/Photovoltaics-Report.pdf>.

CAMPILLO, J. **From Passive to Active Electric Distribution Networks**. [s.l.]

Mälardalen University Sweden, 2016.

CARPENTIER, J. Contribution à l'Étude du Dispatching Économique. **Bulletin de la Societé Francaise des Electriciens**, v. 3 (Aug), p. 431–447, 1962.

CARVALHO, M. R. **Estudo Comparativo de Fluxo de Potência para Sistemas de Distribuição Radial**. [s.l.] Universidade de São Carlos, 2006.

CELESC. **I-432.0004 REQUISITOS PARA A CONEXÃO DE MICRO OU MINIGERADORES DE ENERGIA AO SISTEMA ELÉTRICO DA CELESC DISTRIBUIÇÃO**. [s.l: s.n.].

CEMIG. **ND-5.30 Requisitos para a conexão de Acessantes ao Sistema de Distribuição Cemig - Conexão em Baixa Tensão**. [s.l: s.n.].

CEPEL. **Redefinição dos patamares de carga para a determinação do despacho de geração e formação de preço com os modelos NEWAVE e DECOMP**. [s.l: s.n.]. Available in: <www.mme.gov.br/documents/10584/83952611/%28CEPEL%29Patamares+Carga-12+Julho+2018.pdf/02e39986-b7e3-43c3-aaf2-7015a1c5cc01%0D>.

CHAKRAVORTY, M.; DAS, D. Voltage stability analysis of radial distribution networks. **International Journal of Electrical Power & Energy Systems**, v. 23, n. 2, p. 129–135, 2001.

CHATHURANGI, D., JAYATUNGA, U., RATHNAYAKE, M., WICKRAMASINGHE, A., AGALGAONKAR, A.,PERERA, S.. Potential Power Quality Impacts on LV Distribution Networks With High Penetration Levels of Solar PV. **18th International Conference on Harmonics and Quality of Power (ICHQP)**, 2018.

CIGRE. **Task Force: Development and Operation of Active Distribution Networks C6.11**. [s.l: s.n.]. Available in: <https://e-cigre.org/publication/457-development-and-operation-of-active-distribution-networks>.

CIGRE. **Technical Brochure: Planning and Optimization Methods for Active Distribution Network - C6.19**. [s.l: s.n.].

CIGRE. **Connection of Wind Farms to Weak AC Networks - Working Group B4.62**. [s.l: s.n.]. Available in: <http://b4.cigre.org/Publications/Technical-Brochures/TB-671-2016-B4-62-Connection-of-wind-farms-to-weak-AC-networks>.

COCEL. **NTC 031 CONEXÃO DE MICRO E MINIGERAÇÃO DISTRIBUÍDA**. [s.l: s.n.].

COLOMBARI, L., KUIAVA, R., PERIC, V., RAMOS, R.. Continuation Load Flow Considering Discontinuous Behavior of Distribution Grids. **IEEE Transactions on Power Systems**, v. 34, n. 5, p. 3476–3483, 2019.

COPEL. **NTC 905200 ACESSO DE MICRO E MINIGERAÇÃO DISTRIBUÍDA AO SISTEMA DA COPEL**. [s.l: s.n.].

COPEL. **NTC 905100 - Acesso de Geração Distribuída ao Sistema da Copel (com comercialização de energia)**, 2017.

COPEL. **Tarifa Branca**. Available in: <https://www.copel.com/hpcopel/root/nivel2.jsp?endereco=%2Fhpcopel%2Findustrial%2Fpagcopel2.nsf%2Fdocs%2FB0CA4C8DF4B62F98832581F00058CCF9>.

COPETTI, J. B.; MACAGNAN, M. H. Baterias em Sistemas Solares Fotovoltaicos. **I Congresso Brasileiro de Energia Solar - I CBENS**, 2007.

CORPORATION, P. W. **Power World**. Available in: <https://www.powerworld.com/>.

D'ADAMO, C., TAYLOR, P., JUPE, S., BUCHHOLZ, B., PILO, F., ABBEY, C., MARTI, J.. Active Distribution Networks: general features, present status of implementation and operation practices. **Electra nº246**, 2009.

DAS, C. K., BASS, O., KOTHAPALLI, G., MAHMOUD, T., HABIBI, D.. Overview of energy storaage systems in distribution networks: Placement, sizing, operation, and power quality. **Renewable and Sustainable Energy Reviews**, v. 91, p. 1205–1230, 2018.

DIGSILENT. **DIgSILENT Power Factory 2017 - User Manual**. [s.l: s.n.].

DIVYA, K. C.; OSTERGAARD, J. Battery Energy Storage Technology for Power Systems - An Overview. **Electric Power Systems Reseaarch**, v. 79, p. 511–520, 2009.

DOE. **GridLAB-D Simulatioon Software**. Available in: <https://www.gridlabd.org/>.

DUGAN, R. C.; MONTENEGRO, D. **Reference Guide - The Open Distribution System Simulator (OpenDSS)**EPRI, , 2018. Available in: <https://sourceforge.net/projects/electricdss/>

ELEKTRO. **Norma ND.64 Conexão entre Microgeração Distribuída em Baixa**

Tensão e a Rede de Distribuição da ELEKTRO. [s.l: s.n.].

ELETROPAULO. **NT - 6.012 Requisitos Mínimos para Interligação de Microgeração e Minigeração Distribuída com a Rede de Distribuição da Eletropaulo com Paralelismo Permanente Através do Uso de Inversores - Consumidores de Alta, Média e Baixa Tensão**. [s.l: s.n.].

ENERGISA MT. **NTE - 041 REQUISITOS PARA ACESSO E CONEXÃO DE GERAÇÃO DISTRIBUÍDA AO SISTEMA DE DISTRIBUIÇÃO DA ENERGISA/MT**. [s.l: s.n.].

ENERGY RESEARCH OFFICE - EPE. Distributed Energy Resources: Impacts on Energy Planning Studies. 2018.

ENSSLIN, L. ENSSLIN, S. R., LACERDA, R. T. O., TASCA, J. E.. Processo de Seleção de Portifolio Bibliográfico. **Processo técnico com patente de registro pendente junto ao INPI**, 2010.

EPE. **Projeção da demanda de energia elétrica para os próximos 10 anos (2017 - 2026)**. [s.l: s.n.]. Available in: <http://www.epe.gov.br/sites-pt/publicacoes-dados-abertos/publicacoes/PublicacoesArquivos/publicacao-245/topico-261/DEA 001_2017 - Projeções da Demanda de Energia Elétrica 2017-2026_VF[1].pdf>.

EPRI. **OpenDSS PVSystem Element Model - Version 1**, 2011a.

EPRI. **OpenDSS Storage Element and StorageController Element**, 2011b.

EPRI. **OpenDSS**. Available in: <https://www.epri.com/#/pages/sa/opendss?lang=en>.

EULE, S. **EIA's Annual Energy Outlook 2019—The Future Looks Pleasant**. Available in: <https://www.globalenergyinstitute.org/eias-annual-energy-outlook-2019-future-looks-pleasant>.

FERNANDES, T. S. P. **Um Modelo de Despacho Ótimo de Potência para Sistemas Multi-Usuários.** [s.l.] Universidade Federal de Santa Catarina, 2004.

FRAUNHOFER ISE. **Current and Future Cost of Photovoltaics**. [s.l: s.n.]. Available in:
<https://www.ise.fraunhofer.de/content/dam/ise/de/documents/publications/studies/AgoraEnergiewende_Current_and_Future_Cost_of_PV_Feb2015_web.pdf>.

GABASH, A.; LI, P. Active-reactive optimal power flow in distribution networks with

embedded generation and battery storage. **IEEE Transactions on Power Systems**, 2012.

GAYME, D.; TOPCU, U. Optimal power flow with large-scale storage integration. **IEEE Transactions on Power Systems**, 2013.

GILL, S.; KOCKAR, I.; AULT, G. W. Dynamic Optimum Power flow for Active Distribution Networks. **IEEE Transactions on Power Systems**, v. 29, p. 121–131, 2014.

GODOI.A.A.; AOKI, A. R.; FERNANDES, T. S. . Alocação ótima de bancos de capacitores em redes de distribuição de energia elétrica. **VIII Conferência Brasileira sobre Qualidade de Energia Elétrica**, 2009.

GODOI, A. A. **Alocação de Bancos de Capacitores em Redes Primária e Secundária de Energia Elétrica**. [s.l.] Universidade Federal do Paraná, 2009.

GRANVILLE, S.; MELLO, F. C.; MELLO, A. C. G. Application of Interior Point Methods to Power Flow Unsolvability. **IEEE Transactions on Power Systems**, v. 11, n. 2, p. 1096–1103, 1996.

HALLBERG, P. Active Distribution system Management - A Key tool for the Smooth Integration of Distributed Generation. **A EURELECTRIC**, 2013.

HATZIARGYRIOU, N. ET AL. The impact of battery energy storage systems on distribution networks. **Electra**, v. 297, p. 81–89, 2018.

HAYES, P. **BESS Overview - Components, Drivers, Appications**ABB Group, , 2012.

HOLT, M.; GROSSE_HOLZ, G.; REHTANZ, C. Line Voltage Regulation in Low Voltage Grids. **CIRED Workshop**, 2018.

HUDSON, R.; HEILSCHER, G. PV Grid Integration - Sytem Management Issues and Utility Concerns. **Energy Procedia**, p. 82–92, 2012.

IEA-PVPS. **Trends 2018 in Photovoltaic Applications - Survey Report of Selected IEA Countries between 1992 and 2017.** [s.l: s.n.]. Available in: <http://www.iea-pvps.org/fileadmin/dam/public/report/statistics/2018_iea-pvps_report_2018.pdf>.

IEA. **Word Energy Outlook 2017: China**. Available in: <https://www.iea.org/weo/china/>.

IEA. **World Energy Outlook 2018**. Available in: <https://www.iea.org/weo2018/electricity/>.

IEA. **Technology mix in storage installations excluding pumped hydro, 2011-2016**. Available in: <https://www.iea.org/data-and-statistics/charts/technology-mix-in-storage-installations-excluding-pumped-hydro-2011-2016%0D>.

IEEE. **IEEE Vision for Smart Grid Controls: 2030 and beyond**. [s.l: s.n.].

IEEE POWER ENGINEERING SOCIETY. **Distribution System Analysis Subcommittee - IEEE 13 Node Test Feeder**. [s.l: s.n.]. Available in: <http://sites.ieee.org/pes-testfeeders/resources/>.

IHA, I. H. A. Briefing - 2017 Key Trends in Hydropower. **2017 Hydropower Status Report**, 2017.

INPE. **Centro de Previsão de Tempo e Estudos Climáticos**. Available in: <https://www.cptec.inpe.br/glossario.shtml>. Acesso em: 6 jun. 2019.

KEYSIGHT TECHNOLOGIES. **Instalação e Manutenção de Sistemas Solares Fotovoltaicos - Usando soluções de bancada e de mão para aplicações de energia solar**. [s.l: s.n.]. Available in: <https://literature.cdn.keysight.com/litweb/pdf/5992-1004PTBR.pdf?id=2639367>.

LACHOVICZ, F. J. . **Planejamento de suporte de reativo para rede de distribuição com forte penetração de geração solar fotovoltaica.** [s.l.] Universidade Federal do Paraná, 2018.

LEBID, D. R. **Alocação de Bancos de capacitores e Reguladores de Tensão em Redes de Distribuição Utilizando Cirtérios de Estabilidade de Tensão, Máximo Carregamento, Perfil de Tensão e Perdas Elétricas**. [s.l.] Universidade Federal do Paraná, 2017.

LI, R., WANG, W., CHEN, Z., WU, X.. Optimal planning of energy storage system in active distribution system based on fuzzy multi-objective bi-level optimization. **Journal of Modern Power Systems and Clean Energy**, v. 6, n. 2, p. 342–355, 4 mar. 2018.

LIGHT. **IT DTE/DTP 01/12 PROCEDIMENTOS PARA A CONEXÃO DE MICROGERAÇÃO E MINIGERAÇÃO AO SISTEMA DE DISTRIBUIÇÃO DA LIGHT SESA BT E MT – ATÉ CLASSE 36,2KV**. [s.l: s.n.].

LYON GROUP. **Projects**. Available in: <https://www.lyoninfrastructure.com.au/projects/>.

LYON GROUP. **Riverland Battery Power Plant**. Available in: <https://www.lyoninfrastructure.com.au/projects/riverland-battery-power-plant/>.

MASOUM, M. A. S.; FUCHS, E. F. **Power Quality in Power Systems and Electrical Machines**. 2nd. ed. [s.l.] Elsevier, 2015.

MCDOWALL, J. **Energy of the Future Conference - ESS Technologies**. [s.l: s.n.].

MEYER, F. **Compressed air energy storage power plants**. [s.l: s.n.]. Available in: <http://www.bine.info/fileadmin/content/Publikationen/Englische_Infos/projekt_0507_engl_internetx.pdf>.

NGUYEN, N. T. A. et al. Optimal power flow with energy storage systems: Single-period model vs. multi-period model. **2015 IEEE Eindhoven …**, 2015.

OLIVEIRA, G. A. **Programação diária da operação integrada de redes de distribuição ativas considerando a inserção de veículos elétricos.** [s.l.] Universidade Federal do Paraná, 2019.

ONS. **Capacidade Instalada no SIN - 2018/2023**. Available in: <http://ons.org.br/paginas/sobre-o-sin/o-sistema-em-numeros>. Acesso em: 30 maio. 2019a.

ONS. **Histórico da Operação - Curva de Carga Horária**. Available in: <www.ons.org.br/Paginas/resultados-da-operacao/historico-da-operacao/curva_carga_horaria.aspx%0D>. Acesso em: 14 out. 2019b.

PAIVA, R. R. **Fluxo de Potência Ótimo em Redes de Distribuição de Energia com a Presença de Geração Distribuída: Um Novo Algoritmo para Auxiliar a Análise do Perfil de Tensão**. [s.l.] Universidade Federal de Santa Catarina, 2006.

PALIZBAN, O.; KAUHANIEMI, K. **Energy storage systems in modern grids—Matrix of technologies and applicationsJournal of Energy Storage**Elsevier, , 2016. Available in: <https://www.sciencedirect.com/science/article/pii/S2352152X1630010X>

PEREIRA, R. **O que é Geração Distribuída**. Available in: <https://www.portalsolar.com.br/o-que-e-geracao-distribuida.html>.

PORTAL SOLAR. **O Inversor Solar**. Available in: <https://www.portalsolar.com.br/o-inversor-solar.html>.

REIHANI, E., SEPASI, S., ROOSE, L. R., MATSUURA, M. Energy management at the distribution grid using a Battery Energy Storage System (BESS). **… Journal of Electrical Power & …**, 2016.

REIS, C.; BARBOSA, F. P. M. A Comparison of Voltage Stability Indices. **IEEE MELECON**, p. 1007–1010, 2006.

RHOLDEN, E.; CEBALLOS, S. **The Energy of the Future Conference**CuritibaSchneider Electric and Saft, , 2018.

RODGERS, L. **Batteries** MIT, , 2019. Available in: <http://web.mit.edu/nouyang/Public/Batteries_2.007_Notes_v3.pdf>

SALAS, V., OLIAS, E., DÉBORA, P.J., PÉREZ-REGALADO, M.J.. Overview about International Electrotechnical Commission (IEC) Standards Applied to Grid-Connected Photovoltaic Inverters. **Solar World Congress**, 2011.

SHARENERGY. **O que é o inversor e qual a sua funçãoo em um sistema fotovoltaico**. Available in: <https://sharenergy.com.br/o-que-e-o-inversor-e-como-ele-funciona/>.

SHIREK, G. Assessing the effect of OV generation on distibution system voltages. **Technology and Bussiness for development**, 2014.

SILVA, N. **TRACING THE TRANSITION FROM PASSIVE TO ACTIVE DISTRIBUTION NETWORKS**. Available in: <http://www.incite-itn.eu/blog/tracing-the-transition-from-passive-to-active-distribution-networks/>.

SMA. **PV Inverters - Basic Facts for Planning PV Systems**. Available in: <https://www.sma.de/en/partners/knowledgebase/pv-inverters-basic-facts-for-planning-pv-systems.html>.

SOLARGIS. **Solargis Website**. Available in: <https://solargis.info/>.

SUBRAMANI, C.; DASH, S. S.; BHASKAR, M. A. Line outage contingency screening and ranking for voltage stability assessment. **Power Systems. ICPS'09 International Conference**, p. 1–5, 2009.

SUFYAN, M., RAHIM, N. A., AMAN, M. M., TAN, C. K., RAIHAN, S. R. S.. Sizing and

Applications of Battery Energy Storage Technologies in Smart Grid System: A Review. **Journal of Renewable and Sustainable Energy**, v. 11, 2019.

SUSCHEM. **Battery Energy Storage - White Paper**. [s.l: s.n.].

TAZVINGA, H.; ZHU, B.; XIA, X. Optimal power flow management for distributed energy resources with batteries. **Energy Conversion and Management**, 2015.

THE NOBEL PRIZE. **The Nobel Prize in Chemistry 2019**. Available in: <https://www.nobelprize.org/prizes/chemistry/2019/summary/>.

VIOLA, L. **PLANEJAMENTO DE CURTO PRAZO DA OPERAÇÃO DE BATERIAS E ARMAZENAMENTO DE HIDROGÊNIO EM SISTEMAS DE DISTRIBUIÇÃO DE ENERGIA ELÉTRICA**. [s.l.] Unicamp, 2017.

VIOLA, L.; DA SILVA, L. C. P.; RIDER, M. J. Otimização do Armazenamento de Energia Através de Bateria e Hidrogênio em Sistemas de Distribuição de Energia Elétrica. **XIII Simpósio Brasileiro de Automação Inteligente**, 2017.

WANG, Z., ZHONG, J., CHEN, D., LU, Y. A multi-period optimal power flow model including battery energy storage. **Power and Energy …**, 2013.

WOODBANK COMMUNICATIONS. **Grid Scale Energy Storage Systems**. Available in: <https://www.mpoweruk.com/grid_storage.htm#top%0D>.

YAMAKAWA, E. K. **Sistema de Controle Nebuloso para Bancos de Capacitores Automáticos Aplicados em Alimentadores de Distribuição de Energia Elétrica.** [s.l.] UFPR, 2007.

YANG, C. **Chinese Electricity Consumption Growt Hits 6-Year High**. Available in: <https://www.caixinglobal.com/2019-01-30/chart-of-the-day-chinese-electricity-consumption-growth-hits-6-year-high-101376236.html>.

ZHANG, Y., RAHBARI-ASR, N., DUAN, J.. Day-ahead smart grid cooperative distributed energy scheduling with renewable and storage integration. **IEEE Transactions on …**, 2016.

ANNEX A – IEEE 13 BUSES DATA

TABLE 26 – IEEE 13 BUS OVERHEAD LINE CONFIGURATION DATA.

Config.	Phasing	Phase	Neutral	Spacing
		ACSR	ACSR	ID
601	B A C N	556,500 26/7	4/0 6/1	500
602	C A B N	4/0 6/1	4/0 6/1	500
603	C B N	1/0	1/0	505
604	A C N	1/0	1/0	505
605	C N	1/0	1/0	510

SOURCE: IEEE POWER ENGINEERING SOCIETY (1992).

TABLE 27 - IEEE 13 BUS UNDERGROUND LINE CONFIGURATION DATA.

Config.	Phasing	Cable	Neutral	Space ID
606	A B C N	250,000 AA, CN	None	515
607	A N	1/0 AA, TS	1/0 Cu	520

SOURCE: IEEE POWER ENGINEERING SOCIETY (1992).

TABLE 28 - IEEE 13 BUS LINE SEGMENT DATA.

Node A	Node B	Length(ft.)	Config.
632	645	500	603
632	633	500	602
633	634	0	XFM-1
645	646	300	603
650	632	2000	601
684	652	800	607
632	671	2000	601
671	684	300	604
671	680	1000	601
671	692	0	Switch
684	611	300	605
692	675	500	606

SOURCE: IEEE POWER ENGINEERING SOCIETY (1992).

TABLE 29 - IEEE 13 BUS TRANSFORMER DATA

	kVA	kV-high	kV-low	R - %	X - %
Substation:	5,000	115 - D	4.16 Gr. Y	1	8
XFM -1	500	4.16 – Gr.W	0.48 – Gr.W	1.1	2

SOURCE: IEEE POWER ENGINEERING SOCIETY (1992).

TABLE 30 - IEEE 13 BUS CAPACITOR DATA.

Node	Ph-A	Ph-B	Ph-C
	kVAr	kVAr	kVAr
675	200	200	200
611			100
Total	200	200	300

SOURCE: IEEE POWER ENGINEERING SOCIETY (1992).

TABLE 31 - IEEE 13 BUS REGULATOR DATA

Regulator ID:	1		
Line Segment:	650 - 632		
Location:	50		
Phases:	A - B -C		
Connection:	3-Ph,LG		
Monitoring Phase:	A-B-C		
Bandwidth:	2.0 volts		
PT Ratio:	20		
Primary CT Rating:	700		
Compensator Settings:	Ph-A	Ph-B	Ph-C
R - Setting:	3	3	3
X - Setting:	9	9	9
Volltage Level:	122	122	122

SOURCE: IEEE POWER ENGINEERING SOCIETY (1992).

TABLE 32 - IEEE 13 BUS SPOT LOAD DATA

Node	Load	Ph-1	Ph-1	Ph-2	Ph-2	Ph-3	Ph-3
	Model	kW	kVAr	kW	kVAr	kW	kVAr
634	Y-PQ	160	110	120	90	120	90
645	Y-PQ	0	0	170	125	0	0
646	D-Z	0	0	230	132	0	0
652	Y-Z	128	86	0	0	0	0
671	D-PQ	385	220	385	220	385	220
675	Y-PQ	485	190	68	60	290	212
692	D-I	0	0	0	0	170	151
611	Y-I	0	0	0	0	170	80
	TOTAL	1158	606	973	627	1135	753

SOURCE: IEEE POWER ENGINEERING SOCIETY (1992).

TABLE 33 - IEEE 13 BUS DISTRIBUTED LOAD DATA

Node A	Node B	Load	Ph-1	Ph-1	Ph-2	Ph-2	Ph-3	Ph-3
		Model	kW	kVAr	kW	kVAr	kW	kVAr
632	671	Y-PQ	17	10	66	38	117	68

SOURCE: IEEE POWER ENGINEERING SOCIETY (1992).

TABLE 34 - IEEE 13 BUS IMPEDANCES

Configuration 601:

```
          Z (R +jX) in ohms per mile
0.3465  1.0179   0.1560  0.5017   0.1580  0.4236
                 0.3375  1.0478   0.1535  0.3849
                                  0.3414  1.0348
         B in micro Siemens per mile
           6.2998   -1.9958   -1.2595
                     5.9597   -0.7417
                               5.6386
```

Configuration 602:

```
          Z (R +jX) in ohms per mile
0.7526  1.1814   0.1580  0.4236   0.1560  0.5017
                 0.7475  1.1983   0.1535  0.3849
                                  0.7436  1.2112
         B in micro Siemens per mile
           5.6990   -1.0817   -1.6905
                     5.1795   -0.6588
                               5.4246
```

Configuration 603:

```
          Z (R +jX) in ohms per mile
0.0000  0.0000   0.0000  0.0000   0.0000  0.0000
                 1.3294  1.3471   0.2066  0.4591
                                  1.3238  1.3569
         B in micro Siemens per mile
           0.0000    0.0000    0.0000
                     4.7097   -0.8999
                               4.6658
```

Configuration 604:

```
          Z (R +jX) in ohms per mile
1.3238  1.3569   0.0000  0.0000   0.2066  0.4591
                 0.0000  0.0000   0.0000  0.0000
                                  1.3294  1.3471
         B in micro Siemens per mile
           4.6658    0.0000   -0.8999
                     0.0000    0.0000
                               4.7097
```

SOURCE: IEEE POWER ENGINEERING SOCIETY (1992).

ANNEX B – 90 BUS DATA AND CONFIGURATION FOR MPOPF SIMULATION

TABLE 35 - SYSTEM 90 BUS LINE DATA

Bus From	Bus To	Resistance (Ω)	Reactance (Ω)	Bus From	Bus To	Resistance (Ω)	Reactance (Ω)
1	2	0.0005	0.0012	46	47	0.0009	0.0012
2	3	0.0005	0.0012	5	48	0.0034	0.0084
3	4	0.0005/2	0.0012/2	48	49	0.0851	0.2083
4	5	0.0015	0.0036	49	50	0.2898	0.7091
5	6	0.0251	0.0294	50	51	0.0822	0.2011
6	7	0.3660	0.1864	9	52	0.0928	0.0473
7	8	0.3811	0.1941	52	53	0.3319	0.1114
8	9	0.0922	0.0470	10	54	0.1740	0.0886
9	10	0.0493	0.0251	54	55	0.2030	0.1034
10	11	0.8190	0.2707	55	56	0.2842	0.1447
11	12	0.1872	0.0619	56	57	0.2813	0.1433
12	13	0.7114	0.2351	57	58	1.5900	0.5337
13	14	1.03	0.3400	58	59	0.7837	0.2630
14	15	1.0440	0.3450	59	60	0.3042	0.1006
15	16	1.0580	0.3496	60	61	0.3861	0.1172
16	17	0.1966	0.0650	61	62	0.5075	0.2585
17	18	0.3744	0.1238	62	63	0.0974	0.0496
18	19	0.0047	0.0016	63	64	0.1450	0.0738
19	20	0.3276	0.1083	64	65	0.7105	0.3619
20	21	0.2106	0.0696	65	66	10410	0.5302
21	22	0.3416	0.1129	12	67	0.2012	0.0611
22	23	0.014	0.0046	67	68	0.0047	0.0014
23	24	0.1591	0.0526	13	69	0.7394	0.2444
24	25	0.3463	0.1145	69	70	0.0047	0.0016
25	26	0.7488	0.2475	7	71	0.0257	0.0393
26	27	0.3089	0.1021	17	72	0.0257	0.0393
27	28	0.1732	0.0572	20	73	0.0155	0.0264
3	29	0.0044	0.0108	23	74	0.0155	0.0264
29	30	0.0640	0.1565	25	75	0.0155	0.0264
30	31	0.3978	0.1315	28	76	0.0082	0.0162
31	32	0.0702	0.0232	31	77	0.0257	0.0393
32	33	0.3510	0.1160	36	78	0.0082	0.0162
33	34	0.8390	0.2816	39	79	0.0155	0.0264
34	35	1.7080	0.5646	42	80	0.0155	0.0264
35	36	1.4740	0.4873	44	81	0.0155	0.0264
4	37	0.0044	0.0108	47	82	0.0257	0.0393
37	38	0.0640	0.1565	51	83	0.0257	0.0393
38	39	0.1053	0.1230	53	84	0.0257	0.0393
39	40	0.0304	0.0355	56	85	0.0257	0.0393
40	41	0.0018	0.0021	59	86	0.0257	0.0393
41	42	0.7283	0.8509	62	87	0.0155	0.0264

42	43	0.3100	0.3623	66	88	0.0082	0.0162
43	44	0.0410	0.0478	68	89	0.0257	0.0393
44	45	0.0092	0.0116	70	90	0.0257	0.0393
45	46	0.1089	0.1373				

Source: Adapted from Godoi, Aoki and Fernandes (2009) and Oliveira (2019).

TABLE 36 - INSTALLED POWER IN EACH BUS.

Bus	Active Power (kW)	Reactive Power (kVAr)	Bus	Active Power (kW)	Reactive Power (kVAr)
1	0	0	46	39.22	26.3
2	0	0	47	0	0
3	0	0	48	79	56.4
4	0	0	49	384.7	274.5
5	0	0	50	384.7	274.5
6	2.6	2.2	51	40.5	28.3
7	40.4	30	52	3.6	2.7
8	75	54	53	4.35	3.5
9	30	22	54	26.4	19
10	28	19	55	24	17.2
11	145	104	56	0	0
12	145	104	57	0	0
13	8	5.5	58	0	0
14	8	5.5	59	100	72
15	0	0	60	0	0
16	45.5	30	61	1244	888
17	60	35	62	32	23
18	60	35	63	0	0
19	0	0	64	227	162
20	1	0.6	65	59	42
21	114	81	66	18	13
22	5.3	3.5	67	18	13
23	0	0	68	28	20
24	28	20	69	30.8	20
25	0	0	70	30.8	0
26	14	10	71	26.4	0
27	14	10	72	26.4	0
28	26	18.6	73	39.6	0
29	26	18.6	74	39.6	0
30	0	0	75	39.6	0
31	0	0	76	66	0
32	0	0	77	26.4	0
33	14	10	78	66	0
34	19.5	14	79	39.6	0
35	6	4	80	39.6	0
36	26	18.55	81	39.6	0
37	26	18.55	82	26.4	0

38	0	0	83	26.4	0
39	24	17	84	26.4	0
40	24	17	85	26.4	0
41	1.2	1	86	26.4	0
42	0	0	87	39.6	0
43	6	4.3	88	66	0
44	0	0	89	26.4	0
45	39.22	26.3	90	26.4	0

Source: Adapted from Godoi, Aoki, and Fernandes (2009) and Oliveira (2019).

TABLE 37 - PHOTOVOLTAIC INSTALLED POWER

Bus	Active Power (kW)	Reactive Power (kVAr)	Bus	Active Power (kW)	Reactive Power (kVAr)
1	0	0	46	0	0
2	0	0	47	0	0
3	0	0	48	0	0
4	0	0	49	0	0
5	0	0	50	0	0
6	0	0	51	174.9	74.51
7	174.9	74.51	52	0	0
8	0	0	53	174.9	74.51
9	0	0	54	0	0
10	0	0	55	174.9	74.51
11	0	0	56	0	0
12	0	0	57	0	0
13	0	0	58	0	0
14	0	0	59	0	0
15	174.9	74.51	60	174.9	74.51
16	0	0	61	0	0
17	0	0	62	0	0
18	0	0	63	0	0
19	0	0	64	0	0
20	174.9	74.51	65	174.9	74.51
21	0	0	66	0	0
22	0	0	67	0	0
23	0	0	68	174.9	74.51
24	0	0	69	0	0
25	174.9	74.51	70	174.9	74.51
26	0	0	71	0	0
27	0	0	72	0	0
28	0	0	73	0	0
29	0	0	74	0	0
30	174.9	74.51	75	0	0
31	0	0	76	0	0
32	0	0	77	0	0
33	0	0	78	0	0

34	0	0	79	0	0
35	174.9	74.51	80	0	0
36	0	0	81	0	0
37	0	0	82	0	0
38	174.9	74.51	83	0	0
39	0	0	84	0	0
40	174.9	74.51	85	0	0
41	0	0	86	0	0
42	0	0	87	0	0
43	0	0	88	0	0
44	0	0	89	0	0
45	174.9	74.51	90	0	0

Source: Adapted from Lachovicz (2018) Oliveira (2019).